



**Calhoun: The NPS Institutional Archive**  
**DSpace Repository**

---

Theses and Dissertations

1. Thesis and Dissertation Collection, all items

---

2010-12

# Performance evaluation of photonic Sigma Delta ADCS

Tan, Yean Wee

Monterey, California. Naval Postgraduate School

---

<https://hdl.handle.net/10945/4978>

---

This publication is a work of the U.S. Government as defined in Title 17, United States Code, Section 101. Copyright protection is not available for this work in the United States.

*Downloaded from NPS Archive: Calhoun*



Calhoun is the Naval Postgraduate School's public access digital repository for research materials and institutional publications created by the NPS community. Calhoun is named for Professor of Mathematics Guy K. Calhoun, NPS's first appointed -- and published -- scholarly author.

**Dudley Knox Library / Naval Postgraduate School**  
**411 Dyer Road / 1 University Circle**  
**Monterey, California USA 93943**

<http://www.nps.edu/library>



**NAVAL  
POSTGRADUATE  
SCHOOL**

**MONTEREY, CALIFORNIA**

**THESIS**

**PERFORMANCE EVALUATION OF PHOTONIC SIGMA  
DELTA ADCS**

by

Yean Wee Tan

December 2010

Thesis Advisor:  
Second Reader:

Phillip E. Pace  
David C. Jenn

**Approved for public release; distribution is unlimited**

THIS PAGE INTENTIONALLY LEFT BLANK

REPORT DOCUMENTATION PAGE			Form Approved OMB No. 0704-0188	
Public reporting burden for this collection of information is estimated to average 1 hour per response, including the time for reviewing instruction, searching existing data sources, gathering and maintaining the data needed, and completing and reviewing the collection of information. Send comments regarding this burden estimate or any other aspect of this collection of information, including suggestions for reducing this burden, to Washington headquarters Services, Directorate for Information Operations and Reports, 1215 Jefferson Davis Highway, Suite 1204, Arlington, VA 22202-4302, and to the Office of Management and Budget, Paperwork Reduction Project (0704-0188) Washington DC 20503.				
1. AGENCY USE ONLY (Leave blank)		2. REPORT DATE December 2010	3. REPORT TYPE AND DATES COVERED Master's Thesis	
4. TITLE AND SUBTITLE Performance Evaluation of Photonic Sigma Delta ADCs			5. FUNDING NUMBERS	
6. AUTHOR(S) Yean Wee Tan				
7. PERFORMING ORGANIZATION NAME(S) AND ADDRESS(ES) Center for Joint Services Electronic Warfare Naval Postgraduate School Monterey, CA 93943-5000			8. PERFORMING ORGANIZATION REPORT NUMBER	
9. SPONSORING /MONITORING AGENCY NAME(S) AND ADDRESS(ES) Office of Naval Research, Washington, DC			10. SPONSORING/MONITORING AGENCY REPORT NUMBER	
11. SUPPLEMENTARY NOTES The views expressed in this thesis are those of the author and do not reflect the official policy or position of the Department of Defense or the U.S. Government.				
12a. DISTRIBUTION / AVAILABILITY STATEMENT Approved for public release; distribution is unlimited			12b. DISTRIBUTION CODE A	
13. ABSTRACT (maximum 200 words)  The integration of photonic and electronic components to realize a photonic sigma delta ADC is considered in this thesis. The integration process was broken up into steps. First, the performance of a pair of dual-port Mach-Zehnder interferometers (MZI) modulating a train of narrow high-speed laser pulses from a mode-locked laser was investigated. Various parameters like the half-wave voltage ( $V_{\pi}$ ) and insertion loss were verified. Next, the ability of the MZIs to modulate the laser pulses, including the subtraction of two RF signals going into the two RF ports, was investigated. After that, the performance of a high-speed comparator circuit was evaluated. The comparator circuit was implemented using high-speed analog components capable of supporting data rates of up to 50 Gbps. The comparator components have to be tested individually and then integrated to ensure that they are able to amplitude analyze the modulated laser pulses using their respective matching threshold values. Lastly, the performance of the ring resonator, which was fabricated by the University of California Santa Barbara, was investigated. The ring resonator functions as an accumulator in the photonic ADC.  In addition, a MATLAB simulation designed previously was used to simulate the behavior of the photonic sigma delta ADC. It was modified to speed up the simulation time and incorporate actual hardware parameters, including the time and amplitude jitter of the mode-locked laser. These laser parameters were characterized using a high-speed sampling oscilloscope. Thus, it was possible to predict the performance of the ADC under adverse effects as well as to show how the various electrical and optical signals appear at different parts of the circuit, which greatly adds to the efficiency of the integration process.				
14. SUBJECT TERMS  Photonic Analog to Digital Converter, Sigma delta Analog to Digital Converter, High-speed ADC			15. NUMBER OF PAGES 111	
			16. PRICE CODE	
17. SECURITY CLASSIFICATION OF REPORT Unclassified	18. SECURITY CLASSIFICATION OF THIS PAGE Unclassified	19. SECURITY CLASSIFICATION OF ABSTRACT Unclassified	20. LIMITATION OF ABSTRACT UU	

THIS PAGE INTENTIONALLY LEFT BLANK

**Approved for public release; distribution is unlimited**

**PERFORMANCE EVALUATION OF PHOTONIC SIGMA DELTA ADCS**

Yean Wee Tan  
Singapore Technologies Engineering  
B.Eng., Nanyang Technological University, 2007

Submitted in partial fulfillment of the  
requirements for the degree of

**MASTER OF SCIENCE IN ELECTRICAL ENGINEERING**

from the

**NAVAL POSTGRADUATE SCHOOL  
December 2010**

Author: Yean Wee Tan

Approved by: Phillip E. Pace  
Thesis Advisor

David C. Jenn  
Second Reader

R. Clark Robertson  
Chairman, Department of Electrical and Computer Engineering

THIS PAGE INTENTIONALLY LEFT BLANK

## ABSTRACT

The integration of photonic and electronic components to realize a photonic sigma delta ADC is considered in this thesis. The integration process was broken up into steps. First, the performance of a pair of dual-port Mach-Zehnder interferometers (MZI) modulating a train of narrow high-speed laser pulses from a mode-locked laser was investigated. Various parameters like the half-wave voltage ( $V_{\pi}$ ) and insertion loss were verified. Next, the ability of the MZIs to modulate the laser pulses, including the subtraction of two RF signals going into the two RF ports, was investigated. After that, the performance of a high-speed comparator circuit was evaluated. The comparator circuit was implemented using high-speed analog components capable of supporting data rates of up to 50 Gbps. The comparator components have to be tested individually and then integrated to ensure that they are able to amplitude analyze the modulated laser pulses using their respective matching threshold values. Lastly, the performance of the ring resonator, which was fabricated by the University of California Santa Barbara, was investigated. The ring resonator functions as an accumulator in the photonic ADC.

In addition, a MATLAB simulation designed previously was used to simulate the behavior of the photonic sigma delta ADC. It was modified to speed up the simulation time and incorporate actual hardware parameters, including the time and amplitude jitter of the mode-locked laser. These laser parameters were characterized using a high-speed sampling oscilloscope. Thus, it was possible to predict the performance of the ADC under adverse effects as well as to show how the various electrical and optical signals appear at different parts of the circuit, which greatly adds to the efficiency of the integration process.



THIS PAGE INTENTIONALLY LEFT BLANK

## TABLE OF CONTENTS

<b>I.</b>	<b>INTRODUCTION.....</b>	<b>1</b>
	<b>A. ELECTRONIC SIGMA DELTA ADC.....</b>	<b>1</b>
	<b>B. PHOTONIC SIGMA DELTA ADC.....</b>	<b>2</b>
	<b>C. PREVIOUS WORK.....</b>	<b>3</b>
	<b>D. PRINCIPAL CONTRIBUTIONS .....</b>	<b>3</b>
	<b>E. THESIS OUTLINE.....</b>	<b>4</b>
<b>II.</b>	<b>FIRST-ORDER SIGMA DELTA ADC .....</b>	<b>5</b>
	<b>A. INTRODUCTION.....</b>	<b>5</b>
	<b>B. FIRST-ORDER SIGMA DELTA MODULATOR.....</b>	<b>5</b>
	<b>1. Oversampling .....</b>	<b>6</b>
	<b>2. Accumulator .....</b>	<b>7</b>
	<b>3. Comparator .....</b>	<b>7</b>
	<b>4. Decimation Filter .....</b>	<b>8</b>
	<b>5. Signal-to-Noise Analysis .....</b>	<b>8</b>
	<b>6. Noise Floor of the ADC.....</b>	<b>9</b>
	<b>C. SUMMARY .....</b>	<b>10</b>
<b>III.</b>	<b>PHOTONIC FIRST-ORDER SINGLE-BIT SIGMA DELTA ADC .....</b>	<b>11</b>
	<b>A. PHOTONIC SIGMA DELTA ADC DEVELOPMENT .....</b>	<b>11</b>
	<b>B. PHOTONIC SIGMA DELTA ADC DESIGN .....</b>	<b>11</b>
	<b>1. 10 GHz Signal Generator .....</b>	<b>11</b>
	<b>2. Mode-Locked Laser .....</b>	<b>12</b>
	<b>3. Mach-Zehnder Interferometers (MZI).....</b>	<b>14</b>
	<i>a. Direction MZI .....</i>	<i>16</i>
	<i>b. Magnitude MZI.....</i>	<i>18</i>
	<b>4. Fiber Optic Delay Line .....</b>	<b>19</b>
	<b>5. Photodetector.....</b>	<b>20</b>
	<b>6. Ring Resonator.....</b>	<b>20</b>
	<b>7. High-Speed Comparator .....</b>	<b>22</b>
	<b>8. Decimation Filter .....</b>	<b>25</b>
	<b>C. SUMMARY .....</b>	<b>26</b>
<b>IV.</b>	<b>PERFORMANCE EVALUATION AND RESULT ANALYSIS .....</b>	<b>27</b>
	<b>A. RMS TIMING JITTER ANALYSIS .....</b>	<b>27</b>
	<b>1. 10 GHz Synthesizer.....</b>	<b>30</b>
	<b>2. Mode-Locked Laser .....</b>	<b>32</b>
	<b>3. Timing Jitter Comparison Between Synthesizer and MLL.....</b>	<b>34</b>
	<b>B. AMPLITUDE JITTER ANALYSIS .....</b>	<b>34</b>
	<b>C. MZI RF SIGNAL SUBTRACTION.....</b>	<b>36</b>
	<b>D. HIGH-SPEED COMPARATOR ANALYSIS.....</b>	<b>37</b>
	<b>E. SUMMARY .....</b>	<b>39</b>
<b>V.</b>	<b>MATLAB SIMULATION.....</b>	<b>41</b>

A.	SOFTWARE STRUCTURE .....	41
B.	SIMULATION RESULTS .....	42
C.	COMPARISON OF HARDWARE AND SIMULATION RESULTS .....	46
D.	NOISE FLOOR EVALUATION USING SIMULATION MODELS .....	47
1.	No Jitter ( $f_0$ Varies) .....	48
2.	No Jitter (Record Length Varies) .....	52
3.	Timing Jitter .....	55
4.	Amplitude Jitter .....	58
E.	SUMMARY .....	61
VI.	CONCLUSIONS AND RECOMMENDATIONS .....	63
A.	CONCLUSIONS .....	63
B.	FURTHER IMPROVEMENTS .....	64
1.	Hardware .....	64
2.	MATLAB Simulation .....	64
	APPENDIX A. PHOTONIC SIGMA DELTA ADC FLOW CHART .....	65
	APPENDIX B. MATLAB CODE FOR PHOTONIC SIGMA DELTA ADC .....	67
	APPENDIX C. SUBROUTINE FUNCTIONS .....	73
	APPENDIX D. NOISE FLOW ANALYSIS FLOW CHART .....	79
	APPENDIX E. MATLAB CODE NOISE FLOOR CALCULATION .....	81
	LIST OF REFERENCES .....	89
	INITIAL DISTRIBUTION LIST .....	91

## LIST OF FIGURES

Figure 1.	Block Diagram of a first-order single-bit Sigma delta ADC (From [2]).	5
Figure 2.	Block diagram of first-order sampled data noise model.	8
Figure 3.	Process for examining the noise floor of ADC [From 6].	10
Figure 4.	Block diagram of photonic sigma delta ADC.	12
Figure 5.	Mode-locked laser block diagram (From [10]).	13
Figure 6.	Discrete laser pulse-repetition rate point (From [10]).	14
Figure 7.	Schematic diagram of a transverse LiNbO <sub>3</sub> dual-port MZI (From [2]).	15
Figure 8.	Normalized MZI transmissivity as function of applied voltage $v(t)$ for (a) direction MZI and (b) magnitude MZI (From [4]).	17
Figure 9.	Direction MZI with an applied voltage of a saw tooth function.	18
Figure 10.	Magnitude MZI with an applied voltage of a saw tooth function.	19
Figure 11.	Ring resonator block diagram (From [9]).	20
Figure 12.	Actual ring resonator before waveguide etching (From [9]).	21
Figure 13.	Magnified view of the total internal reflection mirror (From [9]).	22
Figure 14.	High-speed comparator block diagram.	23
Figure 15.	D Flip-flop with (a) clock signal thresholding (b) DC voltage thresholding.	24
Figure 16.	Signal Inverting XOR connection.	24
Figure 17.	Timing jitter in the time domain.	27
Figure 18.	Phase noise in frequency domain (a) ideal sine wave (b) sine wave with timing jitter.	28
Figure 19.	Timing jitter measurement setup (a) time domain (b) frequency domain.	29
Figure 20.	10 GHz clock signal.	30
Figure 21.	Magnified 10 GHz clock signal.	31
Figure 22.	Synthesizer timing jitter versus normal distribution.	32
Figure 23.	Single laser pulse from MLL.	33
Figure 24.	Histogram method of calculating timing jitter.	33
Figure 25.	MLL timing jitter distribution versus normal distribution.	34
Figure 26.	Amplitude jitter measurement.	35
Figure 27.	Amplitude jitter distribution versus normal distribution.	35
Figure 28.	MZI signal subtraction setup.	36
Figure 29.	Display of output waveforms on the oscilloscope.	37
Figure 30.	Comparator Output.	38
Figure 31.	Modulated signals and converted ADC output of a 40 kHz signal.	39
Figure 32.	Simulated Gaussian laser pulse.	43
Figure 33.	Variation of timing and amplitude for pulse to pulse (From [14]).	44
Figure 34.	Simulation output results.	45
Figure 35.	Two-stage decimation filter output.	46
Figure 36.	Results comparison (a) actual comparator and (b) simulation.	47
Figure 37.	Magnitude spectrum for $OSR=100$ with different $f_{RF}$ and no jitter (From [14]).	49
Figure 38.	Magnitude spectrum for $OSR = 10$ , $f_{RF} = 0.13333$ Hz and no jitter.	50

Figure 39.	Plot of OSR versus noise floor for different $f_{RF}$ with no jitter.....	51
Figure 40.	Magnitude spectrum for $OSR = 10$ with different NFFT and no jitter.....	53
Figure 41.	Plot of OSR versus noise floor for different NFFT with no jitter.....	54
Figure 42.	Magnitude spectrum for OSR 10 with timing jitter SD = 0.001 s.....	55
Figure 43.	Magnitude spectrum for OSR 10 with timing jitter.....	56
Figure 44.	Timing jitter noise floor comparison with different $\sigma_t$ .....	57
Figure 45.	Dominant timing jitter test.....	58
Figure 46.	Magnitude spectrum of OSR 20 with different $\sigma_a$ .....	60
Figure 47.	Amplitude jitter noise floor comparison with different $\sigma_a$ .....	60

## LIST OF TABLES

Table 1.	$V_{OA}$ and differential $V_{PP}$ relationship (From [11]).	25
Table 2.	$V_{EC}$ and eye cross percentage relationship (From [11]).	25
Table 3.	Main Parameters for MATLAB simulation.	43
Table 4.	Parameters for noise floor simulation.	48
Table 5.	Noise floor results (dB) with different $f_{RF}$ and no jitter.	50
Table 6.	Parameters for noise floor simulation.	52
Table 7.	Noise floor results (dB) with different NFFT and no jitter.	54
Table 8.	Timing jitter noise (dB) floor results with different $\sigma_t$ .	57
Table 9.	Amplitude jitter noise (dB) floor results with different $\sigma_a$ .	59

THIS PAGE INTENTIONALLY LEFT BLANK

## EXECUTIVE SUMMARY

With the advance of technology, the world is moving from the analog to the digital domain. Since real world signals are analog, there is a need to convert analog signals into the digital domain using analog-to-digital converters (ADC).

Sigma delta ADCs uses pulse-density modulation to encode high resolution signals into lower resolution signals. This was first proposed in the 1960s. However, due to the requirement for a sampling rate that is much higher than the Nyquist rate and the lack of technology available, it was not a practical method to implement. In addition, the digital filters that were required to implement the decimation filter in the sigma delta ADC were very expensive. It was only with the advances in low-cost CMOS processes that could efficiently produce the needed digital integrated circuits that these forms of ADCs came into widespread use. The most common application of the sigma delta ADC can be found in CD players. The bandwidth requirement for a CD player is in the audio range, which is typically below 24 kHz. Thus, even with an oversampling frequency that is much higher than the Nyquist rate, it can easily be implemented with a CMOS sigma delta architecture.

Sigma delta modulators employ oversampling, integration and feedback in iterative loops to obtain a high-resolution representation of the input signal. They digitize the signal through the use of a coarse quantizer, which causes the output to rapidly oscillate between the quantized levels so that its average value over the Nyquist band is an accurate representation of the sampled input signal. The use of a coarse quantizer introduces a large quantization noise; however, the noise is subtracted from the subsequent samples through the use of a feedback loop and an integrator. This has the effect of spreading out the quantization noise over the sampling frequency, which is much higher than the Nyquist frequency. Decimation filtering is then used to attenuate the out-of-band quantization noise, resulting in a high resolution representation of the signal. The decimation also downsamples the signal to the Nyquist band. The price of attaining a high resolution is that the speed of the hardware has to operate at a large oversampling rate much greater than Nyquist rate. In addition, there is an increase in the



complexity of the digital hardware used in the implementation of decimation filtering. The requirement of a large oversampling frequency is the major limitation in the application of the all-electronic sigma delta ADC to higher bandwidth signals.

For the photonic sigma delta approach, however, a very high sampling frequency can be achieved by using pulses from high pulse-repetition frequency mode-locked lasers. Consequently, there is an increase in the signal bandwidth over an all-electronic implementation (audio range) as the carrier medium is a lightwave pulse rather than an electrical current. Thus, the frequency limiting effects of capacitance and inductance can be avoided.

At the heart of the photonic sigma delta architecture are two wideband dual-ported Mach-Zehnder interferometers (MZI). One MZI, known as the direction MZI, is used to detect the polarity of the input RF signal, while the other, the magnitude MZI, is used to determine the magnitude of RF signal. The RF signal is sampled at these MZIs using high-speed narrow laser pulses from a mode-locked laser. The second RF port of the MZIs is used for implementing the subtraction feedback loop. The block diagram of the photonic sigma delta ADC is shown in Figure 1.

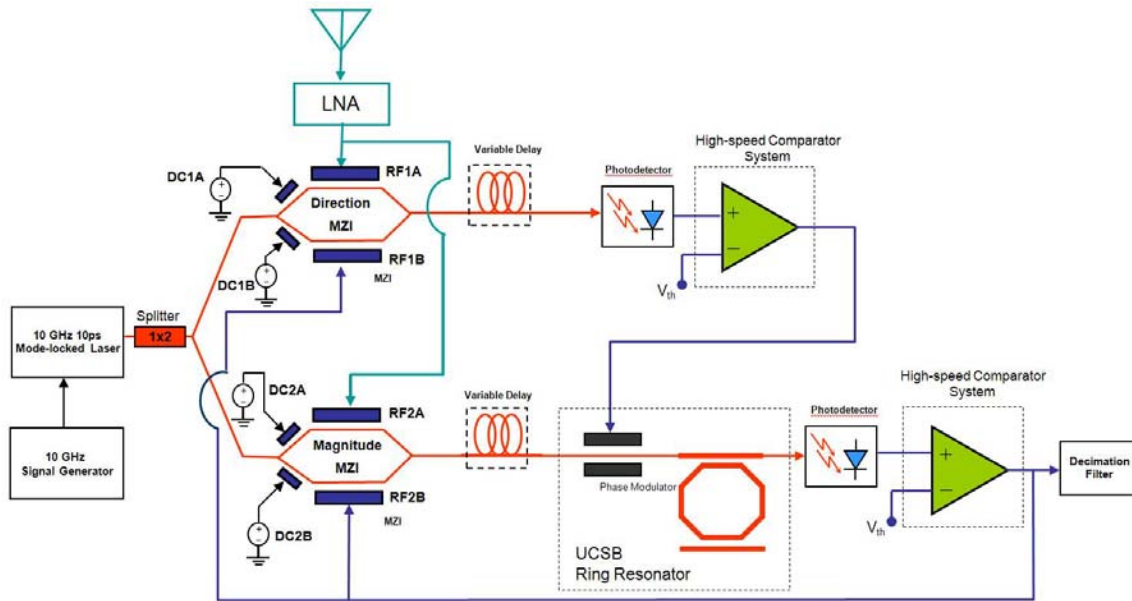


Figure 1. Block diagram of photonic sigma delta ADC.

A photodetector is used at the output of each interferometer to convert the optical signal into an electrical signal. These electrical signals are then passed into two high-speed comparator systems. The output from the comparator for the direction MZI is used to drive the phase modulator within a ring resonator for coherent accumulation of the amplitude modulated laser pulses. The samples from the second comparator (limit cycles) are the modulator's output. The limit cycles are processed by a decimation filter to realize a high resolution representation of the input signal. The limit cycles are also used to drive the second RF port on both MZIs for feedback subtraction.

The integration of photonic and electronic components to realize a photonic sigma delta ADC is the focus of this thesis. The integration process was broken up into steps. First, the performance of a pair of dual-port Mach-Zehnder interferometers (MZI) modulating a train of narrow high-speed laser pulses from a mode-locked laser was investigated. Various parameters, like the half-wave voltage ( $V_{\pi}$ ) and insertion loss, were verified. Next, the ability of the MZIs to modulate the laser pulses, including the subtraction of two RF signals going into the two RF port, was investigated. After that, the performance of a high-speed comparator circuit was evaluated. The comparator circuit was implemented using high-speed analog components capable of supporting data rates of up to 50 Gbps. The comparator components have to be tested individually and then integrated to ensure that they are able to amplitude analyze the modulated laser pulses using their respective matching threshold values. Lastly, the performance of the ring resonator, which was fabricated by the University of California Santa Barbara, was investigated. The ring resonator functions as an accumulator in the photonic ADC.

In addition, a MATLAB simulation designed previously was used to simulate the behavior of the photonic sigma delta ADC. It was modified to speed up the simulation time and incorporate actual hardware parameters including the time and amplitude jitter of the mode-locked laser. These laser parameters were characterized using a high-speed sampling oscilloscope. Thus, it was possible to predict the performance of the ADC under adverse effects, as well as to show how the various electrical and optical signals appear at different parts of the circuit, which greatly adds to the efficiency of the integration process.

THIS PAGE INTENTIONALLY LEFT BLANK

## **ACKNOWLEDGMENTS**

I would like to thank my advisor, Professor Phillip E. Pace, for encouraging me take the challenge of implementing and proving the feasibility of this research. I have learned many interesting concepts while working on this thesis.

To Professor David C. Jenn, thank you for your guidance and patience as I progressed with my research. Your valuable experience and knowledge gave me direction during the early stages of this research.

To Mr. James Calusdian, I humbly thank you for providing much of your knowledge about this research and for helping me integrate various parts of this system.

This work was supported by the Office of Naval Research, Code 31, Washington, DC.

THIS PAGE INTENTIONALLY LEFT BLANK

# I. INTRODUCTION

## A. ELECTRONIC SIGMA DELTA ADC

With the advance of technology, the world is moving from the analog to the digital domain. Since real world signals are analog, there is a need to convert analog signals into the digital domain using analog-to-digital converters (ADC).

Sigma delta ADC uses pulse-density modulation to encode high resolution signals into lower resolution signals and was first proposed in the 1960s. However, due to the requirement for a sampling rate that is much higher than the Nyquist rate and the lack of technology available, it was not practical to implement. In addition, the digital filters that were required to implement the decimation filter in the sigma delta ADC were very expensive. It was only with advances in low-cost CMOS processes that could efficiently produce the needed digital integrated circuits that these forms of ADCs could come into widespread use. The most common application of the sigma delta ADC is found in CD players. The bandwidth requirement for a CD player is in the audio range, which is typically below 24 kHz. Thus, even with an oversampling frequency that is much greater than the Nyquist rate, it can be easily implemented with a CMOS sigma delta architecture.

Sigma delta modulators employ oversampling, integration and feedback in iterative loops to obtain a high-resolution representation of the input signal. The signal is digitized through the use of a coarse quantizer, which causes the output to rapidly oscillate between the quantized levels so that its average value over the Nyquist band is an accurate representation of the sampled input signal. The use of a coarse quantizer introduces a large quantization noise; however, the noise is subtracted from the subsequent samples through the use of a feedback loop and an integrator. This has the effect of spreading out the quantization noise over the sampling frequency, which is much higher than the Nyquist frequency. Decimation filtering is then used to attenuate the out-of-band quantization noise, resulting in a high resolution representation of the signal. The decimation process also downsamples the signal to the Nyquist band. The

price of attaining a high resolution is that the speed of the hardware has to operate at a large oversampling rate much higher than Nyquist rate. In addition, there is an increase in the complexity of the digital hardware used in the implementation of the decimation filtering. The requirement of a large oversampling frequency is the major limitation in the application of the all-electronic sigma delta ADC to higher bandwidth signals.

For the photonic sigma delta approach, however, a very high sampling frequency can be achieved by using pulses from high pulse-repetition frequency mode-locked lasers. Consequently, there is an increase in the signal bandwidth over an all-electronic implementation (audio range) as the carrier medium is a lightwave pulse rather than an electrical current. Thus, the frequency limiting effects of capacitance and inductance can be avoided.

## **B. PHOTONIC SIGMA DELTA ADC**

The implementation of a first-order photonic sigma delta ADC was constructed by integrating commercially available photonic and electronic components. The differences between the all-electronic sigma delta and the photonic sigma delta are the use of optical components for oversampling, subtraction and accumulation.

The architecture uses two wideband dual-port Mach-Zehnder interferometers (MZI) to efficiently couple the radio frequency (RF) signal from the antenna into the optical domain. One MZI, known as the direction MZI, is used to detect the polarity of the input RF signal, while the other, the magnitude MZI, is used to determine the magnitude of RF signal. The RF signal is oversampled at these two MZIs using high-speed narrow laser pulses from a mode-locked laser. The second RF port of the MZIs is used for implementing the subtraction within the feedback loop.

A photodetector is used at the output of each interferometer to convert the optical signal into an electrical signal. These electrical signals are then passed into two high-speed comparator systems. The output from the comparator for the direction MZI is used to drive the phase modulator within the ring resonator for coherent accumulation of the amplitude modulated laser pulses. The samples from the second comparator are the modulator limit cycles. The limit cycles are processed by a decimation filter to realize a

high resolution representation of the input signal [1]. The limit cycles are also used to drive the second RF port on both MZIs for the feedback subtraction.

### **C. PREVIOUS WORK**

A photonic sigma delta ADC was first simulated using MATLAB to provide insight into the performance of the ADC. However, due to computer limitations, certain parameters like the pulse-repetition frequency of the laser pulses and the laser frequency had to be downscaled so that the simulation of a coherent model would be possible [2].

A mode-locked laser was built in hardware to be used as source for sampling RF signals at an MZI. It was shown that an amplitude-analyzing ADC can achieve six bits of resolution when the laser PRF is limited to sampling an 8 GHz signal [3]. Unfortunately, the piezo-electric transducer designed to keep the laser cavity tuned was not stable and the laser had problems keeping the mode locked. The line width of the laser was also not narrow enough to allow coherent integration within the accumulator design, which was based on a fiber-lattice built from discrete components [2, 4].

### **D. PRINCIPAL CONTRIBUTIONS**

The integration of photonic and electronic components to realize a photonic sigma delta ADC is the focus of this thesis. The integration process was broken up into steps. First, the performance of a pair of dual-port Mach-Zehnder interferometers (MZI) modulating a train of narrow high-speed laser pulses from a mode-locked laser was investigated. Various parameters, like the half-wave voltage ( $V_\pi$ ) and insertion loss, were verified. Next, the ability of the MZIs to modulate the laser pulses, including the subtraction of two RF signals going into the two RF port, was investigated. After that, the performance of a high-speed comparator circuit was evaluated. The comparator circuit was implemented using high-speed analog components capable of supporting data rates of up to 50 Gbps. The comparator components have to be tested individually and then integrated to ensure that they are able to amplitude analyze the modulated laser pulses using their respective matching threshold values. Lastly, the performance of the ring resonator, which was fabricated by the University of California Santa Barbara, was investigated. The ring resonator functions as an accumulator in the photonic ADC.



A MATLAB simulation designed previously was modified to simulate the behavior of the photonic sigma delta ADC. It was modified to speed up the simulation time and incorporate actual hardware parameters, including the time and amplitude jitter of the mode-locked laser. The laser's jitter parameters were determined by using a high-speed sampling oscilloscope. By incorporating these measured parameters of the laser into the simulation, the performance of the ADC could be predicted. In addition, the effects of the various electrical and optical signals and how they propagate through the circuit were investigated.

## **E. THESIS OUTLINE**

The sigma delta modulator theory and its application in analog-to-digital conversion is explained in Chapter II.

The photonic ADC architecture was designed and how actual hardware is integrated is described in Chapter III.

The performance of the hardware components of the photonic ADC is evaluated in Chapter IV.

How the MATLAB simulation works and an analysis of the simulation is described in Chapter V.

Lastly, the conclusions and recommendation for future research is discussed in Chapter VI.

## II. FIRST-ORDER SIGMA DELTA ADC

### A. INTRODUCTION

Sigma delta ADCs uses pulse-density modulation to encode high resolution signals into lower resolution signals. It was first proposed in the 1960s. However, due to the requirement for sampling rate that is much higher than Nyquist rate and the technology available then, it was not a practical method to implement. It is a widely used ADC now due to the advance of low cost CMOS fabrication process. However, the applications are mostly in digitization of signals in the audio range due to the oversampling requirements.

### B. FIRST-ORDER SIGMA DELTA MODULATOR

A block diagram of a first-order, single-bit sigma delta modulator is shown in Figure 1. It consists of an accumulator embedded within a feedback loop around a quantizer. The oversampled input signal is first subtracted from the comparator output, and the result is then processed by the accumulator. The output of the accumulator, or limit cycles, are processed by a decimation filter to realize the high resolution representation of the input signal sampled at the Nyquist frequency.

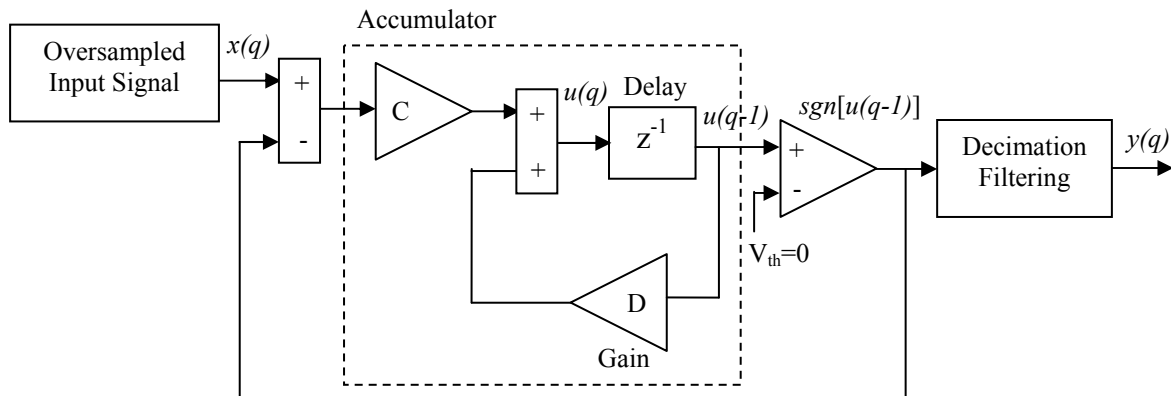


Figure 1. Block Diagram of a first-order single-bit Sigma delta ADC (From [2]).

## 1. Oversampling

Analog-to-digital conversion can be split into two separate operations, uniform sampling in time and amplitude quantization. The process of sampling involves taking a continuous time signal and turning it into a discrete time signal that is uniformly spaced in time. In the frequency domain, this is equivalent to creating a periodically repeated version of the signal spectrum at multiples of the sampling frequency.

Sampling is done using a sample-and-hold circuit which captures the input voltage at a specific time interval and saves this voltage for a specific amount of time. This process repeats at specified time interval. The sample-and-hold circuit functions as an analog memory device.

From the Nyquist theorem, the minimum sampling frequency must be greater than two times the signal bandwidth so that the repeated signal spectrum does not overlap and cause distortion through aliasing.

In the case of a sigma delta ADC, the sampling frequency is much larger than the Nyquist frequency and is defined as the oversampling ratio (OSR), given by

$$OSR = \frac{f_s}{2f_o} = \frac{\text{sampling frequency}}{\text{Nyquist frequency}} \quad (2.1)$$

where  $f_o$  is the signal bandwidth and  $f_s$  is the sampling frequency. Oversampling actually reduces noise in the signal band by spreading it over the sampling frequency, which is much larger than the signal band.

The timing and amplitude jitter of the sample-and-hold circuit greatly affects the performance of the ADC. Timing jitter (sample time uncertainty) causes the sampling period to change from sample to sample. This causes the incorrect input voltage to be captured, which distorts the sampled signal and, hence, the output of the ADC. Amplitude jitter is the variation in output voltage over time for the same input voltage. Likewise, this distorts the sampled signal and affects the output of the ADC. It is a challenge to limit time and amplitude jitter to a minimum acceptable level in high-speed sample-and-hold circuits.

## 2. Accumulator

The accumulator shown in Figure 1 consists of a single delay, a feedback loop and two amplifiers. The input of the accumulator is the difference between the quantizer/comparator output and the oversampled input signal. The feedback loop and the delay act as an accumulator/integrator. In Figure 1, the delay is in the feed forward path. It can also be in the feedback path. The difference between the two configurations is accumulation rate. The feed forward path configuration accumulates faster than the feedback path one. The difference equation describing the first-order modulator is

$$u(q+1) = Du(q) + C \{x(q) - \text{sgn}[u(q)]\} \quad (2.2)$$

where  $x(q)$  is the oversampled input signal,  $C$  is a multiplying factor,  $D$  is the accumulator leakage coefficient, and

$$\text{sgn}[x] = \begin{cases} 1 & \text{for } x \geq 0, \\ 0 & \text{for } x < 0. \end{cases} \quad (2.3)$$

The transfer function for the accumulator is

$$H = \frac{Cz^{-1}}{1 - Dz^{-1}} \quad (2.4)$$

where  $z^{-1}$  is the delay operation. The DC gain of the accumulator is given by

$$H_0 = \frac{1}{1 - D}. \quad (2.5)$$

If the accumulator is ideal, then  $D=1$  (i.e., no leakage),  $H_0 \rightarrow \infty$ , and the feedback connection forces the average value of the comparator output to equal the DC input.

## 3. Comparator

The output of the accumulator is fed into the comparator. When the accumulator output reaches a specified threshold, the comparator outputs a positive voltage which is subtracted from the oversampled input signal. If the accumulator error is lower than the specified threshold, then its output is a negative voltage which is added to the

oversampled input signal. Thus, it can be seen as a single bit quantizer. The output of the comparator is fed back to the subtraction device in front of the accumulator.

#### 4. Decimation Filter

The output of the comparator is then processed by the decimation filter, which attenuates the out-of-band noise, thus, preventing the aliasing of the out-of-band signal into the passband. In addition, the output signal is downsampled to the Nyquist rate. The filter is usually separated into several stages, so that the filter requirements can be relaxed [2].

#### 5. Signal-to-Noise Analysis

Since the comparator is a nonlinear element, the signal-to-noise analysis cannot be based on linear systems theory. Many approaches to the analysis have been reported [5]. A sampled data noise model can be used to simplify the analysis. The quantizer is modeled as white noise. The noise-shaping filter is also replaced by the sampled data equivalent  $H(z)$ . The corresponding first-order sampled data noise model is shown in Figure 2. This results in a linearized system. However, due to the oscillating nature at the ADC output, the quantization noise is not white but contains periodic elements in it. Hence, this model is only able to give a close estimate of the signal-to-noise relationship of the ADC.

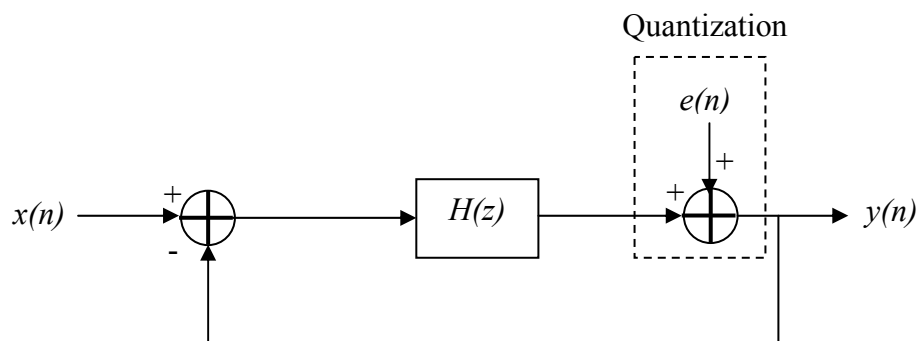


Figure 2. Block diagram of first-order sampled data noise model.

The noise power is given by [6]

$$n_o^2 = \frac{8\pi^2}{3} e_q^2 \left( \frac{f_o}{f_s} \right)^3 \quad (2.6)$$

$$n_o = \frac{\pi}{\sqrt{3}} e_q (OSR)^{-3/2}$$

where  $e_q$  is the variance or power of the quantization noise. This result shows that for every doubling of OSR the noise power is reduced by 9 dB or, in terms of bit resolution, there is an improvement of 1.5 bits. The SNR of the first-order, single-bit sigma delta ADC is given by [6]

$$SNR = 2^{n-1} \sqrt{\left( \frac{18OSR^3}{\pi^2} \right)} \quad (2.7)$$

where  $n$  is the bit resolution of the ADC. The SNR in term of dB is given by [6]

$$SNR = 6.02n - 3.41 + 30 \log(OSR) \text{ (dB)}. \quad (2.8)$$

The SNR in terms of signal and noise power as well as OSR can also be given as [1]

$$SNR = 10 \log(\sigma_x^2) - 10 \log(\sigma_e^2) - 10 \log\left(\frac{\pi^2}{3}\right) + 30 \log(OSR) \text{ (dB)} \quad (2.9)$$

where  $\sigma_x^2$  is the input signal power.

## 6. Noise Floor of the ADC

The dynamic range of an ADC can be determined by examining the noise floor of the DFT output of the ADC. In order to determine the noise floor, spectral averaging must be performed by repeatedly acquiring the digitized signal asynchronously and calculating the DFT for each signal set. The magnitude response of the DFT is averaged over a certain number of runs. The noise floor is dependent on the amount of jitter and thermal noise present. Quantization noise and any other harmonics generated are also present [6]. First, the signal is applied to the ADC, which adds the quantization noise  $\gamma_k$ . The output is then windowed with  $\omega_k$ , and the magnitude is calculated with the DFT.

Point by point spectral averaging is then carried out to obtain the noise floor harmonics. The process for examining the noise floor of the ADC is shown in Figure 3.

In this thesis, the computer simulation results are used to evaluate the noise floor of the photonic sigma delta ADC. The noise floor is evaluated for an OSR ranging from 10 to 100. Simulation results for OSR 10 to 100 are generated so that the noise floor can be determined.

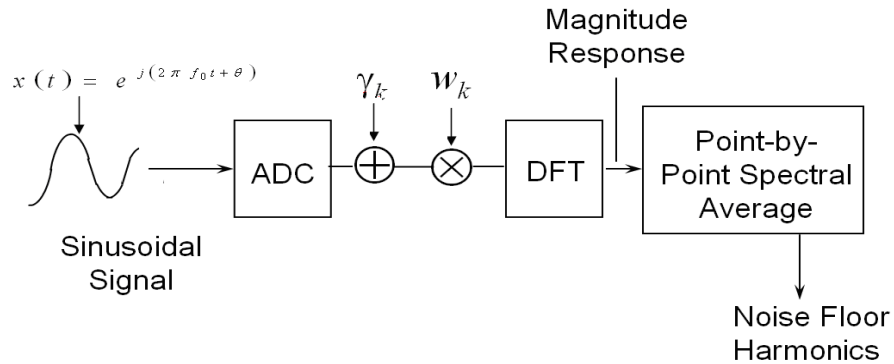


Figure 3. Process for examining the noise floor of ADC [From 6].

### C. SUMMARY

In this chapter, the electronic first-order sigma delta ADC was explained in detail. The ADC was broken into its major components with the function of each component explained in detail. This is followed by a procedure to calculate the performance in terms of SNR and noise floor. In the next chapter, the photonic sigma delta architecture is described.

### **III. PHOTONIC FIRST-ORDER SINGLE-BIT SIGMA DELTA ADC**

A background on the development efforts of the photonic first-order, single-bit sigma delta ADC is first presented in this chapter. This chapter then explains the implementation of the design as well as the operating characteristics of the components and their limitations on the performance of the ADC are then explained.

#### **A. PHOTONIC SIGMA DELTA ADC DEVELOPMENT**

A first-order, single-bit photonic sigma delta ADC was first demonstrated using MATLAB and SIMULINK in [2] and [4]. Subsequently, there was an effort to realize the design with actual hardware, starting with the development and evaluation of the mode-locked laser that was required to perform the oversampling [3]. The design and fabrication of accumulator was also examined in [4, 7]. The design in both papers was based on a fiber-lattice accumulator. To improve the integration function, a ring resonator design using an embedded phase modulator (for accumulation direction control) and several total internal reflection mirrors was proposed [8]. It was simulated using “RSoft OptSim”, and the development of the ring resonator was done at University of California Santa Barbara [9].

#### **B. PHOTONIC SIGMA DELTA ADC DESIGN**

The block diagram of a photonic first-order sigma delta ADC is shown in Figure 4. Every component in the design is discussed below.

##### **1. 10 GHz Signal Generator**

The 10 GHz signal generator is used to generate a RF drive signal for the mode-locked laser. The pulse-repetition frequency of the mode-locked laser is determined by the frequency of the RF drive signal. Hence, this signal generator determines the oversampling frequency of the ADC. In addition, it also serves as a clocking signal for both high-speed comparators so that threshold comparison can be carried out. An output power of 0 dBm is required by the mode-locked laser to properly lock the mode. In



addition, the power level of this signal generator can also serve as a threshold level for the high-speed comparators. This is explained in greater detail in Section B7. A 4-way power divider is used to split the signal to the mode-locked laser and to the two high-speed comparators.

This signal generator is a source of timing jitter for the ADC as it controls the sampling frequency. The timing jitter of the signal generator is characterized in Chapter IV.

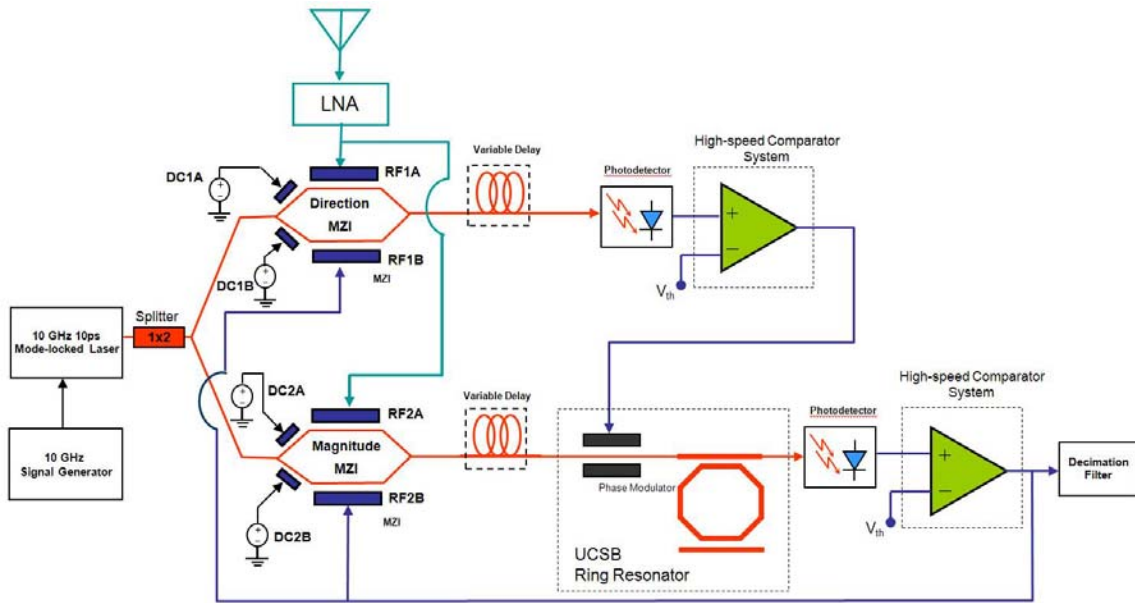


Figure 4. Block diagram of photonic sigma delta ADC.

## 2. Mode-Locked Laser

The sampling in the photonic sigma delta ADC uses narrow laser pulses from the mode-locked laser. The mode-locked laser that was used was manufactured by CALMAR OPTCOM. It produces a laser pulse train at repetition frequency of 5 ~ 11 GHz and pulse width of about 1.5 ~ 10 ps. The wavelength can be adjusted from 1530 nm to 1565 nm. The output power is > 20 mW. In the photonic sigma delta ADC design, the mode-locked laser operates at a PRF of 10 GHz, with a pulse width (full width half maximum) of 10 ps and a wavelength of 1550 nm.

There can be many modes operating within the laser cavity, and the phases between these modes in the frequency domain are often random and incoherent. Therefore, in the time domain, the amplitude of the light coming from the laser will fluctuate as the modes interact constructively and destructively in a random fashion. Techniques exist to force the modes to oscillate coherently and lock them together in phase so that the peak amplitude of these modes oscillating together in phase and combine constructively to form a mode-locked pulse [3].

The mode-locked laser that was used is based on an actively mode-locked fiber laser. The block diagram of the mode-locked laser is shown in Figure 5. The laser cavity of this laser consists of an erbium doped fiber amplifier (EDFA), an output coupler, an electro-optic modulator, a tunable filter and the fiber that connects these devices together. The piezo-electric transducer (PZT) cavity and control adjusts the cavity length to achieve stable mode-locking. The phase locked loop circuit also provides a control voltage to the PZT cavity control to fine tune the laser cavity length to ensure stable operation. The laser cavity has a round trip resonant frequency of  $f_R$  ( $f_R \sim 1.96$  MHz), which depends on cavity length. In order to satisfy the condition of stable mode-locking,  $f_R$  of the laser multiplied by an integer M ( $M \sim 5000$ ) must be matched by the RF drive frequency  $f_D$  precisely.

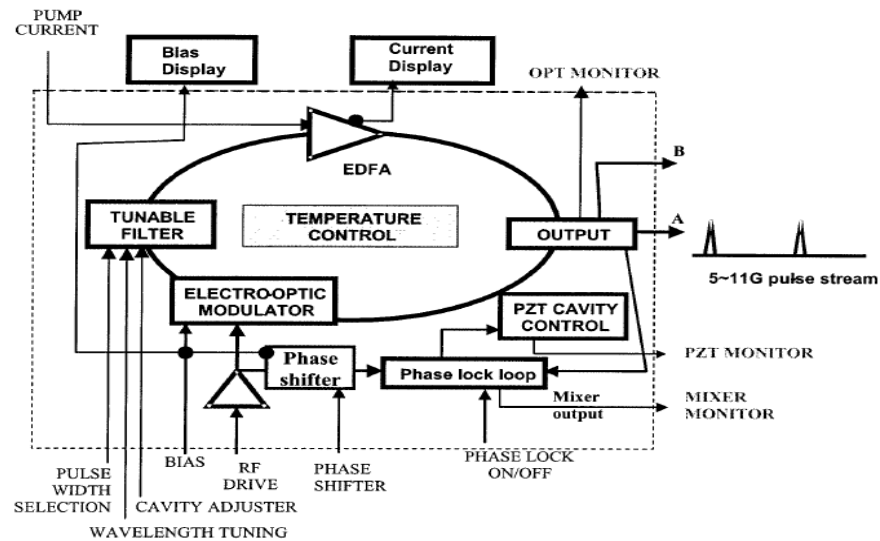


Figure 5. Mode-locked laser block diagram (From [10]).

At constant temperature, the laser can achieve stable mode-locking at discrete (steps of 1.96 MHz) multiple repetition rates according to

$$f_D = M \times f_R \quad M \text{ is an integer} \quad (3.1)$$

since  $M$  can be an arbitrary integer and the cavity length (and resonant frequency  $f_R$ ) can be changed. This is shown in Figure 6. Since cavity length changes about  $1.09 \times 10^5$  m per Celsius, a temperature control system is used so that with a  $\sim 18^\circ\text{C}$  change in temperature, the laser can operate at any frequency point near the 10 GHz range. This is shown by

$$\begin{aligned} \Delta f_D &= -1.09 \times 10^{-5} \times \Delta T \times f_D \\ \Delta f_R &= -1.09 \times 10^{-5} \times \Delta T \times f_R \end{aligned} \quad (3.2)$$

where  $\Delta T$  is the temperature change,  $\Delta f_D$  is the change in pulse-repetition frequency,  $\Delta f_R$  is the change in cavity length frequency [10],  $\Delta T = T - T_o$ ,  $T_o$  is  $18^\circ\text{C}$  and  $T$  is temperature of the cavity.

Timing and amplitude jitter of the mode-locked laser pulses affect the performance of the ADC as the train of pulses is used to oversample the RF signal. Jitter in the laser pulses causes errors in the oversampling results. The timing and amplitude jitter characteristic of the mode-locked laser are characterized and discussed in detail in Chapter IV.

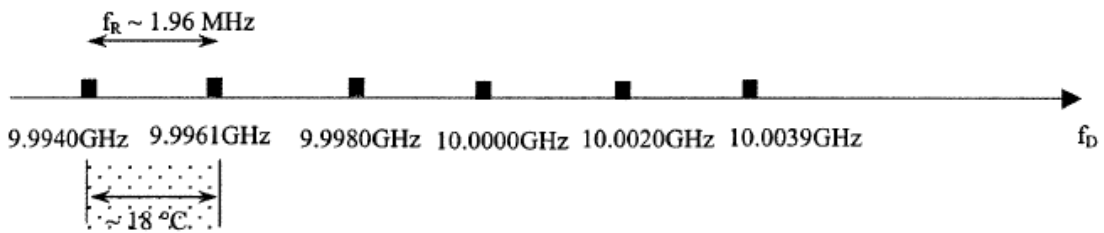


Figure 6. Discrete laser pulse-repetition rate point (From [10]).

### 3. Mach-Zehnder Interferometers (MZI)

The two MZIs are used to convert RF signal into optical signal. Their role is to couple the RF signal efficiently into the optical domain and onto the train of laser pulses

from the mode-locked laser. With the dual-ported MZIs being used, the feedback signal from the output comparator can be subtracted from the RF signal. The schematic diagram of a dual-port MZI is illustrated in Figure 7.

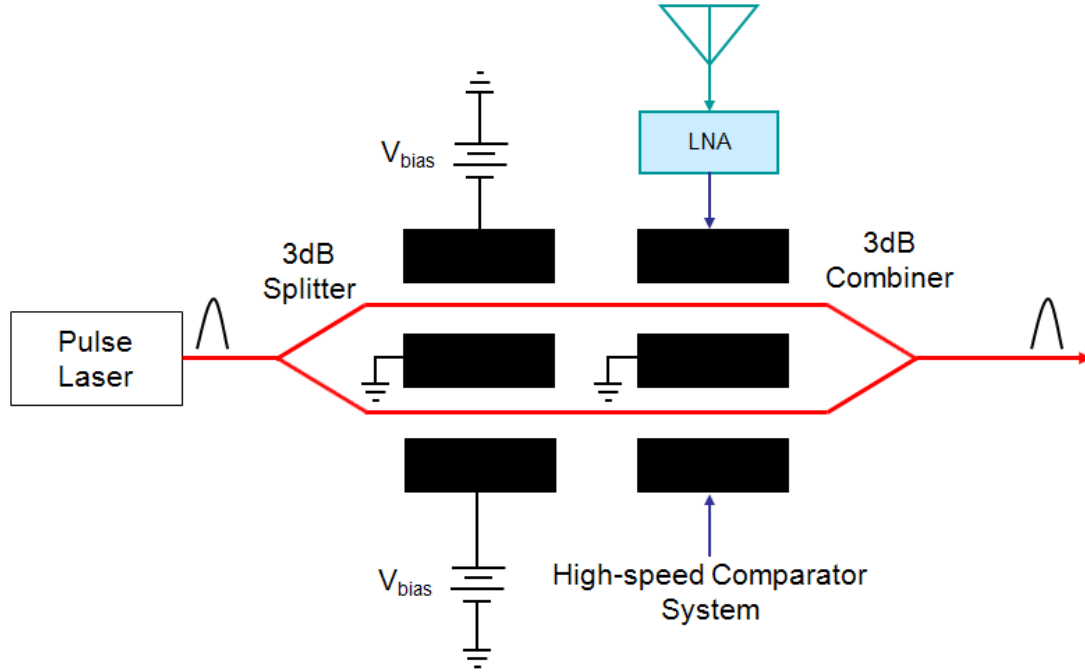


Figure 7. Schematic diagram of a transverse  $\text{LiNbO}_3$  dual-port MZI (From [2]).

Inside the MZI, the input laser pulses are divided by a 3 dB splitter and are fed into two separate optical waveguide arms. The waveguide optical medium is made up of lithium niobate with a higher index of refraction than the substrate due to titanium indiffusion. The applied RF electric field changes the propagation coefficient (or delay) between each MZI arm. One electrode is connected to the RF signal, and one is connected to the feedback signal. Both electrodes form a push-pull configuration. Therefore, the total electrical field generated is the difference between the RF signal and the feedback signal.

When voltage is applied to an electrode, an electric field is generated, which in turn changes the index of reflection of its corresponding optical waveguide. Thus, laser pulses travelling through the optical waveguide experience a change in the propagation coefficient which is proportional to the applied voltage.

The pulses in the two optical waveguides are recombined again at the output of the MZI by a 3 dB combiner. Depending on relative difference of the propagation coefficient between the laser pulses, we see that constructive or destructive interference takes place, either increasing the laser pulse amplitude or decreasing the laser pulse amplitude, respectively. There are also two additional electrodes on the optical waveguides that connect to a DC bias voltage. The DC bias voltage is used to adjust the quadrature point of the interferometer.

The transmissivity function of the MZI, which is the ratio of the output intensity  $I_{out}$  to the input intensity  $I_{in}$  is given by

$$H_{MZI} = \frac{I_{out}}{I_{in}} = \frac{1}{2} + \frac{1}{2} \cos[\Delta\phi(v) + \theta] \quad (3.3)$$

where  $\theta$  is the phase angle that is determined by the DC bias voltage. The phase difference  $\Delta\phi(v)$  between the two optical waveguides depends on the voltage difference  $v(t) = V_{antenna} - V_{feedback}$  and is given by

$$\Delta\phi(v) = \frac{\pi v(t)}{V_{\pi}} \quad (3.4)$$

where the half-wave voltage  $V_{\pi}$  is the voltage required to shift the phase by  $180^{\circ}$ , which (depending on the DC bias) will transition the output intensity from a maximum to a minimum (or vice versa).

#### **a. Direction MZI**

The direction MZI is used to determine the polarity of the applied voltage in order to determine if the magnitude sample is to be integrated up or down. The DC bias voltage is adjusted so that the full swing of  $v(t)$  from positive to negative cycle causes the output intensity to vary from zero to the maximum intensity, with half intensity at  $v(t) = 0$  V as shown in Figure 8(a). After detection, the threshold voltage of the direction comparator is then set to this half intensity level. Thus, depending on the polarity of  $v(t)$ , the direction comparator outputs the corresponding half-wave voltage of

the phase modulator within the ring resonator so that a correct accumulation occurs. The result of the DC bias on the magnitude MZI is illustrated in Figure 8(b). Note that the output intensity is the same and is independent of the applied voltage polarity.

The output of the direction MZI with an applied sawtooth function (upper trace) with a peak-to-peak voltage equal to  $V_\pi$  and the corresponding intensity output (lower trace) are illustrated in Figure 9. The DC bias voltage  $V_{DCbias}$  was adjusted to 18.83 V to achieve the transmissivity characteristics. The optical output of the MZI was converted into an electrical signal using a wideband (45 GHz) photodetector. Due to the bandwidth limit of the oscilloscope the individual 10 ps laser pulses cannot be seen and only the envelope is visible.

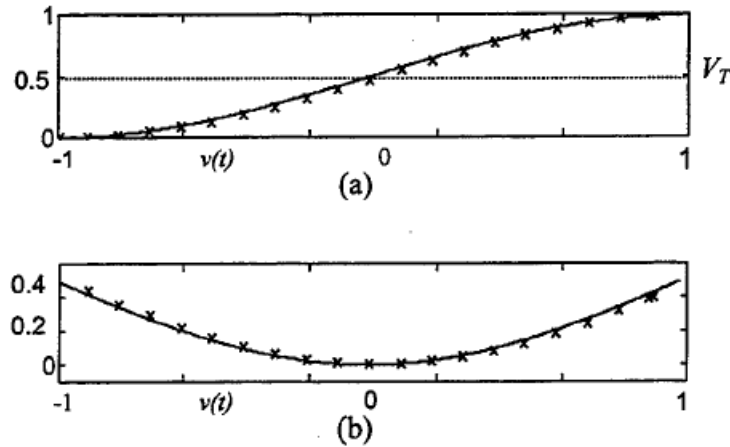


Figure 8. Normalized MZI transmissivity as function of applied voltage  $v(t)$  for (a) direction MZI and (b) magnitude MZI (From [4]).

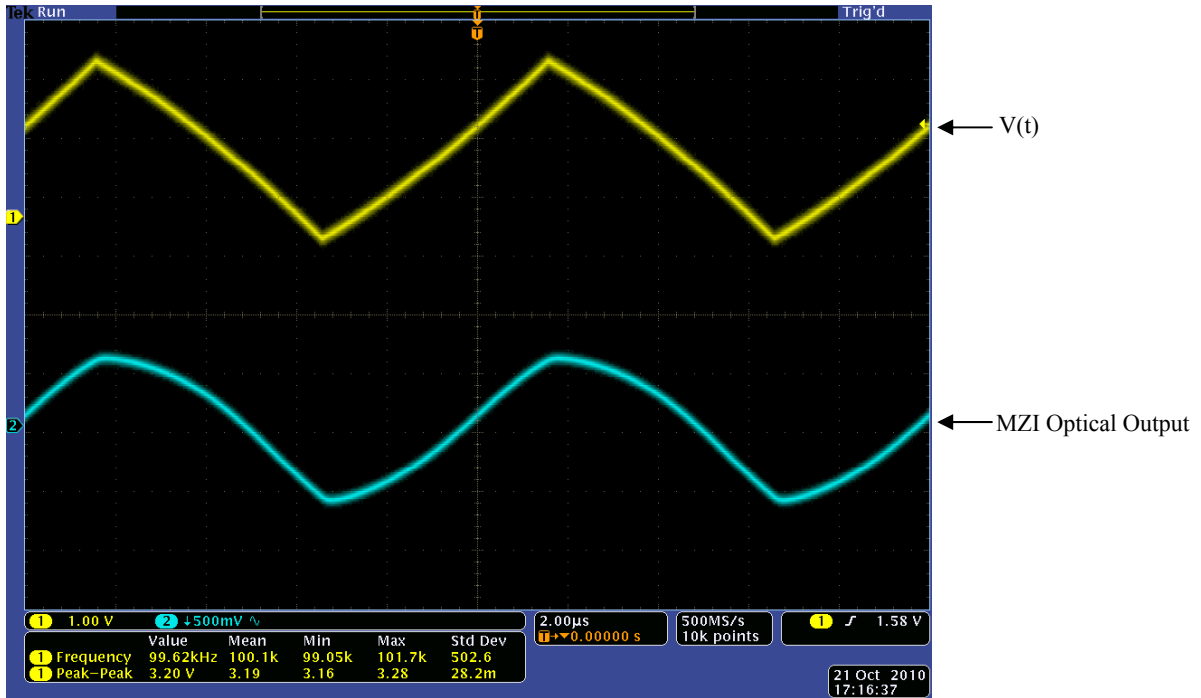


Figure 9. Direction MZI with an applied voltage of a saw tooth function

**b. Magnitude MZI**

The magnitude MZI is used to modulate the magnitude of  $v(t)$ . Therefore, for the full swing of  $v(t)$ , the output intensity varies from zero intensity for  $v(t) = 0$  and half intensity for both maximum and minimum voltage of  $v(t)$ . An actual magnitude MZI with an applied voltage of the same saw tooth function, and its corresponding intensity output is illustrated in Figure 10. The voltage  $V_{DCbias}$  was adjusted to 4.32 V to achieve the transmissivity characteristics.

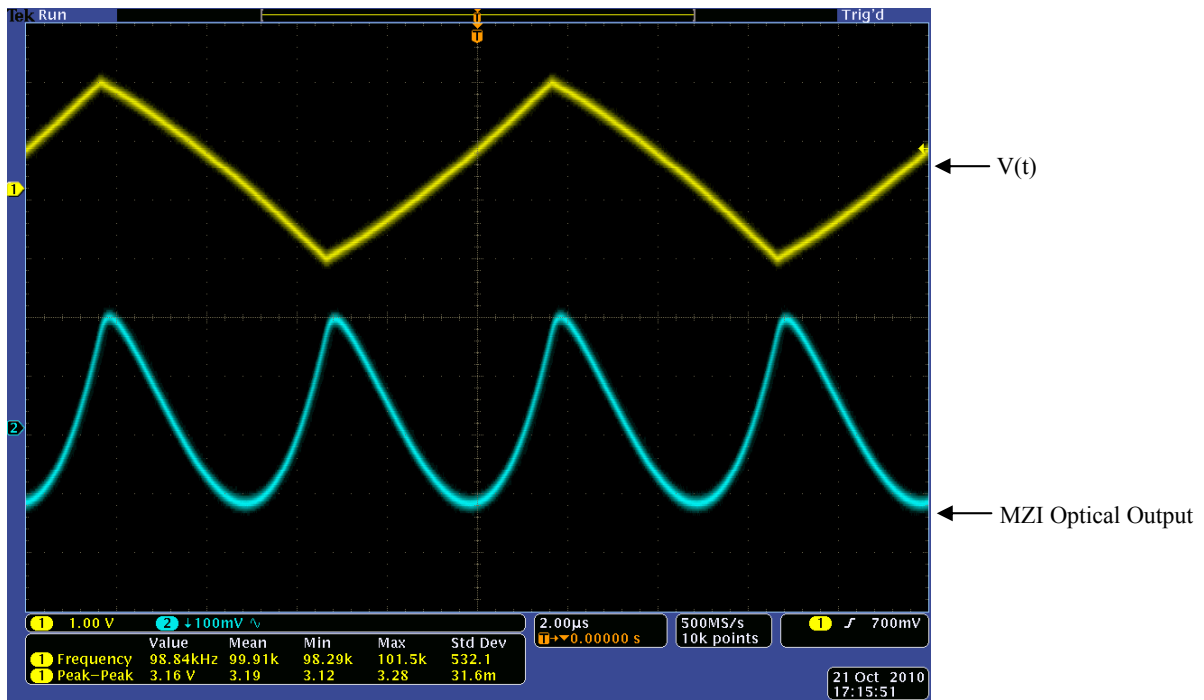


Figure 10. Magnitude MZI with an applied voltage of a saw tooth function.

#### 4. Fiber Optic Delay Line

A fiber optic delay line is used to delay the train of laser pulses at the output of the MZIs. This works by launching the laser pulses into free space using an output collimator and after a certain distance, the laser pulses are collected into the optic fiber again through an input collimator. The amount of time delay is determined by the length of the free space cavity, which is adjustable. The delay line is manufactured by “OZ OPTICS.” The fiber optic delay line used is capable of a maximum of 300 ps delay with a maximum insertion loss of 1.5 dB.

The delay line was necessary because the laser pulses must be synchronized with the clocking signal at the comparators so that proper thresholding can occur. With a PRF of 10 GHz, the distance travel by a laser pulse in a single cycle is about 0.03 m; thus, the time delay needed to synchronize the optical and electrical signal is less 100 ps.



## 5. Photodetector

The photodetectors are used to convert the laser pulses at the output of the direction MZI and the ring resonator into electronic signals. As the pulse width of the laser pulses is 10 ps, an ultra high-speed photodetector is needed so that the laser pulses can be converted into electronic signals without any distortion.

The photodetector used is by “NEW FOCUS”, model 1024. It operates at a wavelength of 950 nm to 1650 nm with a maximum full width at half maximum of 12 ps. The signal conversion is by the Schottky photodiode contained within the detector module.

## 6. Ring Resonator

From the electronic sigma delta modulator discussed in Chapter II, it was seen that the accumulator is composed of a summation device, a feedback loop and two amplifiers. The feedback loop serves as memory storage for the current value of the accumulator and is summed with the new values. The development and fabrication of the ring resonator is undertaken by Professor Nadir Dagli and Byungchae Kim at the University of California Santa Barbara. The block diagram of the ring resonator [9] is illustrated in Figure 11.

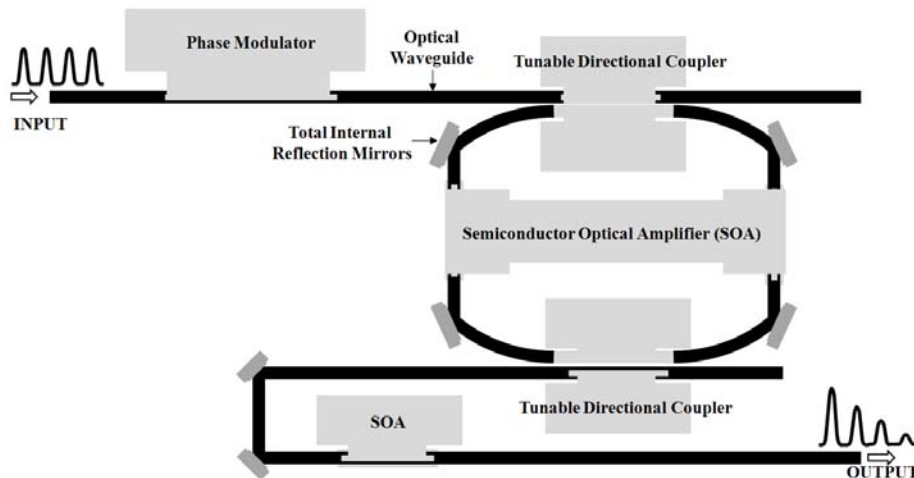


Figure 11. Ring resonator block diagram (From [9]).

The ring resonator is fabricated using optical waveguides, total internal reflection mirrors, phase modulator, semiconductor optical amplifiers and directional coupler on an *indium gallium arsenide phosphide / indium phosphide* (InGaAsP/InP) wafer. The technique can reduce the size of the ring resonator tremendously compared with the fiber-lattice design in [2]. The magnified photo of the actual ring resonator before waveguide etching is shown in Figure 12. The magnified view of the total internal reflection mirror is shown in Figure 13.

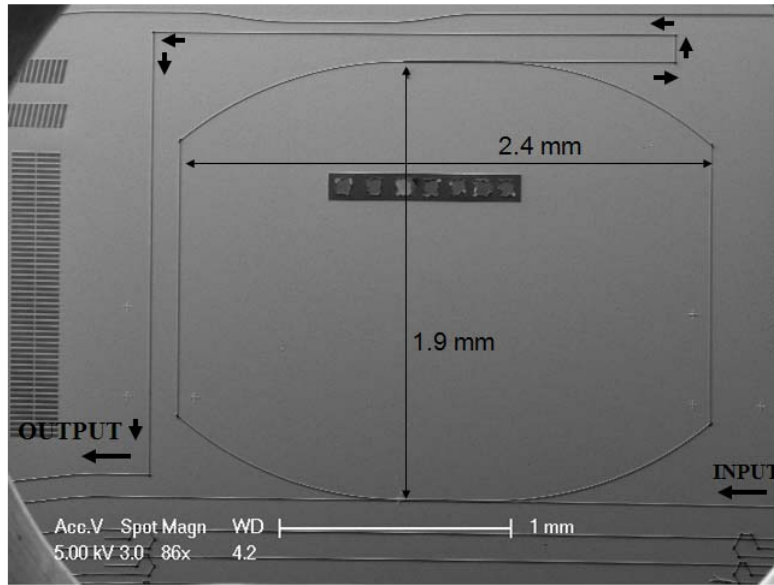


Figure 12. Actual ring resonator before waveguide etching (From [9]).

A single pulse is required to circulate in the ring, and in order to fabricate the ring, the total internal reflection mirrors are used to connect four optical waveguides in a rectangular shape, thus approximating the ring structure. The total length of the ring is chosen so that the total time it takes the pulse to travel a single loop is equal to that of laser pulse-repetition time. A directional coupler, fabricated using etched beam splitters, is used to couple the laser pulse into the ring, while another one is used to take a sample of the circulating laser pulse out of the ring. Due to the losses experienced by the laser pulse as it travels in the ring, two semiconductor optical amplifiers are placed on two sides of the ring so that there will be sufficient gain for the laser pulse to circulate in the ring. In addition, another semiconductor optical amplifier is placed at the output of the ring resonator to amplify the output laser pulse if necessary. The phase modulator is

placed at the input of the ring resonator to change the phase of the incoming laser pulses so that addition or subtraction can take place as directed by the direction MZI.

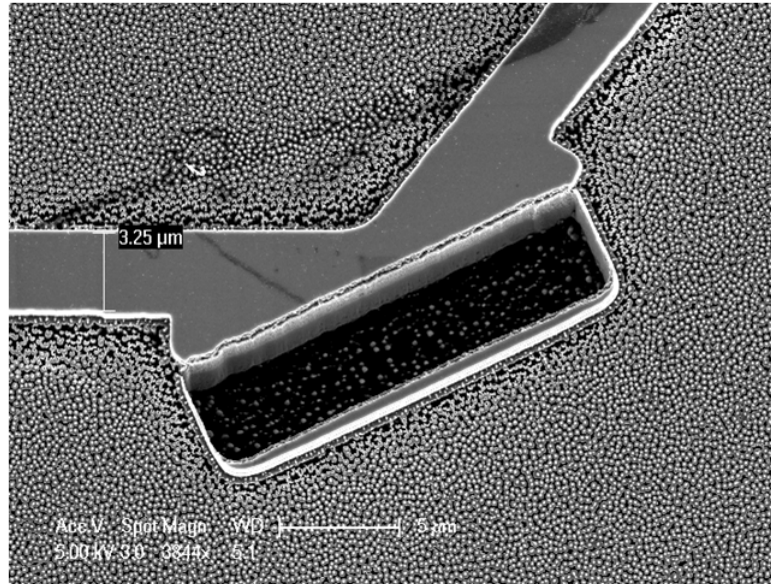


Figure 13. Magnified view of the total internal reflection mirror (From [9]).

## 7. High-Speed Comparator

There are two high-speed comparators in the design of the photonic sigma delta modulator. Both are identical in design. The function of the comparator is to test if the input voltage has exceeded a predetermined threshold and generates a high or a low output for the corresponding input voltage. One is required for the thresholding of the direction MZI, while the other one is for thresholding the ring resonator output. As the PRF of the laser pulse train is 10 GHz, the comparator system has to process  $10 \times 10^9$  pulses per second; hence, a high-speed comparator is needed.

The high-speed comparator is made up of four high-speed analog components from Inphi, Inc. They include a fanout, a D flip-flop, an XOR and a MZI driver. The configuration of the high-speed comparator is illustrated in Figure14. The comparators also requires voltages  $-3.3$  V,  $-5.2$  V and  $+8$  V to function.

As these components are designed for high data rates, they come with an option of being driven differentially or single-ended. For this research, all components are driven single-ended.

The function of the fanout is to amplify the weak signal coming from the photodetector. It functions as a linear amplifier at an input voltage of  $100 \text{ mV}_{pp}$  and a limiting amplifier at an input voltage of greater than  $400 \text{ mV}_{pp}$ .

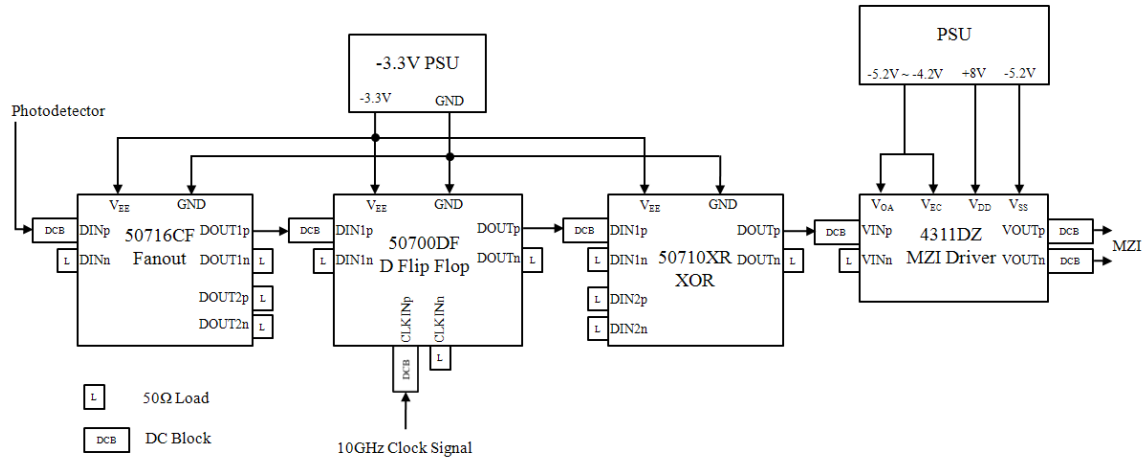


Figure 14. High-speed comparator block diagram.

The D flip-flop functions as the comparator. The output of the fanout is compared to the clock signal. The output of the D flip-flop goes high when the input signal is higher than the clock signal. Hence, the threshold level can be set by changing the signal level of the clock signal with a variable attenuator. Alternatively, the clocking signal can be held constant, and a DC voltage is injected into the negative side of the input port. Being differentially driven, this shifts the signal level of the positive input; thus, the threshold level can also be determined by this DC voltage. Both configurations are shown in Figure 15.

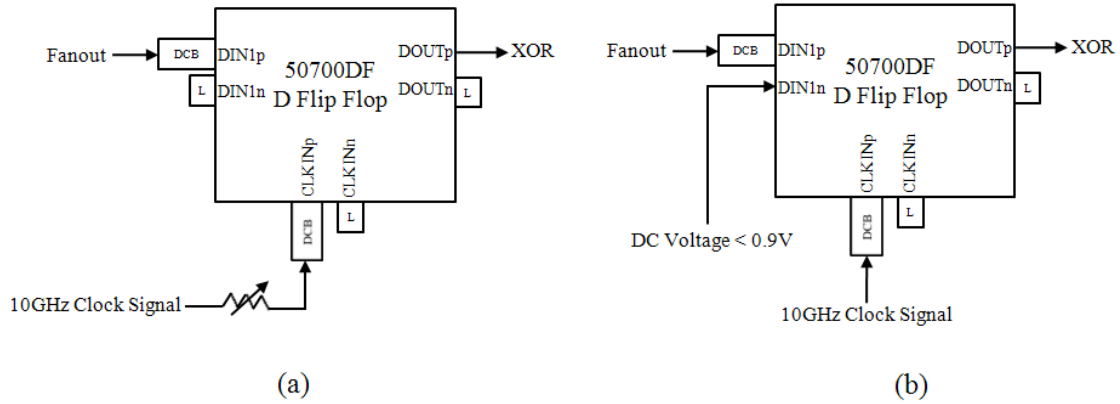


Figure 15. D Flip-flop with (a) clock signal thresholding (b) DC voltage thresholding.

The XOR gate is used as a signal inverter in case there is a need to invert the signal to the phase modulator or the subtraction ports of the MZIs. The connection of the XOR for signal inverting is shown in Figure 16.

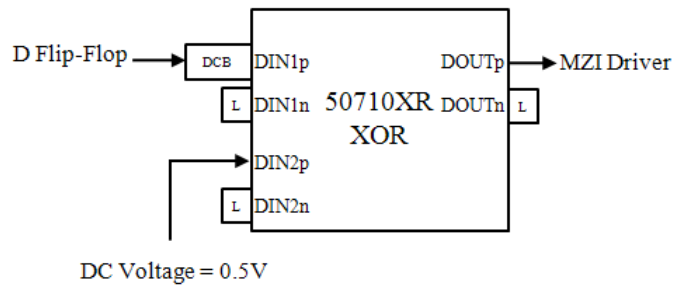


Figure 16. Signal Inverting XOR connection.

The last component in the high-speed comparator is the MZI driver. The RF port of the MZIs has to be driven with a voltage level of  $V_{\pi}$ . As the output of the XOR is too low to achieve this objective, an MZI driver is needed to amplify the output of the XOR. The output of the MZI driver can be varied with  $V_{OA}$ . In addition,  $V_{EC}$  can be used to adjust the eye cross point. The  $V_{OA}$  and differential  $V_{PP}$  relationship are illustrated in Table 1. The  $V_{EC}$  and eye cross percentage relationship are illustrated in Table 2.

Table 1.  $V_{OA}$  and differential  $V_{pp}$  relationship (From [11]).

$V_{OA}$ (V)	Differential $V_{pp}$ (V)	Single-ended $V_{pp}$ (V)
-5.2	4	2
-4.95	5	2.5
-4.7	6	3
-4.45	7	3.5
-4.2	8	4

Table 2.  $V_{EC}$  and eye cross percentage relationship (From [11]).

Eye Cross (%)	$V_{EC1}$ (V)	$V_{EC2}$ (V)
50	-5.2	-5.2
30	-4.2	-5.2
70	-5.2	-4.2

## 8. Decimation Filter

The decimator filter is the last component in the photonic sigma delta ADC. As the single-bit data rate at the output of the ring resonator comparator is expected to be 10 Gbps, it is a challenge to implement a decimator filter using digital signal processing. The comparator output must be lowpass filtered and resampled to the Nyquist rate. Real-time data capturing and digital signal processing of the comparator output at such high-speed using COTS digital I/O and digital signal processing boards is not possible.

In order to overcome this technology limitation and to verify the result of the photonic sigma delta ADC, non real-time digital signal processing is done instead. A high-speed oscilloscope can be used to capture the comparator output. The captured data is then downloaded to a desktop and the decimation filter can be implemented using MATLAB. The decimation filter is broken up into multiple stages so that the filter requirements can be relaxed.

## **C. SUMMARY**

The physical hardware needed to implement the photonic sigma delta ADC was described in this chapter and the working principles of various components like the model locked laser, Mach-Zehnder Interferometers and ring resonators were explained. The design of the high-speed comparator was also discussed in detail. The connection setup as well as various ways of controlling the threshold voltage was shown. In the next chapter, the characterization of the individual components is described. This includes characterization of the laser time and amplitude jitter, the MZI performance and the comparator response.

## IV. PERFORMANCE EVALUATION AND RESULT ANALYSIS

The performance of the individual components in the photonic sigma delta ADC are evaluated in this chapter. Measurements were carried out for individual components and for groups of components. The effects of timing and amplitude jitter are explained. The jitter analysis was done for the 10 GHz clock synthesizer as well as the mode-locked laser. This information will be used in Chapter V and included in the MATLAB simulation to predict the expected performance (once the ring resonator is integrated within the architecture).

### A. RMS TIMING JITTER ANALYSIS

Timing jitter and phase noise are two related quantities. Phase noise is a frequency domain view of the noise spectrum around the oscillator signal, while timing jitter is a time-domain measure of the timing accuracy of the oscillator period [12]. Timing jitter in the time domain, where  $\tau_n$  is the period of the cycle with jitter, and  $\tau_{avg}$  is the period of the ideal cycle is illustrated in Figure 17. Phase noise in the frequency domain where it can be seen that the time jitter causes a spread in the spectrum resulting in phase noise is illustrated in Figure 18.

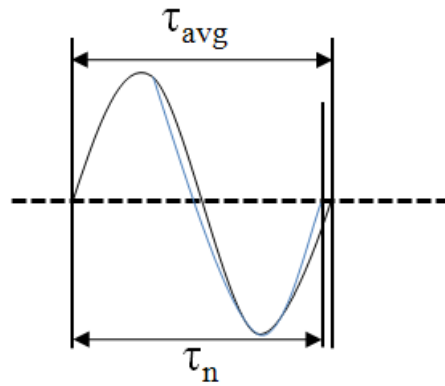


Figure 17. Timing jitter in the time domain.



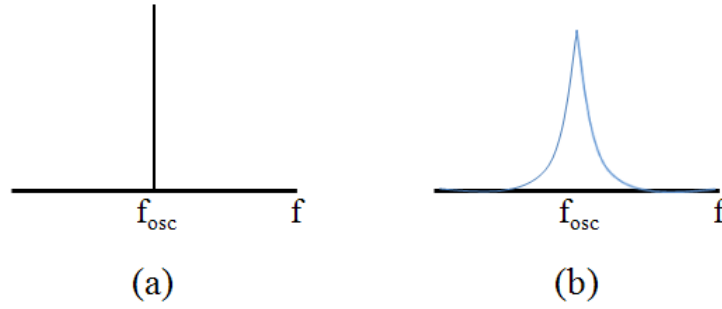


Figure 18. Phase noise in frequency domain (a) ideal sine wave (b) sine wave with timing jitter.

In the time domain, timing jitter is the statistical measure of a noisy oscillation process. The period of each cycle of the oscillation is different due to the noise-induced jitter. Timing jitter  $J_n$  is the time difference between a measured cycle period  $\tau_n$  and the average cycle period  $\tau_{avg}$  [13]:

$$J_n = \tau_n - \tau_{avg} . \quad (4.1)$$

The root mean-squared of the timing jitter can be given as

$$\sigma_t = \sqrt{\langle J_n^2 \rangle} = \sqrt{\frac{J_1^2 + J_2^2 + \dots + J_n^2}{N}} \quad (s) \quad (4.2)$$

where  $N$  is the number of timing jitter measurements.

The  $\sigma_t$  can be measured using a high-speed oscilloscope. Due to timing jitter, the waveform in the time axis is spread over a period of time. The oscilloscope is able to capture up to  $2^{32}$  waveforms in its memory. The waveforms are displayed as a color gradient with white being the highest point of occurrence. From these waveforms the average cycle period and the RMS timing jitter value can be calculated for every waveform. The  $\sigma_t$  value can then be used to calculate the variance, which is the timing jitter power.

The  $\sigma_t$  can also be measured in the frequency domain by measuring the phase noise. The frequency domain method requires integrating the phase noise power over the frequency range of interest. The phase jitter in seconds is given by

$$\sigma_t = \frac{\sqrt{2 \times 10^{A/10}}}{2\pi f_{osc}} \quad (s) \quad (4.3)$$

where  $A$  is the integrated phase noise power in dBc and  $f_{osc}$  is the oscillator frequency. This can be done using the phase noise power integration function of the spectrum analyzer.

The mode-locked laser measurement setup for both the time domain and frequency domain are shown in Figure 19. The high-speed sampling oscilloscope can accept optical or electrical inputs directly, unlike the spectrum analyzer, which requires a photodetector to convert the optical signal to an RF signal. In addition, the oscilloscope can be triggered by the 10 GHz clock signal, which lowers the internal jitter from the clock source of the oscilloscope, and provides a more accurate result. The oscilloscope uses a stored set of sampled data over a period of time to calculate the timing jitter, thus, with sufficient data, it gives an accurate distribution model of the timing jitter. The setup of the synthesizer measurement is similar except that a photodetector is not required.

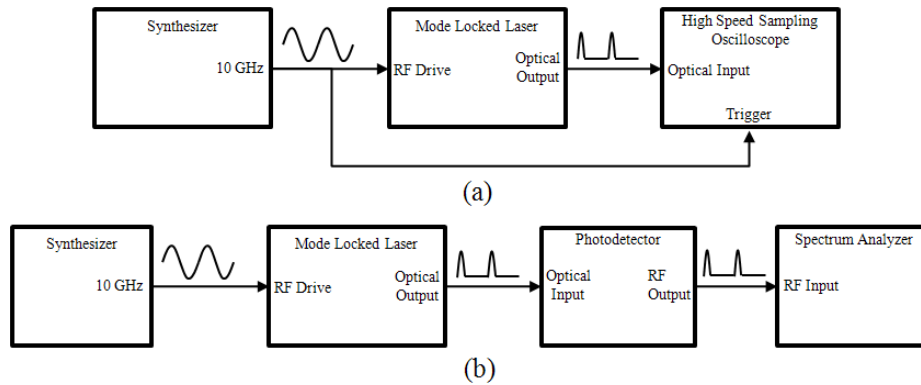


Figure 19. Timing jitter measurement setup (a) time domain (b) frequency domain.

## 1. 10 GHz Synthesizer

The 10 GHz signal is the clock signal for the mode-locked laser as well the high-speed comparator and its timing jitter has a significant impact on the performance of the ADC. The 10 GHz sinusoidal waveform of the synthesizer is illustrated in Figure 20.

The magnified portion of the signal is illustrated in Figure 21. The color gradient illustrates the spread of the samples collected by the oscilloscope. In addition, the histogram of the sampled data is shown at the top of the screen. The histogram data is gathered at the cyan horizontal line indicated on the scope. From the histogram measurement, it can be seen that the standard deviation or timing jitter is 216.6 fs.

In addition, the frequency domain method was employed and a spectrum analyzer was used to measure the phase noise power. The RMS phase noise was measured to be 0.0125 rad, which is equivalent to a timing jitter of 198.95 fs. Both results are shown to be very close.

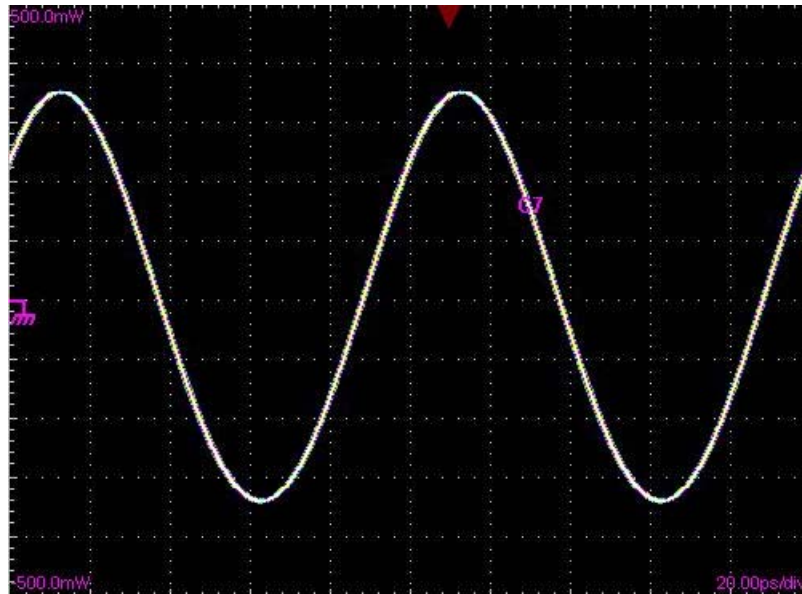


Figure 20. 10 GHz clock signal.

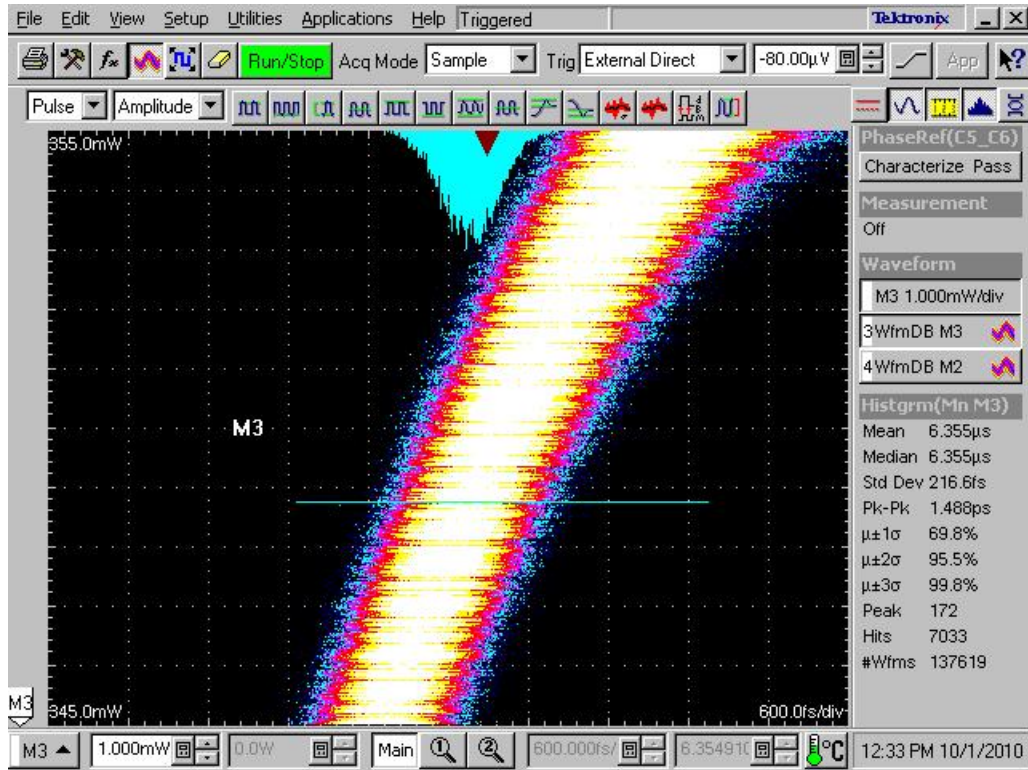


Figure 21. Magnified 10 GHz clock signal.

The histogram data was extracted from the oscilloscope to verify the type of distribution of the timing jitter. The data was ported into MATLAB, and a distribution fitting tool was used to test the distribution type. The timing jitter of the signal was shown to be very close to a normal distribution, the red curve being the normal distribution for the mean and standard deviation of the data set. This is shown in Figure 22.

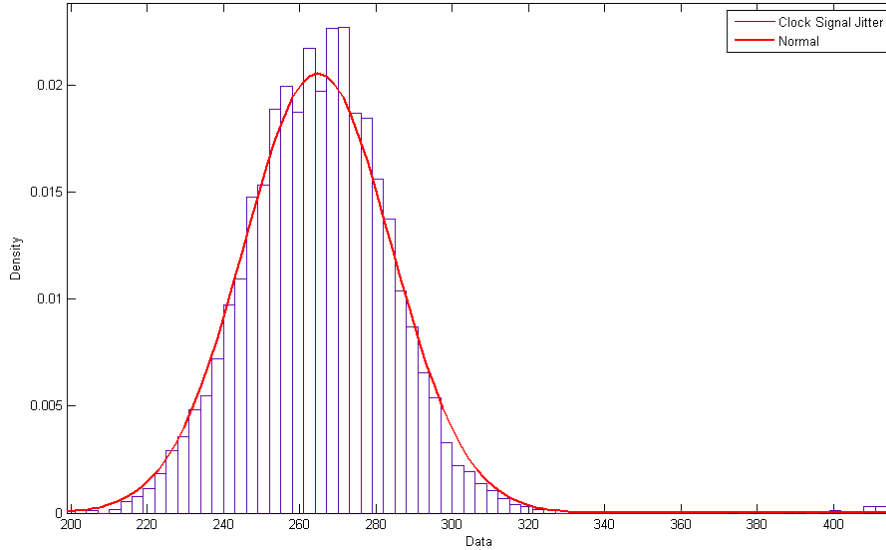


Figure 22. Synthesizer timing jitter versus normal distribution.

## 2. Mode-Locked Laser

A single laser pulse from the mode-locked laser captured with the high-speed sampling oscilloscope is illustrated in Figure 23.

The high-speed sampling oscilloscope also has a built in measurement menu, where different types of measurements can be selected. In Figure 23, the RMS jitter measurement is selected. The oscilloscope then selects the points in which to gather the data for the calculation of the measurement, shown by the two vertical and single horizontal dashed lines. The RMS jitter is shown to be 331.11 fs. The histogram method is also used to calculate the timing jitter, and the result is shown in Figure 24. The RMS jitter is shown to be 333.6 fs. This histogram is also tested for the distribution type, and it is shown to be a normal distribution. This is shown in Figure 25.

The timing jitter was also measured in the frequency domain. The laser pulses are converted to an electrical signal by using a photodetector so that it can be input into the spectrum analyzer. The RMS phase noise was measured to be 0.0245 rad, which gives an equivalent timing jitter of 389.93 fs. Both results are shown to be very close.

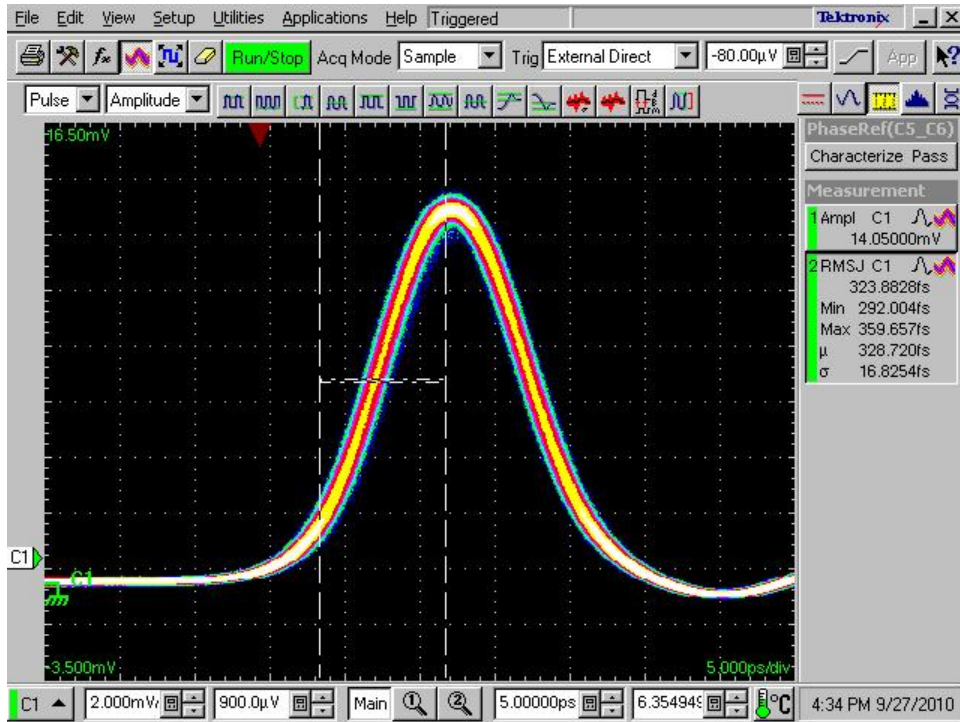


Figure 23. Single laser pulse from MLL.

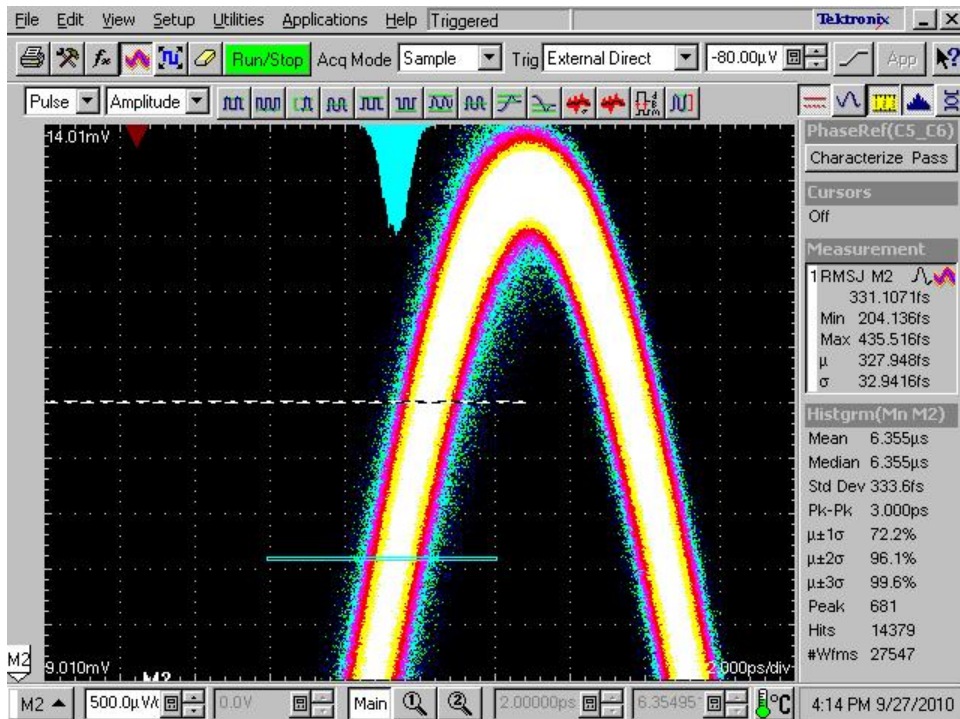


Figure 24. Histogram method of calculating timing jitter.

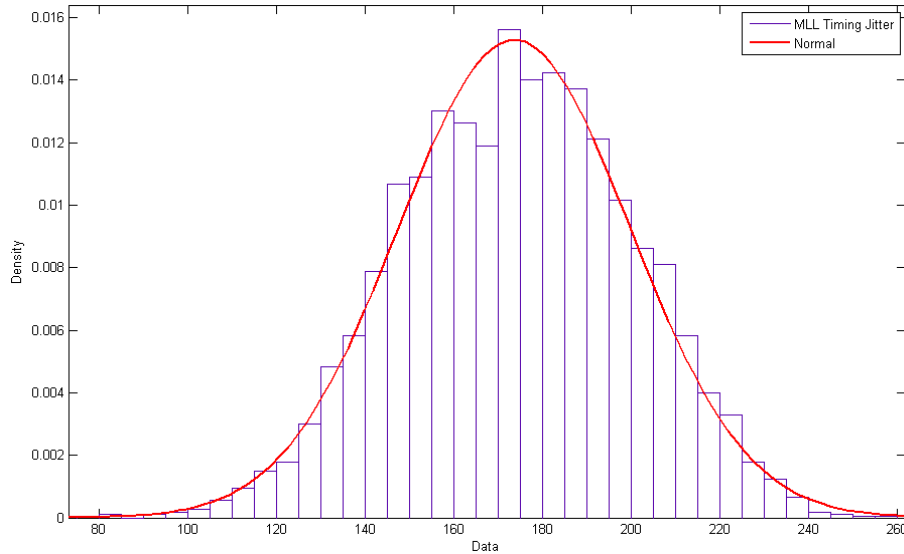


Figure 25. MLL timing jitter distribution versus normal distribution.

### 3. Timing Jitter Comparison Between Synthesizer and MLL

The timing jitter of the mode-locked laser is about 50% higher than that of the synthesizer. Although the clock signal originated from the synthesizer, the MLL adds a significant amount of noise jitter, causing the laser pulse timing jitter to increase.

The time domain mode-locked laser timing jitter was used in the MATLAB simulation of the photonic sigma delta ADC. The timing jitter was generated using the normal distribution random number generator with the timing jitter scaled to the MATLAB simulation's PRF.

#### B. AMPLITUDE JITTER ANALYSIS

The amplitude jitter of the mode-locked laser is measured using the high-speed sampling oscilloscope. The measuring method is the same as for the timing jitter, however, the voltage axis or the Y-axis data is gathered instead. The amplitude jitter measurement is illustrated in Figure 26. The amplitude jitter is 171.9  $\mu\text{V}$ .

The amplitude jitter is also shown to have a normal distribution, as shown in Figure 27. This amplitude jitter value is also used in the MATLAB simulation.

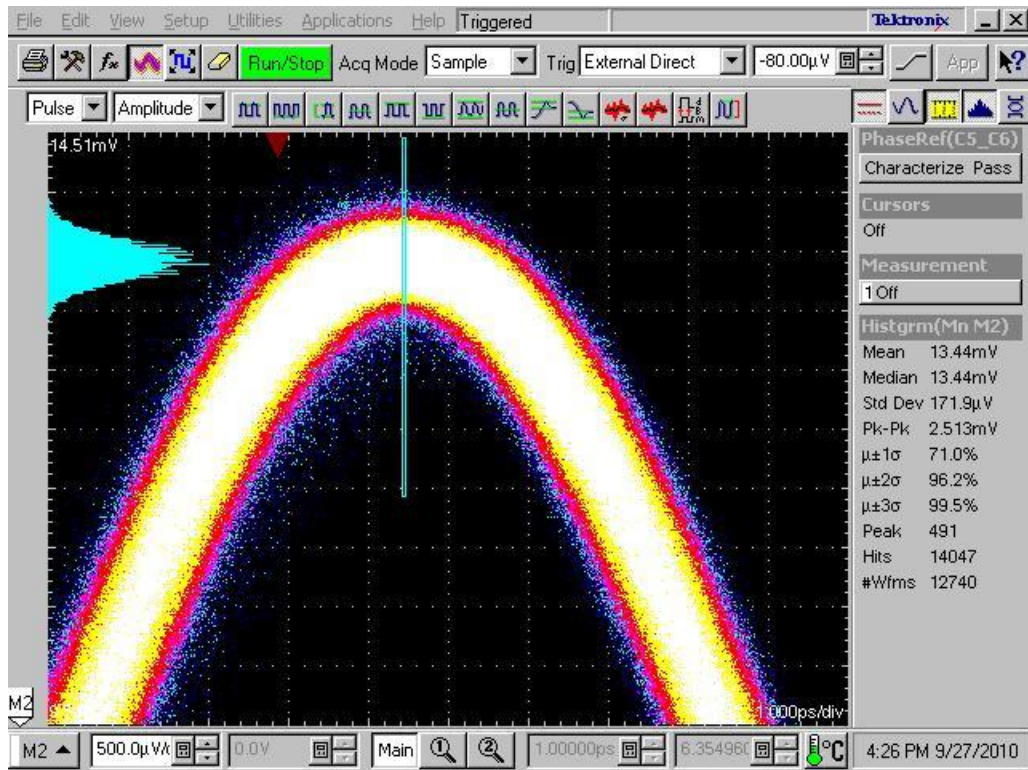


Figure 26. Amplitude jitter measurement.

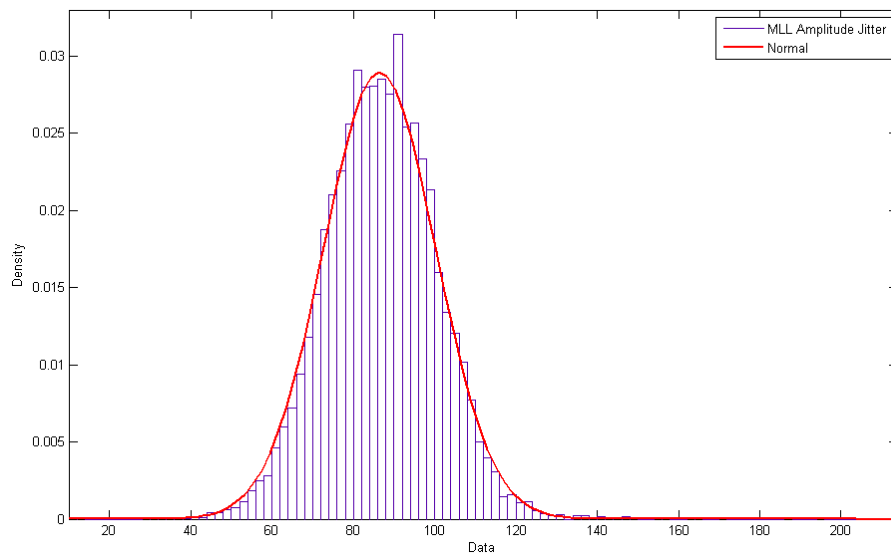


Figure 27. Amplitude jitter distribution versus normal distribution.



### C. MZI RF SIGNAL SUBTRACTION

As the MZIs are configured in a push pull manner, the modulation waveform of the MZI is supposed to be the difference between the two RF ports. In order to verify the ability of the MZI to perform the signal subtraction, the test setup in Figure 28 was used.

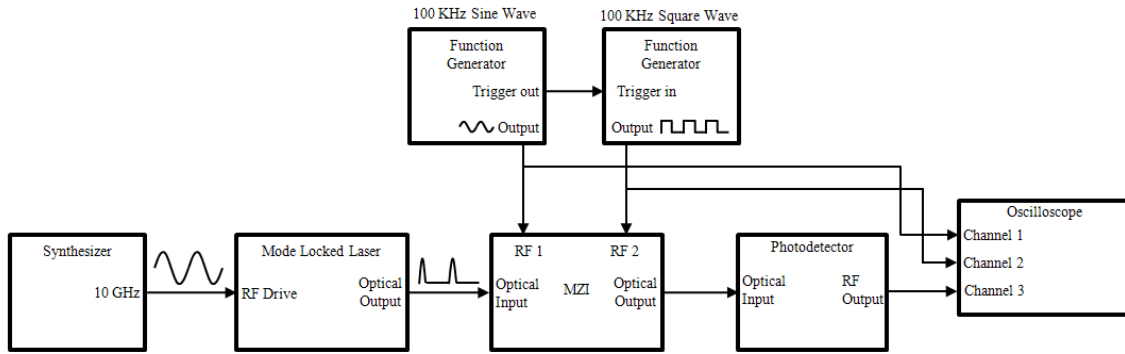


Figure 28. MZI signal subtraction setup.

Two function generators, one set to generate a 100 kHz sine wave and the other a 100 kHz square wave, are connected together and one generator is used to trigger the other so that the waveform generated by both function generators are synchronized. The phase difference between the two waveforms can be adjusted. The sine wave is injected into the RF 1 port of the MZI, while the square wave is injected in the RF 2 port. Both waveforms are fed into ‘Channel 1’ and ‘Channel 2’ of the oscilloscope, respectively. The modulated optical output of the MZI is fed into ‘Channel 3’ via the photodetector. Shown in Figure 29 is the oscilloscope display for all three waveforms. The fourth waveform is the mathematical computation of ‘Channel 2’ minus ‘Channel 1’, the result of which is identical to the waveform shown in ‘Channel 3’.

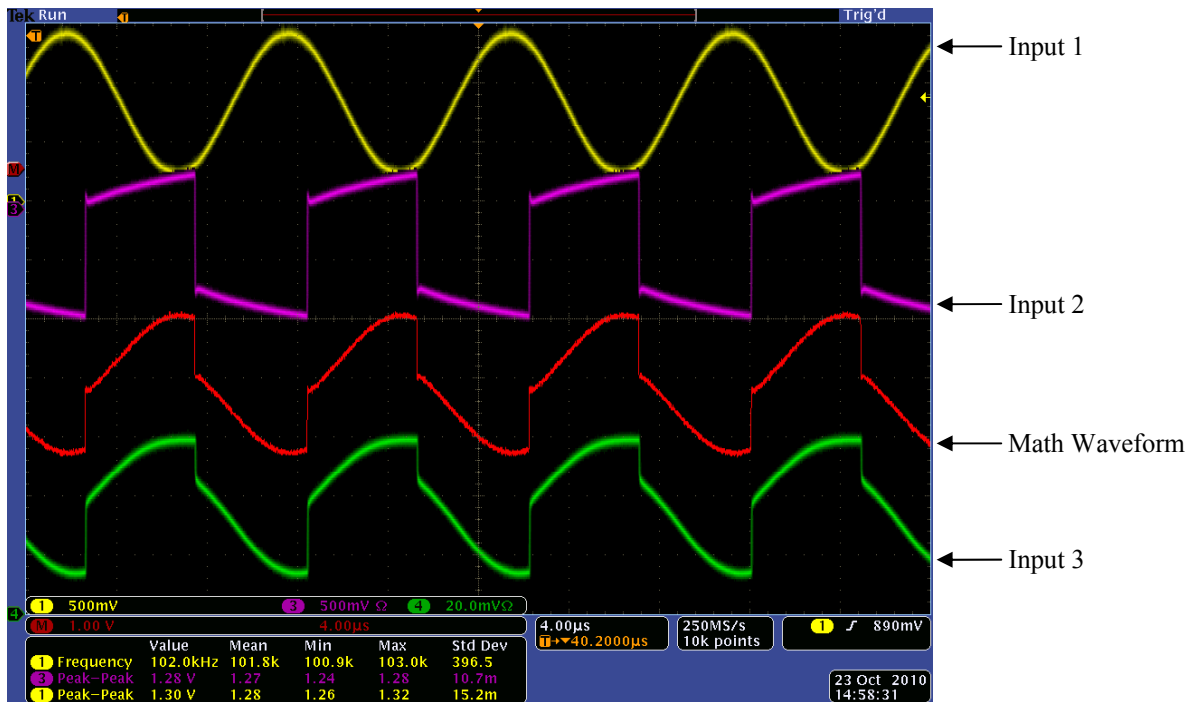


Figure 29. Display of output waveforms on the oscilloscope.

#### D. HIGH-SPEED COMPARATOR ANALYSIS

The configuration of the high-speed comparator was discussed briefly in Chapter III Section B7. The comparator output with respect to a sinusoidal train of pulses and varying level of clock signal are illustrated in Figure 30. The diagram is not drawn to scale.

The DC component of the photodetector output is removed by a DC block before going into the high-speed comparator. The D flip-flop is the component that is doing the thresholding. The threshold is set by varying the clock signal amplitude with a variable attenuator. For pulses that are higher than the positive clock cycle, the D flip-flop outputs a high, and for pulses that are lower, a low is output. In addition, the delay line has to be adjusted so that the clock signal is synchronized with the laser pulses. For the case of the ring resonator's comparator, the threshold is set so that in the positive cycle of the RF signal outputs a high, while the negative cycle outputs a low (i.e., 50% duty cycle) square wave.

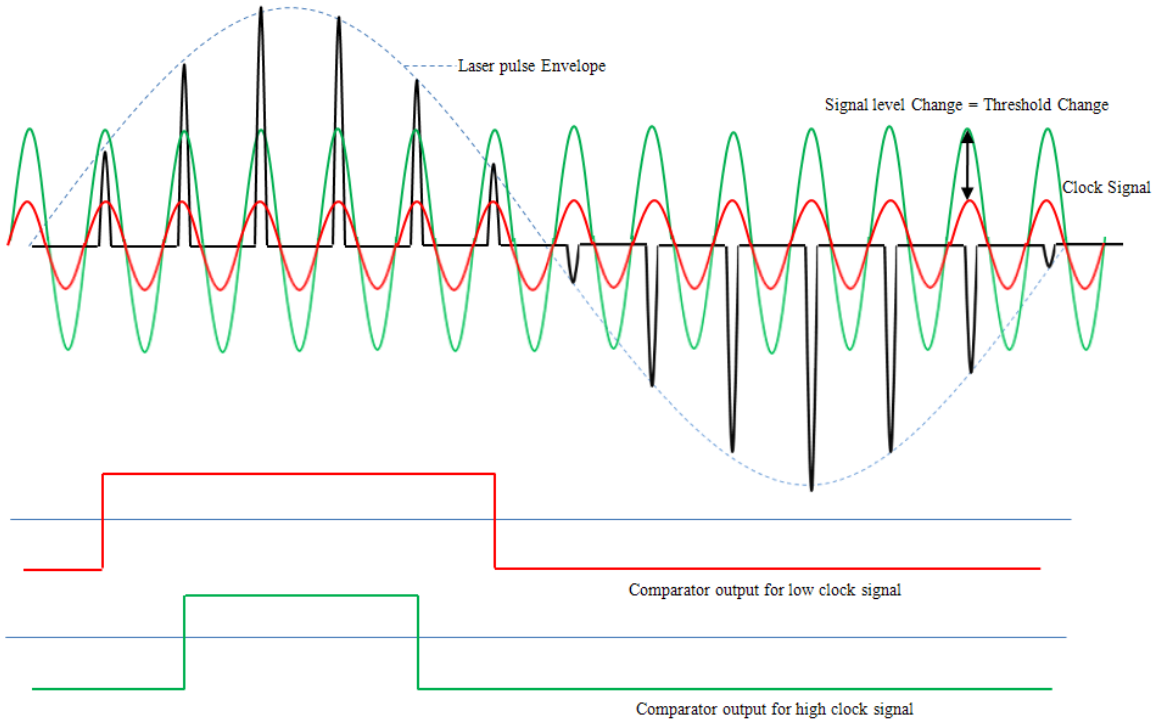


Figure 30. Comparator Output.

The actual output of the comparator on an oscilloscope is seen in Figure 31. A 55 MHz sine wave is used to modulate the laser pulses. The modulated laser pulses are then converted into an electrical signal using a photodetector. The output is then DC-blocked and sent into the high-speed comparator. With the correct threshold level of the clock signal set by the variable attenuator, as well as the correct delay line setting, the high duration of the comparator can be set. The comparator output in Figure 31 is measured from the XOR component is inverted because the signal was measured on the negative port of the differential output.

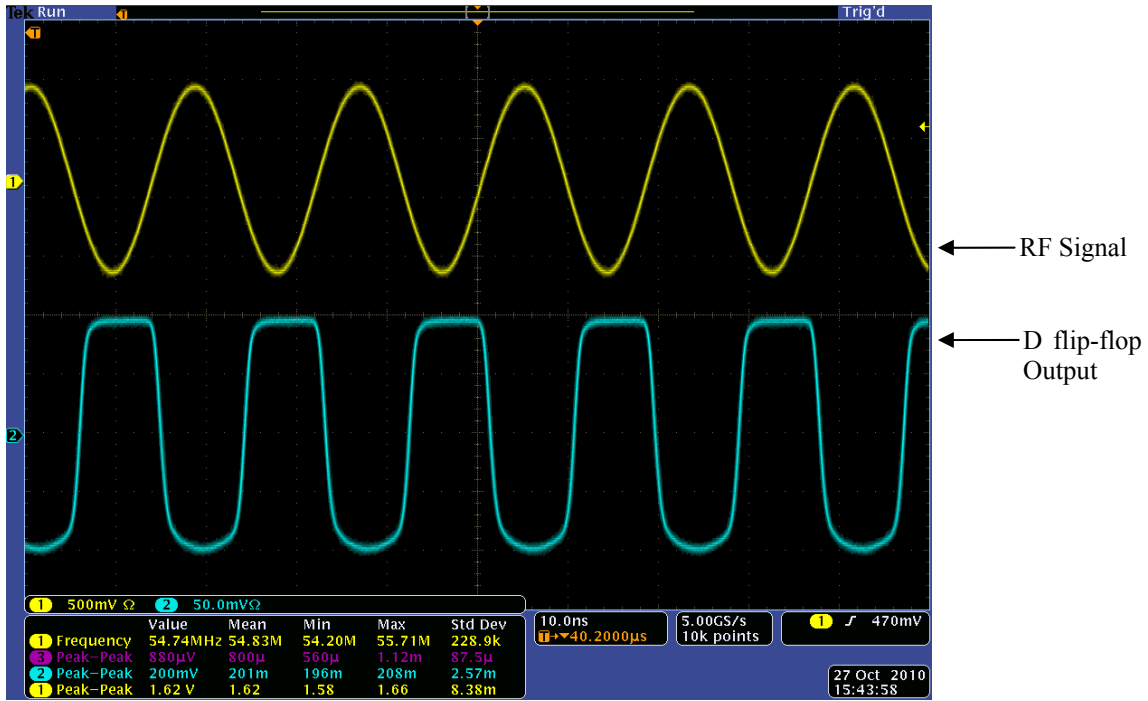


Figure 31. Modulated signals and converted ADC output of a 40 kHz signal.

## E. SUMMARY

Actual measurements of various components in the ADC were shown in this chapter. A detailed analysis of timing and amplitude jitter was carried out. The jitter for the synthesizer and the mode-lock laser were characterized. All jitter was shown to be Gaussian in nature. The actual jitter parameters were recorded and used in the MATLAB simulation for the photonic sigma delta ADC. The RF subtraction of the MZI was evaluated to ensure that the feedback subtraction for the sigma delta loop is able to function as simulated. Lastly, analysis of the high-speed comparator was done to ensure that the threshold could be set and the comparator is able to operate at 10 Gsamples/s.

In the next chapter, the MATLAB simulation to predict the performance of the photonic sigma delta ADC under various laser pulse timing and amplitude jitter conditions are evaluated.

THIS PAGE INTENTIONALLY LEFT BLANK

## V. MATLAB SIMULATION

A MATLAB simulation of the photonic sigma delta ADC is described in this chapter. The simulation was first designed to generate results at various positions within the ADC. For example, the output of the two MZIs, the output of the ring resonator, and the output of the comparators can be evaluated. This information is used in the integration of the hardware. In order to use the simulation to evaluate the ADC's performance in the presence of timing and amplitude jitter, the sigma delta modulator simulation was modified to include a multi-stage decimation process (lowpass filtering, and down sampling to the Nyquist band) and an asynchronous spectral averaging process for examining the sigma delta ADC's noise floor.

The first version of the software was written by Mr. Chang Ho Nam, a visiting researcher from the South Korean Agency for Defense Development. For the timing and amplitude jitter performance analysis, the software was modified to speed up the simulation time as well as to reflect the actual hardware parameters.

### A. SOFTWARE STRUCTURE

The software structure follows closely that of the physical hardware, and a flow diagram is shown in Appendix A. The simulation starts by generating the laser pulse train and the RF signal in discrete time. The RF signal is a sinusoidal waveform. The pulse train is generated by multiplying the envelope of a pulse train with a CW signal at the laser frequency.

The RF waveform is applied to separate functions that simulate the magnitude and direction MZIs transmissivity function, the results of which are used to modulate the laser pulse train. The direction MZI output is applied to a comparator function to determine the polarity of the RF signal. The result is then used to control the ring resonator function, which accumulates (adds or subtracts) the output laser pulse from the magnitude MZI with the previous magnitude pulse that is circulating within the ring. The output from the ring resonator is applied to the output comparator. The comparator output is then fed back to the MZI functions again.

Parameters, such as the laser frequency, the laser pulse width and the laser pulse-repetition frequency can be set. However, due to the limited memory space and processing time, these parameters have to be scaled down. Timing jitter and amplitude jitter of the laser pulses are generated using normal (Gaussian) pseudo-random numbers scaled by the standard deviation. This also includes the measured mode-locked laser jitter values.

Due to the use of feedback in the sigma delta ADC, the simulation is written using a for-loop. The feedback subtraction of the comparator output from the RF signal is also calculated within the for-loop. The result of this subtraction then goes into the comparator and accumulation. The loop executes until the last index of the sampled RF signal vector and laser pulse train.

The simulation was written using function modules for easy debugging and trouble shooting. It also makes modification of the simulation easier.

## **B. SIMULATION RESULTS**

The main simulation parameters used and their comparison with the hardware parameters and corresponding scale factors are shown in Table 3.

The simulated Gaussian laser pulse is illustrated in Figure 32. A Gaussian envelope is first simulated and then multiplied with the laser frequency cycles. The pulse-repetition frequency chosen must allow for an integer number of laser cycles within each pulse. Due to the scaling, each pulse contains fewer number of laser frequency cycles than the actual mode-locked laser pulse. This is because coherence must be maintained so that proper constructive (summation) or destructive (subtraction) interference of the laser pulses within the accumulator can take place. For the laser pulses, timing and amplitude jitter are simulated as well. The variation of the laser pulse-repetition interval and laser pulse amplitude respect to the ideal scaled values of 0.1 s and 1 V, respectively, are illustrated in Figure 33.

Table 3. Main Parameters for MATLAB simulation.

	Actual Parameters in hardware	Scaled Parameters for Simulation	Scale Factor
Laser PW	10 ps	0.01 s	$1 \times 10^9$
Laser PRI / PRF	100 ps / 10 GHz	0.1 s / 10 Hz	$0.1 \times 10^9 / \sim 1 \times 10^9$
Laser Frequency ( $f_L$ )	193.55 THz	800 Hz	$\sim 2.41938 \times 10^{11}$
RF Signal frequency ( $f_{RF}$ )	55 MHz	0.25 Hz	$\sim 0.22 \times 10^9$
Signal Bandwidth	110 MHz	0.5 Hz	$\sim 0.22 \times 10^9$
Over Sampling Ratio	45.45	10	–
RF Signal Voltage	$\pm 0.8$ V	$\pm 0.8$ V	1
No. of Laser Pulses	–	200	–
Modulator, $V_\pi$	3.2 V	3.2 V	1
Sample Time	–	$1.5625 \times 10^{-4}$ s	–
Timing Jitter SD, $\sigma_t$	$333.6 \times 10^{-15}$ s	$3.336 \times 10^{-5}$ s	$\sim 0.1 \times 10^9$
Amplitude Jitter SD, $\sigma_a$	$171.9 \times 10^{-6}$ V	0.01279 V	$\sim 74.4$

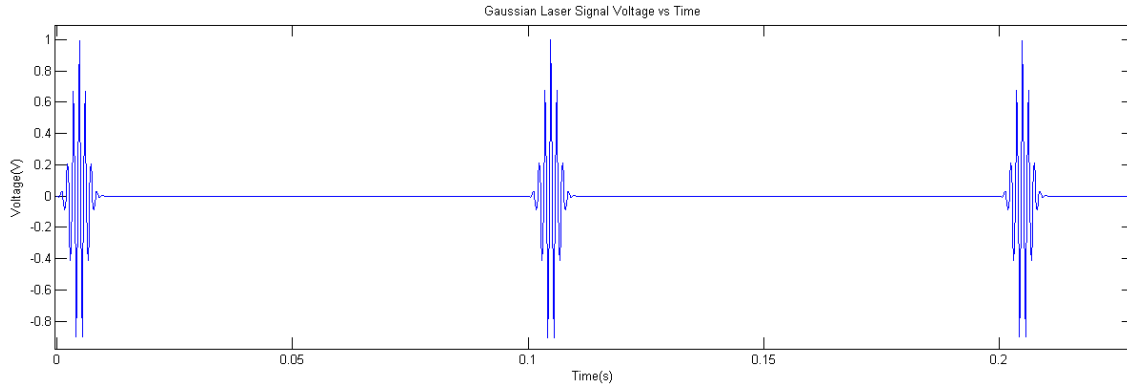


Figure 32. Simulated Gaussian laser pulse.

The RF input signal (sinusoid), the output of the ring resonator, the output of the ring resonator’s photodetector with respect to the RF signal, as well as the two ring resonator outputs, one without and one with laser pulse amplitude and timing jitter are illustrated in Figure 34. Note that timing and amplitude jitter cause distortion at the ring resonator comparator output. The effects of timing and amplitude jitter are discussed in detail in Section D. In addition to these outputs, the simulation is able to plot the outputs of the two MZIs as well.



The magnitude channel output is passed through a decimation filter. The decimation filter is broken up into two stages. The first stage consists of a 30<sup>th</sup> order low pass finite impulse response (FIR) filter and a decimation factor of five, while in the second stage, the same low pass filter is used but with a decimation factor of two (OSR = 10). The output signal after decimation is sampled at the Nyquist rate. The output of the two-stage decimation filter is shown in Figure 35 (no timing or amplitude jitter).

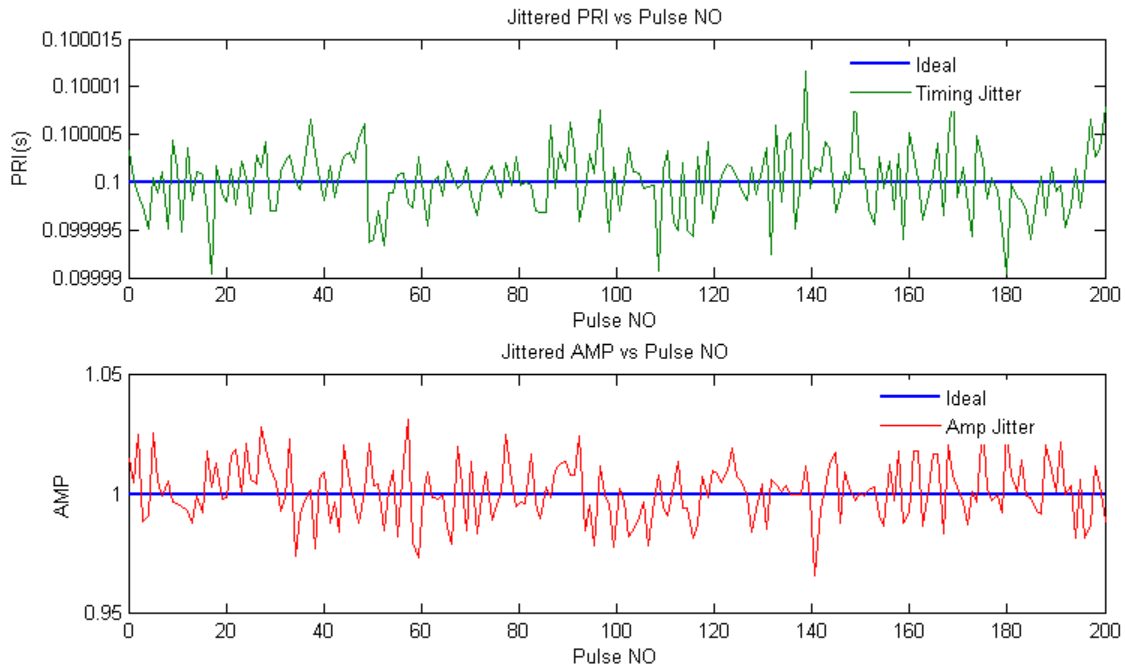


Figure 33. Variation of timing and amplitude for pulse to pulse (From [14]).

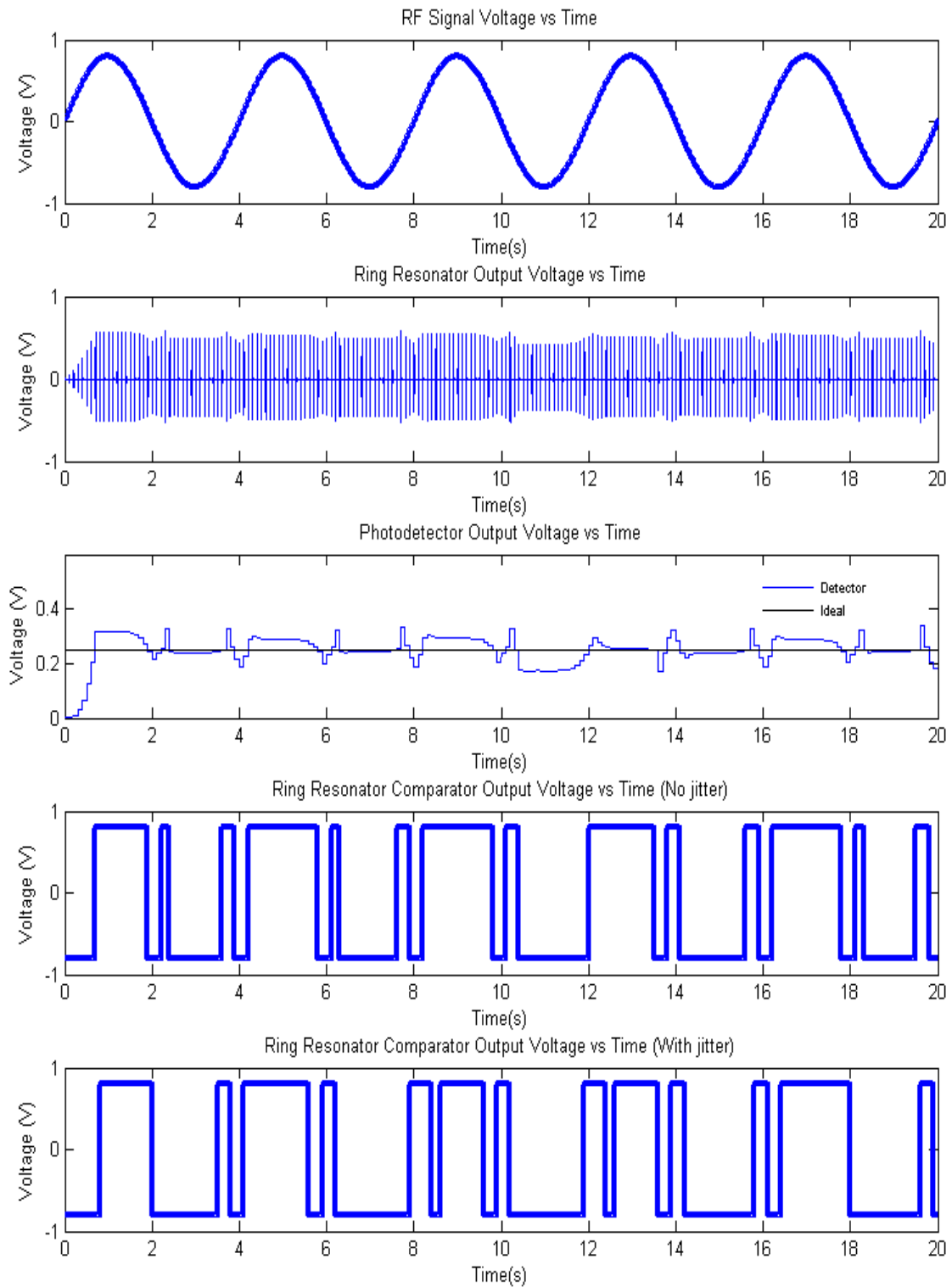


Figure 34. Simulation output results.

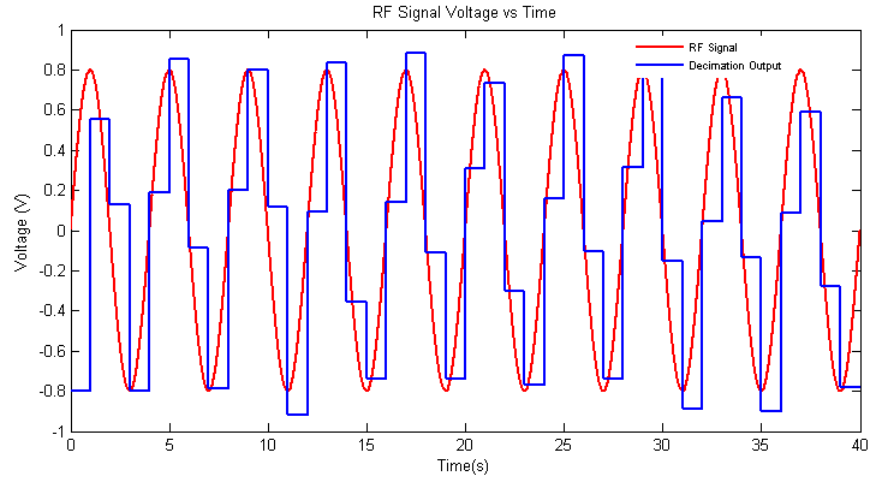


Figure 35. Two-stage decimation filter output.

### C. COMPARISON OF HARDWARE AND SIMULATION RESULTS

The hardware test results can be used to verify the simulation results are correct. The measurement of the direction comparator is illustrated in Figure 36(a) and the simulated results are illustrated in Figure 36(b). Both results are without feedback into the second RF port of the MZI. For the negative cycle of the sine wave, the direction comparator sends the ring resonator's internal phase modulator  $V_{\pi}$ , which generates a  $180^{\circ}$  phase shift for the incoming magnitude laser pulses. This phase shift enables a subtraction to occur in the resonator. Both figures are very similar; thus, the simulation results and the hardware correlate.

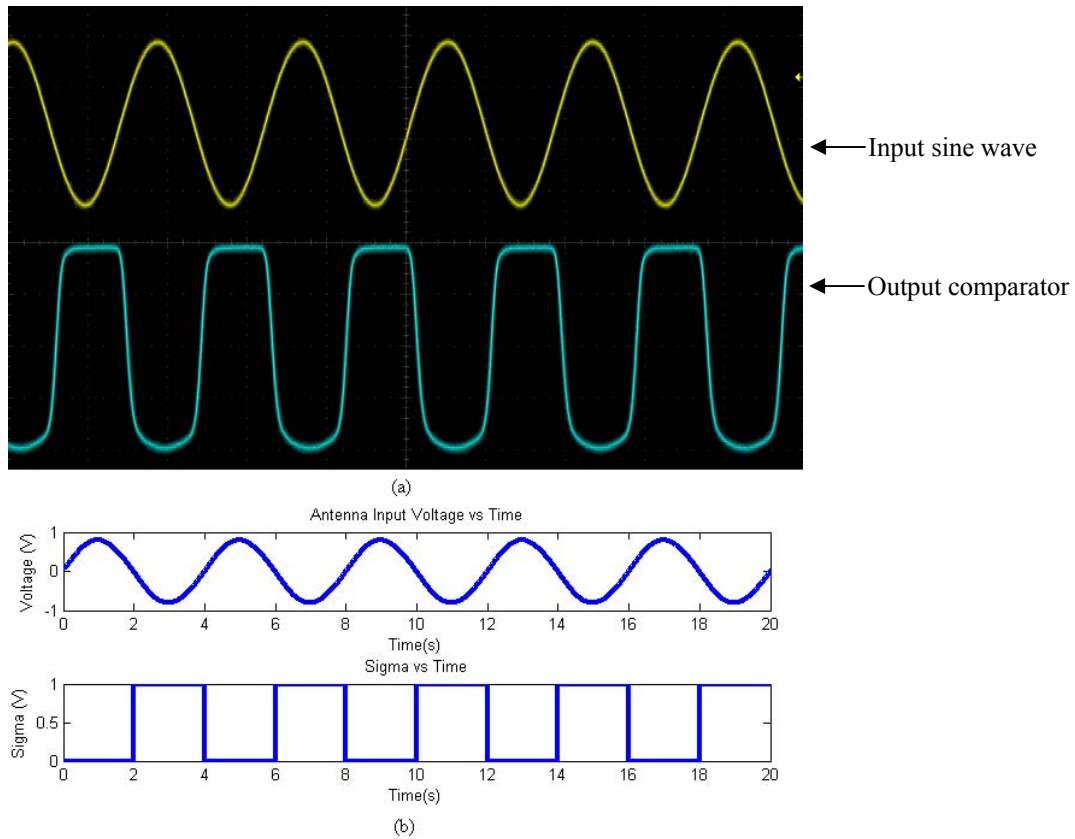


Figure 36. Results comparison (a) actual comparator and (b) simulation.

#### D. NOISE FLOOR EVALUATION USING SIMULATION MODELS

The MATLAB simulation was next modified to examine the noise floor performance of the ADC. The comparison of the simulation noise floor to the theoretical values helps in verifying that the simulation is accurate. In order to evaluate the ADC noise floor, the magnitude spectrum is calculated using the output of the decimation filter. Asynchronous spectral averaging of the magnitude spectrum is carried out next. For each simulation, the RF input is phase shifted, and the process is repeated until 20 collections are saved. The record length is the total number of samples integrated into the magnitude spectrum calculation. For example, with an OSR of ten, a scaled laser frequency of 200 Hz, and 1,100 pulses used for a 1024 point spectral calculation, the simulation requires 11,000 pulses with a total of 1,760,000 samples. The number of pulses and samples processed increases with an increase in OSR. To speed up the processing, the original simulation is modified to run in a single file, memory pre-

allocation is done wherever possible, and the number of for loops used is reduced to two. The program flow chart for the noise floor simulation is shown in Appendix C.

### 1. No Jitter ( $f_0$ Varies)

The simulation was run for the range of OSR values from 10 to 100, in steps of 10, with scaled RF signal frequency; 0.03333 Hz, 0.13333 Hz, 0.23333 Hz, 0.26666 Hz, 0.33333 Hz and 0.43333 Hz. The remaining parameters are shown in Table 4.

Table 4. Parameters for noise floor simulation.

	Scaled Parameters for Simulation
Laser PW	0.1 * PRI
Signal Bandwidth	0.5 Hz
RF Signal Voltage	$\pm 0.5$ V
Modulator, $V_\pi$	1 V
No of Spectral Averages	20
Record Length, NFFT	1024
Timing Jitter SD, $\sigma_t$	0 s
Amplitude Jitter SD, $\sigma_a$	0 V

The theoretical noise floor is given by [6]

$$NF = 10 \log \left( \frac{3N}{4E_B} \right) + 10 \log \left[ \sqrt{1.5} \left( 2^n - 2 + \frac{4}{\pi} \right) \right] + 30 \log \sqrt{OSR} \text{ dB} \quad (5.1)$$

where record length  $N = 1024$ , and  $E_B$  is the equivalent noise bandwidth of the window function. For the Blackman–Harris window  $E_B = 2$ . The value of  $n$  is the number of bits in the quantizer, which is  $n = 1$  for the single-bit first order sigma delta.

The normalized asynchronous averaging of the magnitude spectrum for  $OSR = 100$  and six different frequencies  $f_{RF}$  are shown in Figure 37. For the lowest frequency (0.03333 Hz), there are odd harmonics present in the Nyquist band. For the  $OSR = 10$ , in addition to the even harmonics, there is a strong presence of spurious noise as shown in Figure 38.

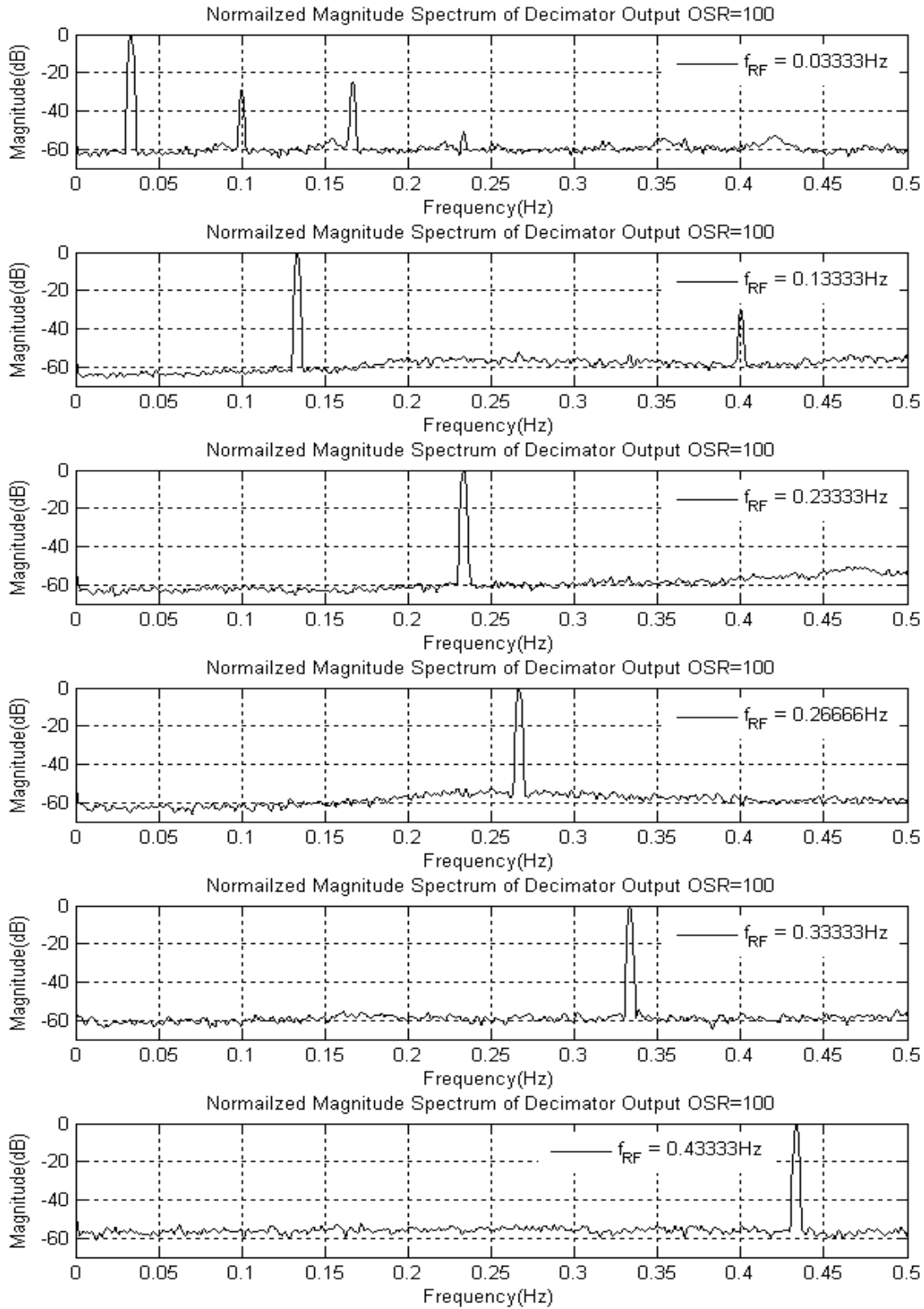


Figure 37. Magnitude spectrum for OSR=100 with different  $f_{RF}$  and no jitter (From [14]).

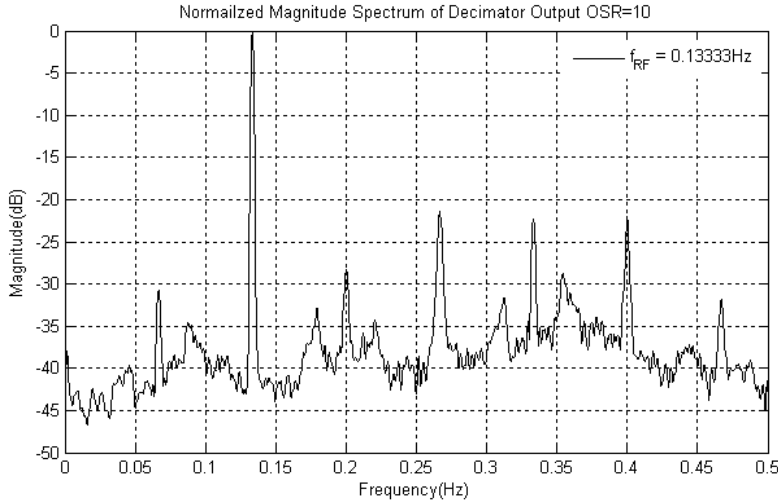


Figure 38. Magnitude spectrum for  $OSR = 10$ ,  $f_{RF} = 0.13333$  Hz and no jitter.

The noise floor results for the OSR values 10 through 100 are shown in Table 5, together with the theoretical noise floor values. Also shown is the scaled laser frequency. The noise floor results are also plotted in Figure 39. The laser frequency has to be varied for some of the OSR values. This is due to the fact that as the pulse-repetition frequency (OSR) changes, the number of laser cycles within a pulse-repetition interval has to be an integer in order to maintain coherence.

Table 5. Noise floor results (dB) with different  $f_{RF}$  and no jitter.

OSR	$f_{RF}$ (Hz)							PRF (Hz)	$f_L$ (Hz)
	Theo.	0.03333	0.13333	0.23333	0.26666	0.33333	0.43333		
10	-42.77	-42.16	-38.65	-37.45	-37.42	-42.31	-41.75	10	200
20	-47.29	-47.67	-46.5	-45.37	-42.15	-44.48	-44.88	20	200
30	-49.93	-51.09	-48.92	-47.27	-46.70	-48.94	-42.73	30	210
40	-51.80	-54.96	-51.89	-49.89	-53.45	-49.83	-49.17	40	200
50	-53.26	-56.15	-53.05	-53.76	-52.82	-52.39	-48.39	50	200
60	-54.45	-57.17	-54.64	-53.98	-54.50	-54.29	-49.72	60	240
70	-55.45	-57.43	-56.6	-55.77	-56.01	-53.92	-53.69	70	210
80	-56.32	-58.48	-57.29	-57.33	-57.37	-54.58	-54.35	80	240
90	-57.09	-58.88	-58.81	-57.81	-57.91	-57.42	-53.78	90	270
100	-57.77	-59.49	-59.03	-59.78	-58.94	-59.26	-56.19	100	200

In Figure 39, the noise floor (in dB) is shown as a function of the OSR. For  $f_{RF} \leq 0.3333$  Hz, the simulation results are more consistent across all OSR. For  $f_{RF} = 0.4333$  Hz there are certain OSR that show an abnormal fluctuation of the noise floor. This is due to the fact that the frequency is near the edge of the signal's Nyquist bandwidth of 0.5 Hz, resulting in fewer samples than those frequencies that are further away. The noise floor is generally lower with the smaller frequencies, and the theoretical noise floor also follows more closely. The noise floor values converge as the OSR gets larger. The smallest spread in noise floor values occurs at OSR = 100. Also shown in Figure 39 is the theoretical noise floor, which is given by (5.1).

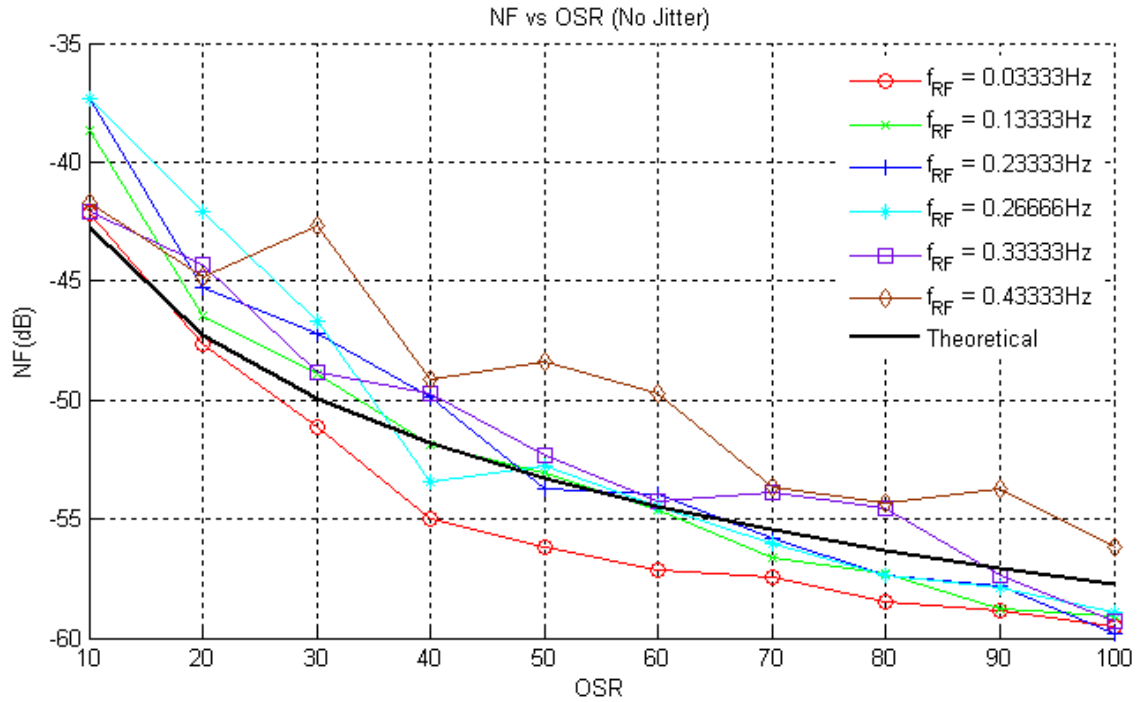


Figure 39. Plot of OSR versus noise floor for different  $f_{RF}$  with no jitter.



## 2. No Jitter (Record Length Varies)

The simulation was run for the range of OSR from 10 to 100, in steps of 10, with record length values: 126, 256, 512, 1024 and 2048. The rest of the parameters are shown in Table 6.

Table 6. Parameters for noise floor simulation.

	Scaled Parameters for Simulation
Laser PW	0.1 * PRI
RF signal Frequency, $f_{RF}$	0.13333 Hz
Signal Bandwidth	0.5 Hz
RF Signal Voltage	$\pm 0.5$ V
Modulator, $V_{\pi}$	1 V
No of Spectral Averages	20
Timing Jitter SD, $\sigma_t$	0 s
Amplitude Jitter SD, $\sigma_a$	0 V

The normalized result of magnitude spectrum asynchronous averaging for  $OSR = 10$  as a function of the record length, NFFT, is shown in Figure 40.

From the magnitude spectrum, it can be seen that an increase in the record length increases the frequency resolution and also decreases the noise floor. The magnitude spectrum plot for  $OSR = 10$  also has more spurious noise compared with spectrum for  $OSR = 100$ . A summary of the noise floor results for the remaining OSR values are shown in Table 7, together with the theoretical calculated noise floor. For  $NFFT = 2048$ , the results for  $OSR = 90$  and  $OSR = 100$  could not be calculated due to computer memory limitations.

In Figure 41, the noise floor values as a function of OSR are shown for various values of the record length NFFT. The noise floor decreases in a consistent manner. From Table 7, it can be seen that that every doubling of NFFT, the noise floor decreases by  $\sim 3$  dB as predicted in (5.1). The theoretical noise floor given by (5.1) for different record length, NFFT, is also shown.

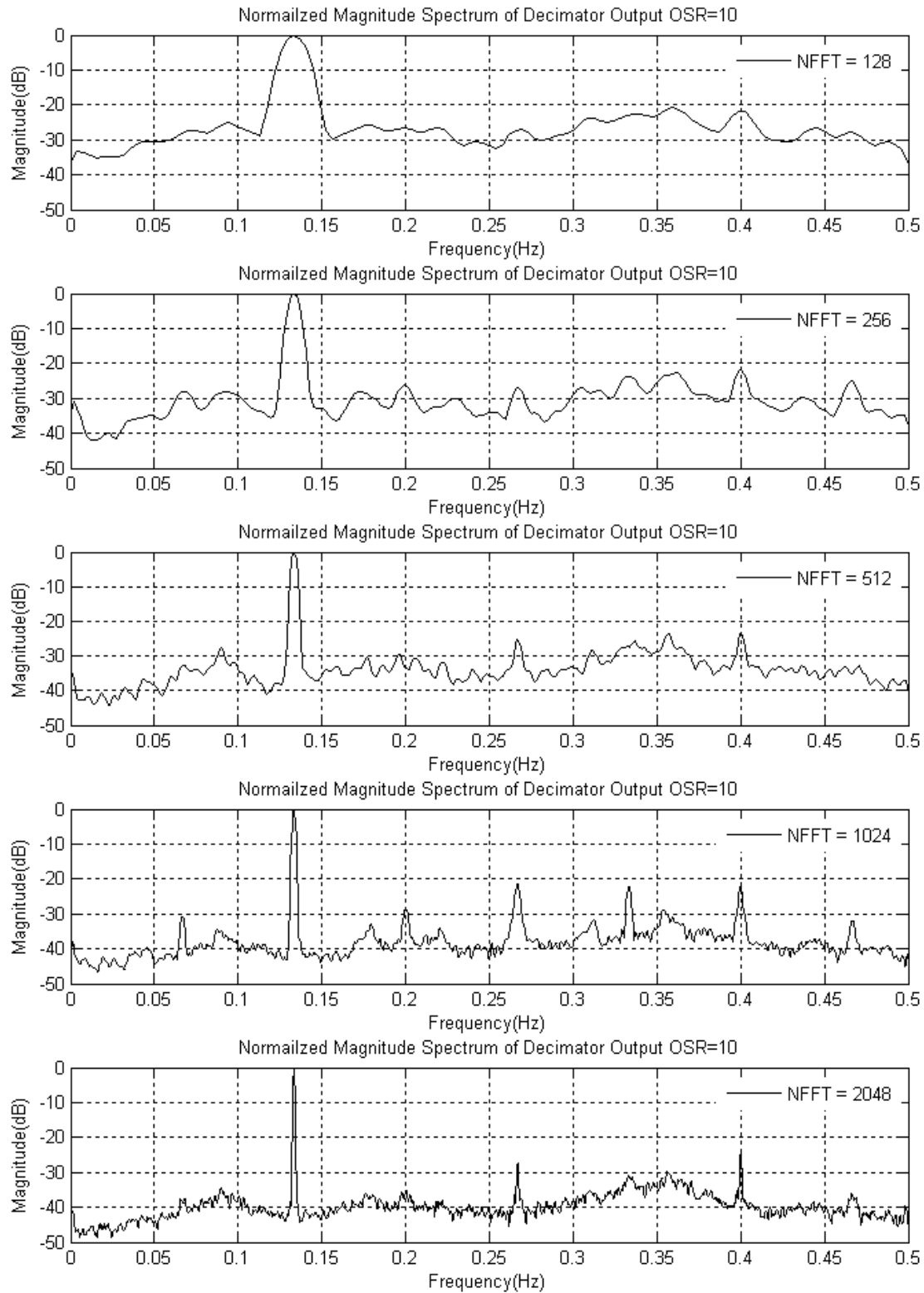


Figure 40. Magnitude spectrum for  $OSR = 10$  with different NFFT and no jitter.

Table 7. Noise floor results (dB) with different NFFT and no jitter.

OSR	NFFT					PRF (Hz)	f <sub>L</sub> (Hz)
	128	256	512	1024	2048		
10	-28.32	-31.28	-34.63	-38.64	-40.06	10	200
20	-41.61	-42.14	-46.33	-46.47	-51.45	20	200
30	-39.07	-42.84	-45.79	-48.92	-51.53	30	210
40	-42.36	-45.12	-48.24	-51.89	-54.26	40	200
50	-44.51	-46.97	-50.49	-53.05	-55.91	50	200
60	-45.33	-47.47	-51.55	-54.64	-57.50	60	240
70	-47.21	-51.08	-53.58	-56.60	-59.55	70	210
80	-48.05	-50.52	-54.61	-57.30	-60.08	80	240
90	-48.96	-52.31	-55.65	-58.81	-	90	270
100	-49.36	-53.06	-56.40	-59.04	-	100	200

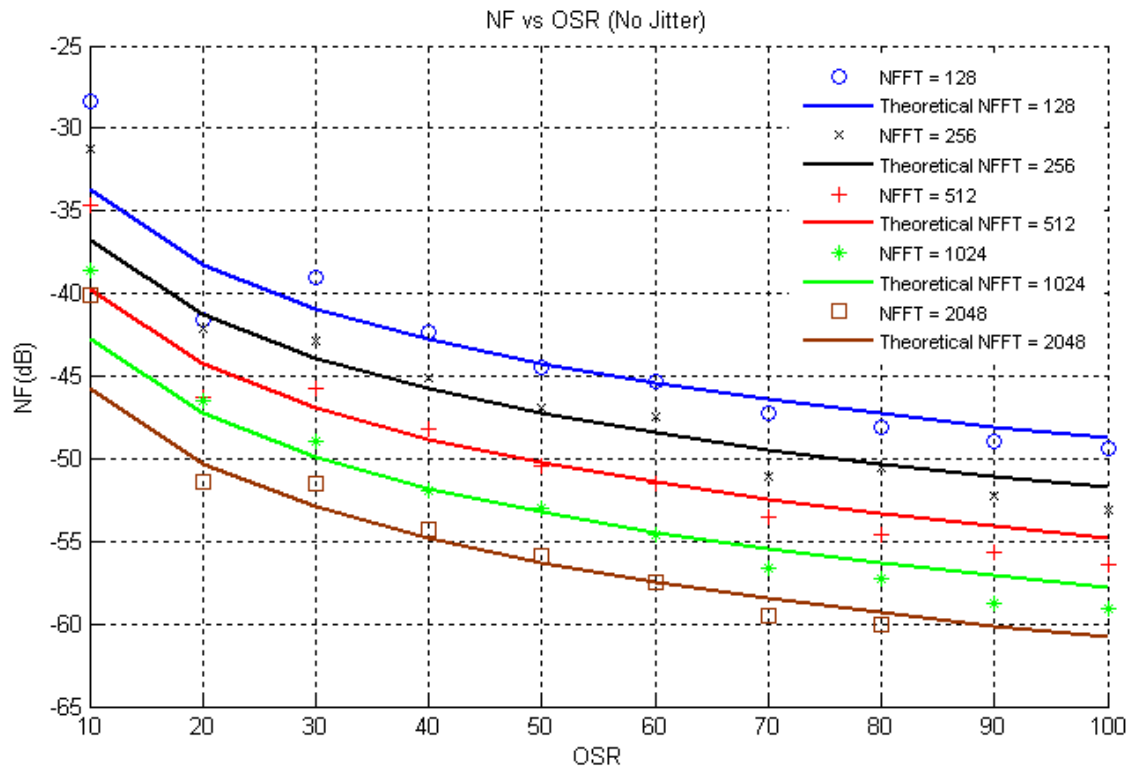


Figure 41. Plot of OSR versus noise floor for different NFFT with no jitter.

### 3. Timing Jitter

The effects of timing jitter were simulated next. This was done for OSRs of 10, 20, 50, 80 and 100. The standard deviation for the timing jitter was varied from 0.00001 s to 0.00011 s. For standard deviation of 0.00001 s to 0.00006 s, the noise floor values are the same as the no jitter scenario. However, from standard deviation of 0.00006 s onwards, the timing jitter distorts the output so much that RF input could not be recovered at the decimation filter. The quantization noise is distorted as well; hence, what is seen is only the noise floor of the FFT process. This is because the comparator is clocked by the ideal PRF cycle, while a timing jitter is simulated into the laser pulse train; hence, if the standard deviation is too high the comparator will apply the threshold outside the peak of pulse or even not on the pulse itself. This results in the distortion of the ring resonator comparator output. The timing jitter effect of the comparator is illustrated in Figure 42.

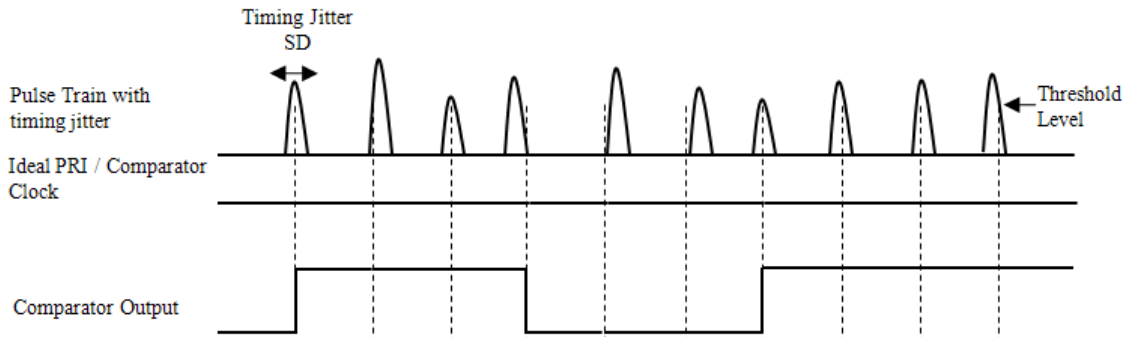


Figure 42. Magnitude spectrum for OSR 10 with timing jitter SD = 0.001 s.

The magnitude spectrum for OSR 10 with timing jitter  $\sigma_t$  of 0 s, 0.0003336 s and 0.001 s is illustrated in Figure 43. The timing jitter  $\sigma_t$  of 0.0003336 s is the scaled  $\sigma_t$  of the mode-locked laser. A DC component is seen in the spectrum plot with timing jitter  $\sigma_t$  of 0.001 s; the timing jitter sometimes introduces a DC component at the output of the decimation filter. The third magnitude spectrum plot shows the distortion of the RF input signal by the timing jitter, which resulted in the total loss of the signal. The noise floor

results for the rest of the OSR are shown in Table 8, together with the scaled timing jitter standard deviation. Next, the noise floor versus timing jitter standard deviation is shown in Figure 44.

It can be seen that the noise floor remains constant for timing jitter standard deviation from  $1 \times 10^{-5}$  s to  $6 \times 10^{-5}$  s and the results are very close to the results of the simulation with no jitters shown previously in Table 5. For standard deviation greater than 0.0001 s, the noise floor drops drastically. This was due to the distortion of the RF input signal by the timing jitter, which resulted in the total loss of the signal. Hence, the noise floor is that of the FFT noise floor.

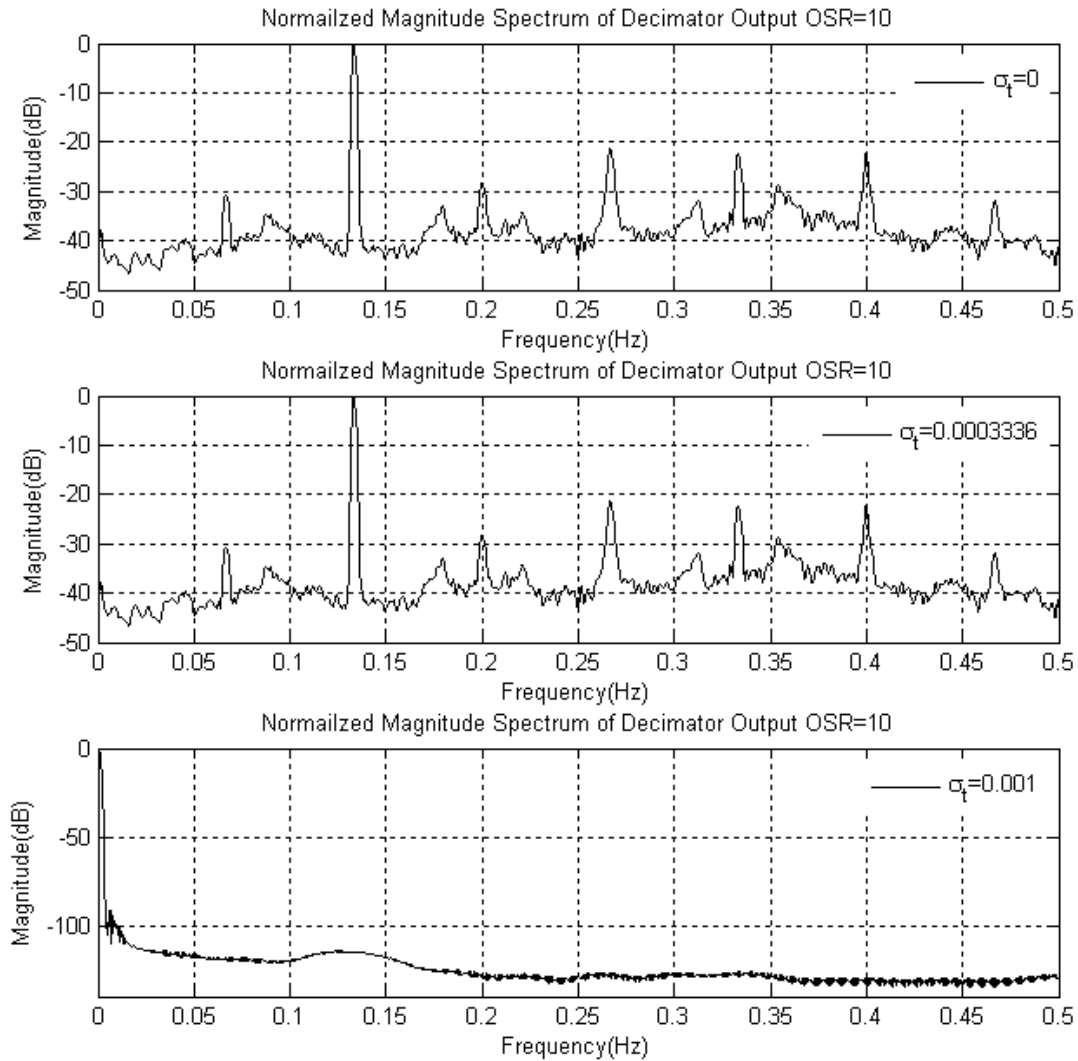


Figure 43. Magnitude spectrum for OSR 10 with timing jitter.

Table 8. Timing jitter noise (dB) floor results with different  $\sigma_t$ .

OSR	Timing Jitter $\sigma_t$ (s)								PRF (Hz)
	1e-5	5e-5	6e-5	7e-5	8e-5	9e-5	1e-4	1.1e-4	
10	-38.64	-38.63	-38.63	-38.63	-37.60	-37.42	-37.13	-36.20	10
20	-46.46	-46.49	-46.48	-46.48	-46.48	-54.38	-83.08	-90.73	20
50	-53.07	-53.08	-53.08	-53.08	-52.70	-92.71	-113.82	-128.38	50
80	-57.33	-57.32	-50.70	-65.77	-114.83	-127.98	-128.80	-128.86	80
100	-59.04	-59.03	-59.03	-59.03	-67.75	-93.89	-122.92	-126.52	100

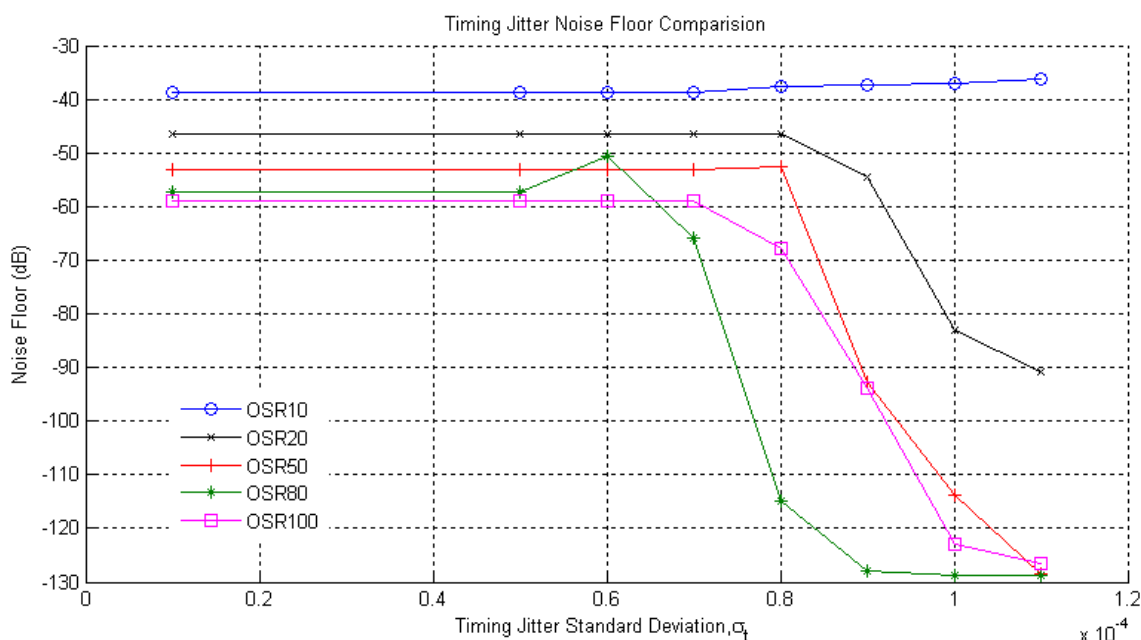


Figure 44. Timing jitter noise floor comparison with different  $\sigma_t$ .

In order to determine if the timing jitter is a dominant source of noise, two simulations where one input frequency is 0.13333 Hz and the other is 0.2666 Hz were done. The spectrum plots of the simulation are shown in Figure 45.

The frequencies were chosen such that one is half of the other. If the noise floor drops by 6 dB when the input frequency is reduced by one-half, then timing jitter is dominant [6]. In our simulation result, the noise reduced by 1 dB; hence, we conclude that other noise sources, for example, quantization noise are far more significant.

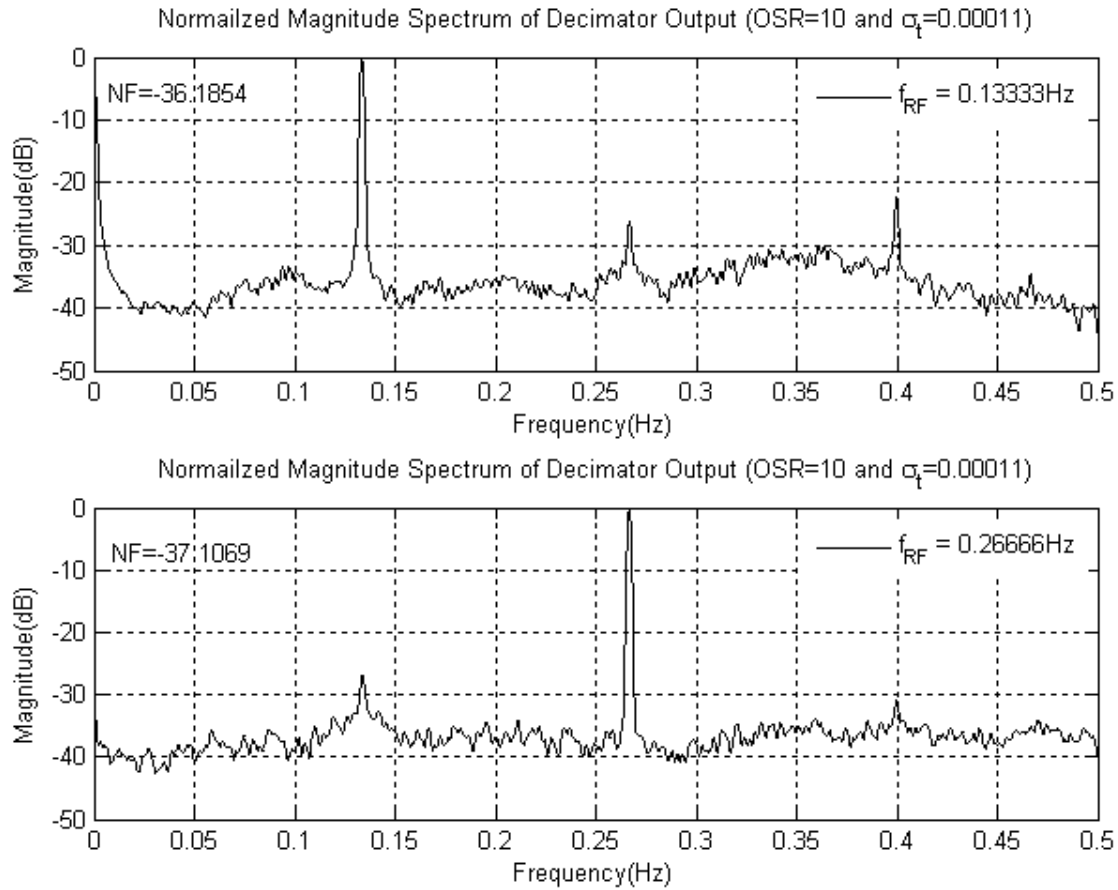


Figure 45. Dominant timing jitter test.

#### 4. Amplitude Jitter

The effects of amplitude jitter were simulated next. Amplitude jitter is the fluctuation of the amplitude of the laser pulse train that is used to sample the RF input signal. This fluctuation introduces errors to the different parts of the ADC. For example, the direction comparator incorrectly detects the polarity of the RF input signal if the amplitude jitter is opposite to that of the actual signal and is high enough to cause the overall signal level to cross the threshold of the comparator. For the case of the ring resonator, the amplitude jitter causes errors in the accumulation and there is an error at the output of the ring resonator comparator.

The simulation was done for OSRs of 10, 20, 50, 80 and 100. The amplitude jitter standard deviation was also varied from 0.001 V to 0.02 V in steps of 0.001 V. The normalized magnitude spectrum for OSR 20 and amplitude jitter standard deviation  $\sigma_a$  is

0 and 0.01279, which is the scaled amplitude jitter of the mode-locked laser, are shown in Figure 46. From the spectrum plot, it can be seen that the plot with the amplitude jitter has less spurious peaks on the noise floor compared with the plot of the case without amplitude jitter. Ignoring the second harmonics of both plots, we see that the spurious free range is now about 40 dB for the plot with amplitude jitter compared to 35 dB for the plot without amplitude jitter. However, the noise floor has risen by 0.5 dB with the addition of amplitude jitter.

The decrease in spurious peaks on the noise floor is because the amplitude jitter added to the laser pulse train is Gaussian in nature; hence, the periodic nature of the quantization noise is destroyed, resulting in the rise of the noise floor as well as the removal of the spurious peaks from the signal. The deliberate act of adding noise to remove periodic noise is known as dithering.

The simulation for OSRs of 10, 20, 50, 80 and 100 and amplitude jitter  $\sigma_a$  from 0.001 V to 0.02 V is tabulated in Table 9. The result is also plotted in Figure 47. For all five curves, it can be seen that there is a general trend of the rise in noise floor as the amplitude jitter increases. The noise floors are higher for all OSRs compared with the noise floor values of the no jitter simulations.

Table 9. Amplitude jitter noise (dB) floor results with different  $\sigma_a$ .

OSR	Amplitude Jitter, $\sigma_a$ (V)											PRF (Hz)
	0.002	0.004	0.006	0.008	0.01	0.012	0.01279	0.014	0.016	0.18	0.2	
10	-52.26	-43.98	-43.80	-40.39	-41.21	-42.25	-39.86	-39.54	-40.04	-39.31	-40.40	10
20	-47.03	-46.63	-46.84	-46.65	-46.32	-46.50	-46.32	-46.21	-46.18	-46.27	-46.27	20
50	-52.49	-52.39	-50.85	-48.21	-50.64	-49.30	-47.31	-49.87	-49.94	-47.07	-47.07	50
80	-56.76	-56.01	-55.04	-50.82	-50.29	-53.38	-52.98	-50.14	-51.39	-49.10	-49.10	80
100	-58.55	-57.66	-54.76	-51.98	-53.15	-51.25	-55.02	-50.27	-50.27	-54.17	-54.17	100



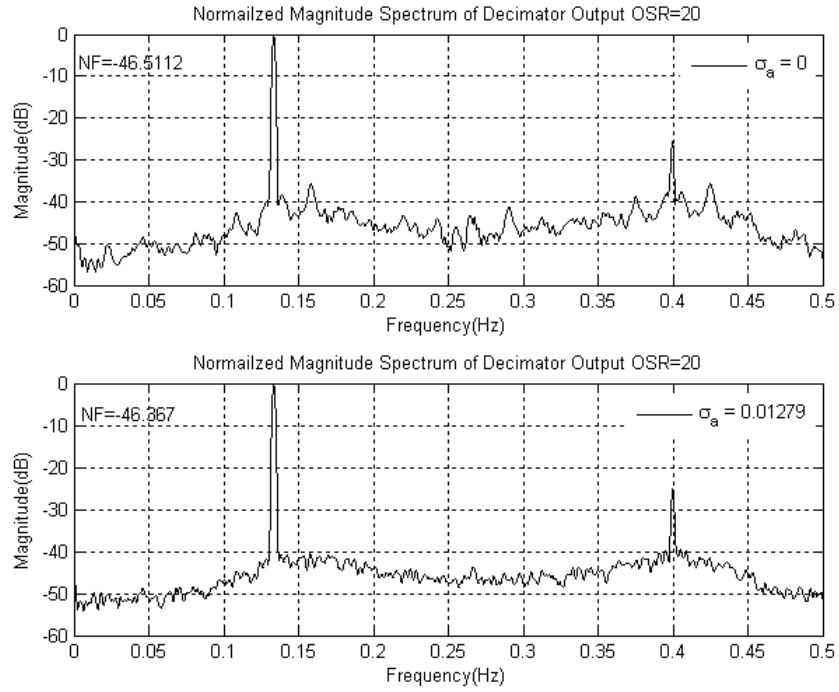


Figure 46. Magnitude spectrum of OSR 20 with different  $\sigma_a$ .

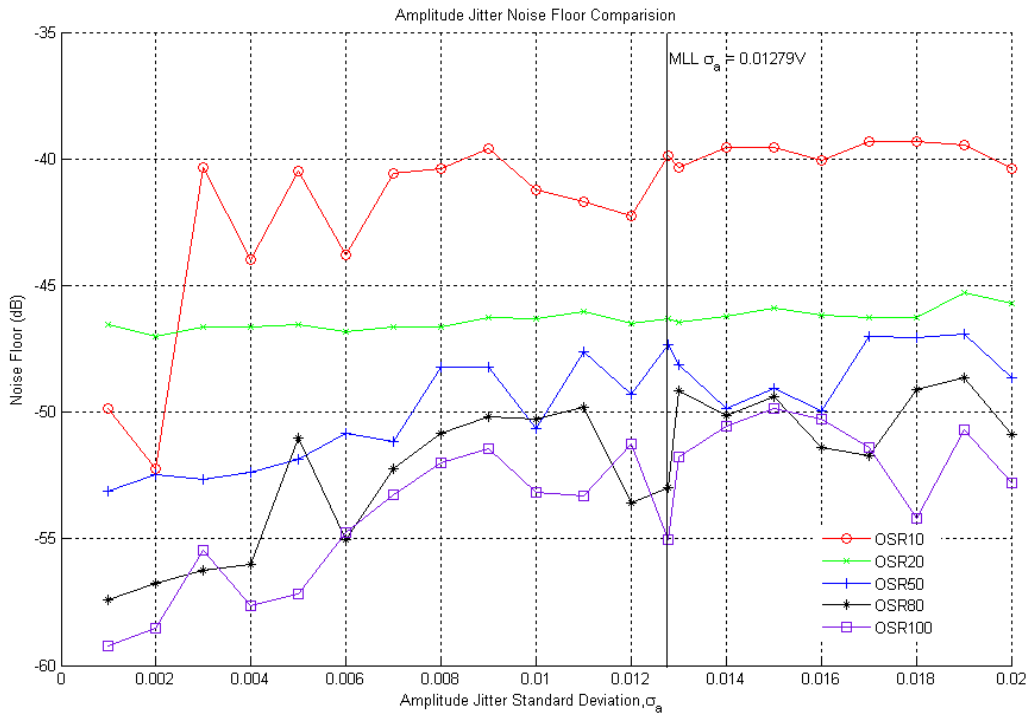


Figure 47. Amplitude jitter noise floor comparison with different  $\sigma_a$ .

## **E. SUMMARY**

The design of the MATLAB simulation for the photonic sigma delta ADC was dealt with in this chapter. The simulation is first used to evaluate the feasibility of the photonic sigma delta ADC as well as the integration of the actual hardware photonic sigma delta ADC. The simulation was modified and used to evaluate the performance of the ADC in the presence of timing and amplitude jitter. The effects of the timing and amplitude jitter on the output of the decimation filter were shown. The noise floor of the ADC was calculated using spectral averaging. The noise floor indicates the dynamic range of the ADC.

In the next chapter, the conclusion as well as the recommendations for the follow-on research are discussed.

THIS PAGE INTENTIONALLY LEFT BLANK

## VI. CONCLUSIONS AND RECOMMENDATIONS

The implementation of the photonic sigma delta ADC using actual photonics and electronic components was studied in this thesis. The performance of various components in the ADC were evaluated and compared with a MATLAB simulation of the ADC. However, due to the absence of the ring resonator, a full integration was not possible.

### A. CONCLUSIONS

The integration of the photonic sigma delta ADC was attempted in this thesis. Various optical and electronic components of the ADC were first tested to identify performance specification as well as their parameters. Next the integration was done in stages. The MZI was first tested to ensure that the RF input signal is able to modulate the laser pulse trains. The  $V_{\text{bias}}$  was also determined so that the MZI could operate at the correct conditions.

The high-speed comparator, which was made up of four individual high-speed analog components, was integrated and tested to verify its design. The setting of the threshold for the comparator was investigated and tested to ensure that the thresholding operation could be carried out.

The use of a high-speed sampling oscilloscope enabled the study of the laser pulse characteristics of the mode-locked laser. The timing and amplitude jitter of the mode-locked laser could be determined by this oscilloscope. With the jitter information, the MATLAB simulation model can be used to determine the effects of the jitter on the noise floor and dynamic range of the ADC.

The ring resonator, which is developed by Professor Nadir Dagli at the University of California Santa Barbara, was not available. Hence, the full integration of the photonic sigma delta ADC could not be achieved. However, the test and measurements carried out on the rest of the available components showed that the concept is feasible and can be implemented as the ring resonator becomes available.

There was also a considerable amount of effort spent on modifying the MATLAB simulation to test the performance of the ADC in the presence of timing and amplitude jitter. A number of simulation runs for different scenarios were conducted to determine the effects of the jitter and to ascertain the performance of the ADC under these different conditions.

## **B. FURTHER IMPROVEMENTS**

### **1. Hardware**

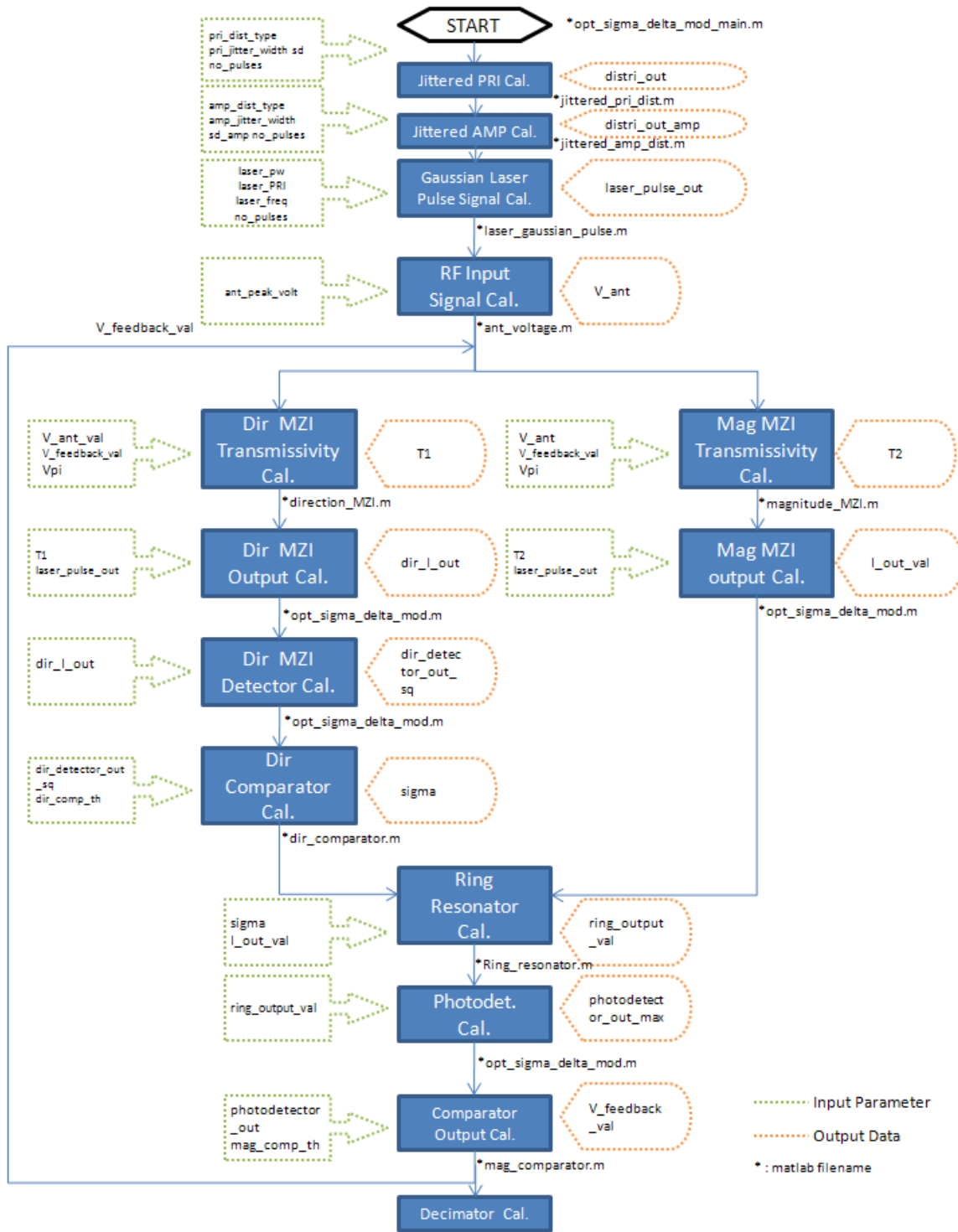
In the high-speed comparator system, as the input was coming from a photodetector, the voltage and current of the signal is very low. The use of the fanout, which is a limiting amplifier, as the first stage in the system was not sufficient to generate an output that is high enough for the rest of the components in the high-speed comparator. This resulted in an output at the MZI driver that is too low to drive the MZI itself. It is recommended that a transimpedance amplifier be used instead of the fanout. This ensures that the output at the MZI driver will be high enough to drive the MZI and the proper feedback subtraction can occur.

Alternatively, the use of a fully optical comparator can be investigated so that the thresholding can be done optically, bypassing the need for high-speed analog components.

### **2. MATLAB Simulation**

The MATLAB simulation does not take into account the delay experienced by the laser pulse train as it passed through various components in the ADC. These delays may result in degradation of performance. In future work, these delays can be included in the simulation so that the effects of these delays on the performance of the photonic sigma delta ADC can be analyzed.

# APPENDIX A. PHOTONIC SIGMA DELTA ADC FLOW CHART



THIS PAGE INTENTIONALLY LEFT BLANK

## APPENDIX B. MATLAB CODE FOR PHOTONIC SIGMA DELTA ADC

Program File Name: opt\_sigma\_delta\_mod\_main.m

```
%%%%%%%%%%%%%%%%%%%%%%%%%%%%%%%%%%%%%%%%%%%%%%%%%%%%%%%%%%%%%%%%%%%%%%%%%
%Simulation for photonic sigma delta ADC.
%The following parameters can be set
%Line 40 -> Vpi - half wave length voltage
%Line 41 -> dir_comp_th - direction comparator threshold
%Line 42 -> mag_comp_th - output comparator threshold
%Line 43 -> a - amplitude of laser pulse
%Line 47 -> f_l - scaled laser freq. for simulation
%Line 48 -> f_0 - RF input Signal frequency
%Line 49 -> f_0_bw - Signal bandwidth
%Line 50 -> osr_temp - Oversampling ratio
%Line 67 -> no_of_laser_pulses - number of laser pulse to simulate
%Line 79 -> sd - Standard deviation for timing jitter
%Line 90 -> sd_amp - Standard deviation for amplitude jitter
%Line 104 -> ant_peak_volt - peak voltage of RF input signal
%%%%%%%%%%%%%%%%%%%%%%%%%%%%%%%%%%%%%%%%%%%%%%%%%%%%%%%%%%%%%%%%%%%%%%%%%
% Modified by: Yean Wee Tan
% Electrical and Computer Engineering Department
% Naval Postgraduate School
%
% Originally written: by Chang Ho Nam
%%%%%%%%%%%%%%%%%%%%%%%%%%%%%%%%%%%%%%%%%%%%%%%%%%%%%%%%%%%%%%%%%%%%%%%%%

%Simulation of the sigma delta modulator

clear all;
close all;

%V_ant is the signal coming from the antenna
%V_feedback is the signal from feedback

global a; % amp. of laser pulse
global f_l; % frequency of laser pulse
global no_of_laser_pulses;
global Vpi;
global samp_no_total;

% ----- Hardware parameter setting -----
Vpi=3.2;
dir_comp_th=0.25;% direction comparator threshold
mag_comp_th=0.25;% output comparator threshold
a=1; % amplitude of laser pulse

% ----- Scaled laser freq, PRI and PW for simulation -----

f_l=200; %scaled laser freq. for simulation
f_0=0.25; %RF Signal frequency
```



```

f_0_bw=0.5; %Signal bandwidth
osr_temp=10;
pri_temp=1/(2*f_0_bw*osr_temp);

laser_freq_period=1/f_l;
no_of_cycle=pri_temp/laser_freq_period; % no of laser cycles in PRI
pri=round(no_of_cycle)*laser_freq_period; %Multiples of laser_freq_period
laser_pw_ratio=0.1; % duty cycle of laser signal
laser_pw=laser_pw_ratio*pri; % pulsewidth of lase pulse
prf=1/pri;
OSR=prf/(2*f_0_bw);

%———— Determine sample size and step————

no_of_laser_pulses=200;
sampling_clock=4*2*f_l;
samp_time=1/sampling_clock;
samp_no_cycle=laser_freq_period/samp_time; %number of samples in laser frequency period
samp_no_pri=(round(no_of_cycle)*round(samp_no_cycle)); %number of samples in laser pulse pri –
multiple of samp_no_cycle
samp_no_pw=round(laser_pw/samp_time); %number of samples in laser pulse pulsewidth
samp_no_total=no_of_laser_pulses*samp_no_pri;

%———— Generation of jittered PRI —————

pri_dist_type=2; % 1 : uniform distribution, 2 : Gaussian distribution
pri_jitter_width=0.0; %jitter_width to pri of uniform distribution
sd=0.001;% standard deviation of Gaussian distribution
distri_out=jittered_pri_dist(pri_dist_type, pri_jitter_width, sd, no_of_laser_pulses);
delta_pri=distri_out; % uniform or Gaussian distribution of PRI jitter
jitter_pri=pri+(pri*delta_pri); %
samp_no_jitter_pri=round(jitter_pri/samp_time);

%———— Generation of jittered AMPLITUDE —————

pulse_amp=1.0;
amp_dist_type=2; % 1 : uniform distribution, 2 : Gaussian distribution
amp_jitter_width=0.2; %amp jitter_width to "amp=1" of uniform distribution
sd_amp=0;% standard deviation of Gaussian distribution
distri_out_amp=jittered_amp_dist(amp_dist_type, amp_jitter_width, sd_amp, no_of_laser_pulses);
delta_amp=distri_out_amp; % uniform or Gaussian distribution of PRI jitter
jitter_amp=pulse_amp+(pulse_amp*delta_amp); %

%———— Gaussian laser pulse signal calculation —————

[begin_samp1,end_samp1,ttl1,gaussian_env_samp,laser_pulse_out_1d_2,y,laser_pulse_out]=laser_gaussia
n_pulse(samp_time,pri,samp_no_pw,samp_no_pri,samp_no_jitter_pri,jitter_amp,
samp_no_total,no_of_laser_pulses,laser_pw_ratio);
% ——> laser pulse * Gaussian envelope
I_in_pulse=laser_pulse_out;

%———— ant voltage signal calculation —————

ant_peak_volt=0.8; % antenna peak voltage

```

```
V_ant=rf_voltage(samp_time,pri,samp_no_pri,no_of_laser_pulses,ant_peak_volt,samp_no_total,f_0);
```

```
%———— Variable pre-allocation to speed up loop speed————\\
```

```
V_feedback_samp=zeros(1,samp_no_total);  
sigma=0.0;  
pulse_count=0.0;  
pulse_count_no=zeros(1,no_of_laser_pulses);  
V_feedback_samp_tmp=zeros(1,samp_no_total);  
dir_transmissivity=zeros(1,samp_no_total);  
dir_I_out=zeros(1,samp_no_total);  
dir_I_out_sq=zeros(1,samp_no_total);  
mag_transmissivity=zeros(1,samp_no_total);  
I_out=zeros(1,samp_no_total);  
sigma_samp_tmp=zeros(1,samp_no_total);  
ring_output_array=zeros(1,samp_no_total);  
photodetector_out=zeros(1,samp_no_total);  
ab=zeros(1,no_of_laser_pulses);  
ae=zeros(1,no_of_laser_pulses);  
ax=zeros(1,no_of_laser_pulses);  
sigma_pulse=zeros(1,no_of_laser_pulses);  
output_envelope_detector=zeros(1,no_of_laser_pulses);  
V_feedback_pulse=zeros(1,no_of_laser_pulses);
```

```
%———— Start of Optical Sigma Delta Modulator Loop —————
```

```
for ni=1:samp_no_total
```

```
    residue1=mod(ni,samp_no_pri);  
    if (residue1==1)  
        pulse_count=pulse_count+1;  
    end
```

```
    nk=pulse_count;  
    pulse_count_no(nk)=pulse_count;
```

```
    if (pulse_count == 1)
```

```
        V_feedback_val=0.0;  
        sigma=0.0;
```

```
    else  
        V_feedback_val=V_feedback_pulse(pulse_count-1);  
        sigma=sigma_pulse(pulse_count-1);  
    end;
```

```
    V_feedback_samp_tmp(ni)=V_feedback_val;
```

```
%———— direction_MZI transmissivity calculation —————
```

```
    V_ant_val=V_ant(ni);  
    [T1]=direction_MZI(V_ant_val,V_feedback_val);  
    dir_transmissivity(ni)=T1;
```

```
%———— direction_MZI output calculation —————
```

```

dir_I_out(ni)=T1*laser_pulse_out(ni); % direction_MZI_output
dir_I_out_val=dir_I_out(ni);

%———— direction_MZI detector output calculation —————
dir_I_out_sq(ni) = (abs(dir_I_out_val)^2);% square of direction_MZI detector output

%———— magnitude_MZI transmissivity calculation —————

[T2]=magnitude_MZI(V_ant_val,V_feedback_val);
mag_transmissivity(ni)=T2;

%———— magnitude_MZI output calculation —————

I_out(ni)=T2*laser_pulse_out(ni); % magnitude_MZI_output
I_out_val=I_out(ni);

%———— Ring resonator output calculation —————

sigma_samp_tmp(ni)=sigma;
ring_output_val=ring_resonator(ni,pulse_count,samp_no_pri,no_of
_laser_pulses,I_out_val,sigma);
ring_output_array(ni)=ring_output_val;

%———— photodetector output calculation —————

photodetector_out(ni) = (abs(ring_output_val)^2);% square of fiber lattice output

residue2=mod(ni,samp_no_pri);
if (residue2==0) % pulse-to-pulse calculation
%———— direction comparator output calculation —————

begin_pulse=(pulse_count-1)*samp_no_pri+1;
end_pulse=pulse_count*samp_no_pri;
ab(pulse_count)=begin_pulse;
ae(pulse_count)=end_pulse;
dir_I_out_max=max(dir_I_out_sq(begin_pulse:end_pulse));
ax(pulse_count)=dir_I_out_max;
dir_comparator_output=dir_comparator(dir_I_out_max,dir_comp_th);
sigma_pulse(pulse_count)=dir_comparator_output;
sigma_samp(begin_pulse:end_pulse)=sigma_pulse(pulse_count);

%———— output comparator output calculation —————

photodetector_out_max=max(photodetector_out(begin_pulse:
end_pulse));
output_envelope_detector(pulse_count)=photodetector_out_max;
output_envelope_detector_samp(begin_pulse:end_pulse)=output_envelope_detector(pulse_count);
output_comparator_output=mag_comparator(photodetector_out_max,mag_comp_th,ant_peak_volt);
V_feedback_pulse(pulse_count)=output_comparator_output;
V_feedback_samp(begin_pulse:end_pulse)=V_feedback_pulse(pulse_count);

end

end

```

```

%———— End of Optical Sigma Delta Modulator Loop —————

%———— Decimation Filter —————
%for OSR=10
dda1=decimate(V_feedback_pulse,5,30,'fir');
dda2=decimate(dda1,2,30,'fir');
dda3=upsample(dda2,6400);
for x=1:length(dda3)
    if dda3(x)==0
        dda3(x)=dda3(x-1);
    end
end
figure(3);
hold on
plot(time,V_ant,'LineWidth',3);
plot(time,dda3);
xlabel('Time(s)')
ylabel('Voltage(V)')
title('Decimator Output Voltage vs Time')

%———— Plot figures —————
figure(1);

tt=no_of_laser_pulses*pri;
time=linspace(0,tt,samp_no_total);

subplot(3,1,1),plot(time,(I_in_pulse));
xlabel('Time(s)')
ylabel('Voltage(V)')
title('Gaussian Laser Signal Voltage vs Time')

subplot(3,1,2), plot(time,V_ant,'LineWidth',3);
xlabel('Time(s)')
ylabel('Voltage (V)')
title('RF Signal Voltage vs Time')

subplot(3,1,3);
plot(time,real(sigma_samp),'LineWidth',3);
xlabel('Time(s)')
ylabel('Sigma (V)')
title('Sigma vs Time')

figure(2)

subplot(4,1,1), plot(time,V_ant,'LineWidth',3);
xlabel('Time(s)')
ylabel('Voltage (V)')
title('RF Signal Voltage vs Time')

subplot(4,1,2);
plot(time,real(ring_output_array));
xlabel('Time(s)')
ylabel('Voltage (V)')
title('Ring Resonator Output Voltage vs Time')

```

```

subplot(4,1,3);

plot(time,output_envelope_detector_samp);
xlabel('Time(s)')
ylabel(' Voltage (V)')
title('Photodetector Output Voltage vs Time')

subplot(4,1,4);
plot(time,V_feedback_samp,'LineWidth',3);
xlabel('Time(s)')
ylabel('Voltage (V)')
title('Ring Resonator Comparator Output Voltage vs Time (With jitter)')

figure(3);

tt=no_of_laser_pulses;
pulse_no=linspace(0,tt,no_of_laser_pulses);

pri_fig(1:no_of_laser_pulses)=pri;
subplot(2,1,1),plot(pulse_no,pri_fig,'b','LineWidth',2);
hold on;
plot(pulse_no,jitter_pri,'m','LineWidth',1);
hold on;
xlabel('Pulse NO')
ylabel('PRI(s)')
title('Jittered PRI vs Pulse NO')

amp_fig(1:no_of_laser_pulses)=pulse_amp;
subplot(2,1,2),plot(pulse_no,amp_fig,'b','LineWidth',2);
hold on;
plot(pulse_no,jitter_amp,'m','LineWidth',1);
hold on;
xlabel('Pulse NO')
ylabel('AMP')
title('Jittered AMP vs Pulse NO')

```

## APPENDIX C. SUBROUTINE FUNCTIONS

Program File Name: dir\_comparator.m

```
%%%%%%%%%%%%%%%%%%%%%%%%%%%%%%%%%%%%%%%%%%%%%%%%%%%%%%%%%%%%%%%%%%%%%%%%%  
% Written: by Chang Ho Nam  
% Electrical and Computer Engineering Department  
% Naval Postgraduate School  
%%%%%%%%%%%%%%%%%%%%%%%%%%%%%%%%%%%%%%%%%%%%%%%%%%%%%%%%%%%%%%%%%%%%%%%%%  
  
%———— direction comparator output calculation —————  
Function dir_comparator_output=dir_comparator(dir_I_out_max,dir_comp_th)  
  
if (dir_I_out_max>dir_comp_th)  
  
    dir_comparator_output = 0.0;%Vpi phase modulator – comparator output–integrate up  
else  
    dir_comparator_output = 1.0;%Vpi phase modulator – comparator output–integrate down  
end
```

Program File Name: direction\_MZI.m

```
%%%%%%%%%%%%%%%%%%%%%%%%%%%%%%%%%%%%%%%%%%%%%%%%%%%%%%%%%%%%%%%%%%%%%%%%%  
% Written: by Chang Ho Nam  
% Electrical and Computer Engineering Department  
% Naval Postgraduate School  
%%%%%%%%%%%%%%%%%%%%%%%%%%%%%%%%%%%%%%%%%%%%%%%%%%%%%%%%%%%%%%%%%%%%%%%%%  
  
%———— direction_MZI transmissivity calculation —————  
  
function [T1,Vpi]=direction_MZI(V_ant_val,V_feedback_val)  
  
global Vpi;  
  
DC1 = ones(1,length(V_ant_val))*0;  
DC2 = ones(1,length(V_ant_val))*0;  
V = V_ant_val-V_feedback_val;  
VDC = DC1-DC2;  
VpiDC = 2;  
phi = (pi*V/Vpi);  
phase = -pi/2;  
theta = (pi*VDC/VpiDC)+phase;  
T1 = (1/2)+(1/2)*cos(phi+theta);%direction transmissivity
```

Program File Name: jittered\_amp\_dist.m

```

%%%%%%%%%%%%%%%%%%%%%%%%%%%%%%%%%%%%%%%%%%%%%%%%%%%%%%%%%%%%%%%%%%%%%%%%
% Written: by Chang Ho Nam
% Electrical and Computer Engineering Department
% Naval Postgraduate School
%%%%%%%%%%%%%%%%%%%%%%%%%%%%%%%%%%%%%%%%%%%%%%%%%%%%%%%%%%%%%%%%%%%%%%%%

```

```
function distri_out_amp=jittered_amp_dist(amp_dist_type, amp_jitter_width, sd_amp, no_of_laser_pulses)
```

```

if(amp_dist_type==1) % UNIFORM (
    a = 0; b = amp_jitter_width;
    y11 = a + (b-a) * rand(no_of_laser_pulses,1) - b/2;
else % GUASSIAN
    a = 0; b = sd_amp; %————— a=mean, b=standard deviation —————
    y11 = a + b * randn(no_of_laser_pulses,1);
end
distri_out_amp=y11;

```

Program File Name: jittered\_pri\_dist.m

```

%%%%%%%%%%%%%%%%%%%%%%%%%%%%%%%%%%%%%%%%%%%%%%%%%%%%%%%%%%%%%%%%%%%%%%%%
% Written: by Chang Ho Nam
% Electrical and Computer Engineering Department
% Naval Postgraduate School
%%%%%%%%%%%%%%%%%%%%%%%%%%%%%%%%%%%%%%%%%%%%%%%%%%%%%%%%%%%%%%%%%%%%%%%%

```

```
function distri_out=jittered_pri_dist(pri_dist_type, pri_jitter_width, sd, no_of_laser_pulses)
```

```

if(pri_dist_type==1)
    a = 0; b = pri_jitter_width;
    y11 = a + (b-a) * rand(no_of_laser_pulses,1) - b/2;
else
    a = 0; b = sd; %————— a=mean, b=standard deviation —————
    y11 = a + b * randn(no_of_laser_pulses,1);
end
distri_out=y11;

```

Program File Name: laser\_gaussian\_pulse.m

```

%%%%%%%%%%%%%%%%%%%%%%%%%%%%%%%%%%%%%%%%%%%%%%%%%%%%%%%%%%%%%%%%%%%%%%%%
% Written: by Chang Ho Nam
% Electrical and Computer Engineering Department
% Naval Postgraduate School
%%%%%%%%%%%%%%%%%%%%%%%%%%%%%%%%%%%%%%%%%%%%%%%%%%%%%%%%%%%%%%%%%%%%%%%%

```

```

function
[begin_samp1,end_samp1,ttl,gaussian_env_samp,laser_pulse_out_1d_2,y,laser_pulse_out]=laser_gaussian_pulse(samp_time,pri,samp_no_pw,samp_no_pri,samp_no_jitter_pri,jitter_amp,samp_no_total,no_of_laser_pulses,laser_pw_ratio)
%function
[laser_pulse_out_1d_2,y_total,laser_pulse_out]=laser_gaussian_pulse(pri,samp_no_pw,samp_no_pri,samp_no_total,no_of_laser_pulses,laser_pw_ratio)

```

```

global a;
global f_l;

```

```

global no_of_laser_pulses;
global samp_no_total;

clear laser_pulse_out_1d;
clear laser_pulse_out;
clear laser_pulse;

tt1=samp_time.*linspace(1,samp_no_pri,samp_no_pri);

cmplx_laser=cos(2*pi*f_1*tt1(1:samp_no_pw))+i*sin(2*pi*f_1*tt1(1:samp_no_pw));

optical_intensity_laser_pulse=cmplx_laser;

laser_pulse_out_1d(1:samp_no_pw)=a*optical_intensity_laser_pulse;
laser_pulse_out_1d(samp_no_pw+1:samp_no_pri)=0.0;

cmplx_laser1=cos(2*pi*f_1*tt1(1:samp_no_pri))+i*sin(2*pi*f_1*tt1(1:samp_no_pri));
laser_pulse_out_1d_1(1:samp_no_pri)=a*cmplx_laser1;

%—————CW Laser Generation—————
tt2=samp_time.*linspace(1,samp_no_total,samp_no_total);
t11=tt2;
laser_pulse_out_1d_2=zeros(1,samp_no_total);

for nns=1:samp_no_total
    cmplx_laser2=cos(2*pi*f_1*t11(nns))+i*sin(2*pi*f_1*t11(nns));
    laser_pulse_out_1d_2(nns)=a*cmplx_laser2;
end

%————— Gaussian Envelope Generation—————

mu=laser_pw_ratio/2.0; %center of gaussian distribution
samp_spacing=1/samp_no_pri;
laser_pw=laser_pw_ratio*pri;
y=zeros(no_of_laser_pulses,samp_no_pri);
T=zeros(no_of_laser_pulses,samp_no_pri);

for pulse_no=1:no_of_laser_pulses
    normalized_end_pri=1+((samp_no_jitter_pri(pulse_no)-samp_no_pri)/samp_no_pri);
    T(pulse_no,1:samp_no_jitter_pri(pulse_no))=samp_spacing:samp_spacing:normalized_end_pri;
    %samples in PRI(at .1sec)(100ps@ 1:10^9 scale)
    sigma=laser_pw;
    y11 = (1/(sigma*sqrt(2*pi)))*exp(-(T(pulse_no,1:samp_no_jitter_pri(pulse_no))-
mu).^2)/(2*((sigma).^2));
    y_max=max(y11);
    y(pulse_no,1:samp_no_jitter_pri(pulse_no))=y11/y_max; %normalize
end

%————— in case of jittered PRI————— %

gaussian_env_samp_1(1:samp_no_total)=0.0;
gaussian_env_samp_1=zeros(1,samp_no_total);

```



```

begin_samp1=zeros(1,no_of_laser_pulses);
end_samp1=zeros(1,no_of_laser_pulses);

for pulse_count1=1:no_of_laser_pulses
    if(pulse_count1==1)
        begin_samp1(pulse_count1)=1;
    else
        begin_samp1(pulse_count1)=end_samp1(pulse_count1-1)+1;
    end
    end_samp1(pulse_count1)=begin_samp1(pulse_count1)+(samp_no_jitter_pri(pulse_count1)-1);

    gaussian_env_samp_1(begin_samp1(pulse_count1):end_samp1(pulse_count1))=jitter_amp(pulse_count1)*
    y(pulse_count1,1:samp_no_jitter_pri(pulse_count1)); %gaussian_env_samp is the gaussian envelope signal
    samples(1-dim array)
end

gaussian_env_samp(1:samp_no_total)=gaussian_env_samp_1(1:samp_no_total);
laser_pulse_out=zeros(1,samp_no_total);
for ns=1:samp_no_total
    laser_pulse_out(ns)=(gaussian_env_samp(ns).^(.5)).*laser_pulse_out_1d_2(ns); %the laser pulses from
    the pulsed laser * Gaussian Envelope
end

```

Program File Name: mag\_comparator.m

```

%%%%%%%%%%%%%%%%%%%%%%%%%%%%%%%%%%%%%%%%%%%%%%%%%%%%%%%%%%%%%%%%%%%%%%%%
% Written: by Chang Ho Nam
% Electrical and Computer Engineering Department
% Naval Postgraduate School
%%%%%%%%%%%%%%%%%%%%%%%%%%%%%%%%%%%%%%%%%%%%%%%%%%%%%%%%%%%%%%%%%%%%%%%%

```

```

function
output_comparator_output=mag_comparator(photodetector_out_max,mag_comp_th,ant_peak_volt)

if (photodetector_out_max>mag_comp_th)

    output_comparator_output = ant_peak_volt;%comparator output : V_feedback=1V
else
    output_comparator_output = -1*ant_peak_volt;%comparator output : V_feedback=-1V
end

```

Program File Name: magnitude\_MZI.m

```

%%%%%%%%%%%%%%%%%%%%%%%%%%%%%%%%%%%%%%%%%%%%%%%%%%%%%%%%%%%%%%%%%%%%%%%%
% Written: by Chang Ho Nam
% Electrical and Computer Engineering Department
% Naval Postgraduate School
%%%%%%%%%%%%%%%%%%%%%%%%%%%%%%%%%%%%%%%%%%%%%%%%%%%%%%%%%%%%%%%%%%%%%%%%

```

```

%————— magnitude_MZI transmissivity calculation —————

```

```
function [T2,Vpi]=magnitude_MZI(V_ant,V_feedback)
```

```
global Vpi;
```

```
DC1 = ones(1,length(V_ant))*0;  
DC2 = ones(1,length(V_ant))*0;  
V = V_ant-V_feedback;  
VDC = DC1-DC2;  
VpiDC = 2;  
phi = (pi*V/Vpi);  
phase = pi;  
theta = (pi*VDC/VpiDC)+phase;  
T2 = (1/2)+(1/2)*cos(phi+theta);%magnitude transmissivity
```

Program File Name: rf\_voltage.m

```
%%%%%%%%%%%%%%%%%%%%%%%%%%%%%%%%%%%%%%%%%%%%%%%%%%%%%%%%  
% Written: by Chang Ho Nam  
% Electrical and Computer Engineering Department  
% Naval Postgraduate School  
%%%%%%%%%%%%%%%%%%%%%%%%%%%%%%%%%%%%%%%%%%%%%%%%%%%%%%%%
```

```
%----- rf voltage signal calculation -----
```

```
function
```

```
V_ant=rf_voltage(samp_time,pri,samp_no_pri,no_of_laser_pulses,ant_peak_volt,samp_no_total,f_0)
```

```
time1=samp_time.*linspace(1,samp_no_total,samp_no_total);  
V_ant1=sin(2*pi*f_0*time1);  
V_ant=ant_peak_volt*V_ant1;%RF voltage – SINE function
```

Program File Name: ring\_resonator.m

```
%%%%%%%%%%%%%%%%%%%%%%%%%%%%%%%%%%%%%%%%%%%%%%%%%%%%%%%%  
% Written: by Chang Ho Nam  
% Electrical and Computer Engineering Department  
% Naval Postgraduate School  
%%%%%%%%%%%%%%%%%%%%%%%%%%%%%%%%%%%%%%%%%%%%%%%%%%%%%%%%
```

```
%----- ring resonator output calculation -----
```

```
function ring_output_val=ring_resonator(ni,pulse_count,samp_no_pri,no_of_laser_pulses,I_out_val,sigma)
```

```
global ring_output;
```

```
if (sigma==1)
```

```
    phase_mod_out(ni) = (-1)*(I_out_val);%phase modulator output for destructive  
interference(sigma=Vpi=1)
```

```

else
    phase_mod_out(ni) = (I_out_val);%phase modulator output for constructive interference(sigma=0)
end

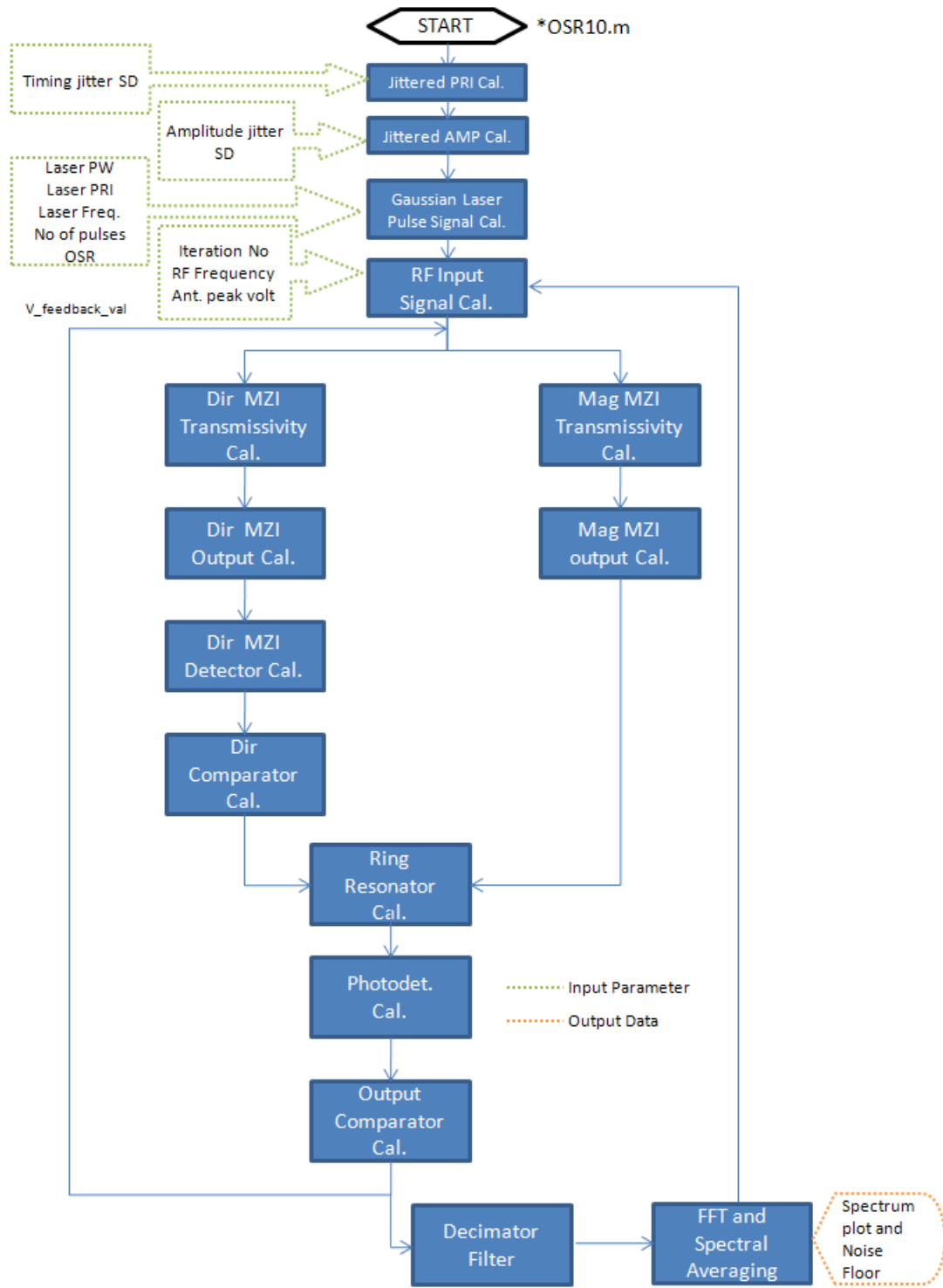
a_0=.4;
a_1=.6;
G=4.166;
c=(1-a_0)*(1-a_1);
d=(a_0*a_1)*G;

if (pulse_count==1)
    ring_output(ni) = (I_out_val);%MZI output of pulse#1
else
    ring_output(ni) =c*phase_mod_out(ni) + d*ring_output(ni-samp_no_pri);
end

ring_output_val= ring_output(ni); % 1-pulse delayed fiber-lattice-accumulator output

```

## APPENDIX D. NOISE FLOW ANALYSIS FLOW CHART



THIS PAGE INTENTIONALLY LEFT BLANK

## APPENDIX E. MATLAB CODE NOISE FLOOR CALCULATION

Program File Name: OSR10.m

```
%%%%%%%%%%%%%%%%%%%%%%%%%%%%%%%%%%%%%%%%%%%%%%%%%%%%%%%%%%%%%%%%%%%%%%%%%
%Simulation to calculate the noise floor photonic sigma delta ADC.
%The following parameters can be set
%Line 35 -> Vpi – half wave length voltage
%Line 36 -> dir_comp_th – direction comparator threshold
%Line 37 -> mag_comp_th – output comparator threshold
%Line 38 -> a – amplitude of laser pulse
%Line 42 -> f_l – scaled laser freq. for simulation
%Line 43 -> f_0 – RF input Signal frequency
%Line 44 -> f_0_bw – Signal bandwidth
%Line 45 -> osr_temp – Oversampling ratio
%Line 57 -> pulse_no_fft – pulse no after decimation
%Line 63 -> iteration – number of runs for spectral averaging
%Line 69 -> sd – Standard deviation for timing jitter
%Line 87 -> sd_amp – Standard deviation for amplitude jitter
%Line 155 -> ant_peak_volt – peak voltage of RF input signal
%
%
%%%%%%%%%%%%%%%%%%%%%%%%%%%%%%%%%%%%%%%%%%%%%%%%%%%%%%%%%%%%%%%%%%%%%%%%%
% Modified by: Yean Wee Tan
% Electrical and Computer Engineering Department
% Naval Postgraduate School
%
% Originally written: by Chang Ho Nam
%%%%%%%%%%%%%%%%%%%%%%%%%%%%%%%%%%%%%%%%%%%%%%%%%%%%%%%%%%%%%%%%%%%%%%%%%
%Simulation of the sigma delta modulator

clc
clear all;
close all;

%V_ant is the signal coming from the antenna
%V_feedback is the signal from feedback

Vpi = 1.0;
dir_comp_th=0.25;% direction comparator threshold
mag_comp_th=0.25; % output comparator threshold
a=1;

%———— scaled laser freq. and PRI for simulation —————

f_l=200; %scaled laser freq. for simulation
f_0=0.2; %RF signal frequency
f_0_bw=0.5; %Signal Bandwidth
osr_temp=10 %Temp OSR
prf_temp=2*f_0_bw*osr_temp;
pri_temp=1/prf_temp;
laser_freq_period=1/f_l;
```

```

sampling_clock=4*2*f_1;
samp_time=1/sampling_clock;
no_of_cycle=pri_temp/laser_freq_period; % no of laser cycles in PRI
pri=round(no_of_cycle)*laser_freq_period; %PRI = multiples of laser_freq_period
laser_pw_ratio=0.1; % duty cycle of laser signal
laser_pw=laser_pw_ratio*pri; % pulsewidth of laser pulse
prf=1/pri; %Actual PRF
oversampling_ratio=prf/(2*f_0_bw); %Actual OSR
pulse_no_fft=1100; %pulse no after decimation
no_of_laser_pulses=oversampling_ratio*pulse_no_fft;
samp_no_cycle=laser_freq_period/samp_time; %number of samples in laser frequency period
samp_no_pri=(round(no_of_cycle)*round(samp_no_cycle)); %number of samples in laser pulse pri –
multiple of samp_no_cycle
samp_no_pw=round(laser_pw/samp_time); %number of samples in laser pulse pulsewidth
samp_no_total=no_of_laser_pulses*samp_no_pri;
iteration_no=1; %number of runs for spectral averaging
decimator_output_modulator_sum_11=0.0;
%———— Generation of jittered PRI —————

pri_dist_type=2; % 1 : uniform distribution, 2 : Gaussian distribution
pri_jitter_width=0; %jitter_width to pri of uniform distribution
sd=0;% standard deviation of Gaussian distribution(% of PRI)
if (pri_dist_type==1)
    mean = 0;
    y11 = mean + (pri_jitter_width–mean) * rand(no_of_laser_pulses,1) – pri_jitter_width/2;
else
    mean = 0;
    y11 = mean + sd * randn(no_of_laser_pulses,1);
end
delta_pri=y11; % uniform or Gaussian distribution of PRI jitter
jitter_pri=pri+(pri*delta_pri); % % use this!!
sd_pri=pri*sd;
samp_no_jitter_pri=round(jitter_pri/samp_time);

%———— Generation of jittered AMPLITUDE —————

pulse_amp=1.0;
amp_dist_type=2; % 1 : uniform distribution, 2 : Gaussian distribution
amp_jitter_width=0.2; %amp jitter_width to "amp=1" of uniform distribution
sd_amp=0;% standard deviation of Gaussian distribution(% of amplitude)
if (amp_dist_type==1) % UNIFORM
    mean = 0;
    y11 = mean + (amp_jitter_width–mean) * rand(no_of_laser_pulses,1) – amp_jitter_width/2;
else % GUASSIAN
    mean = 0;
    y11 = mean + sd_amp * randn(no_of_laser_pulses,1);
end
delta_amp=y11; % uniform or Gaussian distribution of PRI jitter
jitter_amp=pulse_amp+(pulse_amp*delta_amp); % use this!!

% ————— Generation of laser Gaussian envelope —————

tt1=samp_time.*linspace(1,samp_no_pri,samp_no_pri);
cmplx_laser=cos(2*pi*f_1*tt1(1:samp_no_pw))+1i*sin(2*pi*f_1*tt1(1:samp_no_pw));

```

```

optical_intensity_laser_pulse=cmplx_laser;

laser_pulse_out_1d(1:samp_no_pw)=a*optical_intensity_laser_pulse;
laser_pulse_out_1d(samp_no_pw+1:samp_no_pri)=0.0;

cmplx_laser1=cos(2*pi*f_1*tt1(1:samp_no_pri))+1i*sin(2*pi*f_1*tt1(1:samp_no_pri));
laser_pulse_out_1d_1(1:samp_no_pri)=a*cmplx_laser1;

%—————CW Laser Generation—————

tt2=samp_time.*linspace(1,samp_no_total,samp_no_total);
ttt1=tt2;
laser_pulse_out_1d_2=a.*(cos(2*pi*f_1*ttt1)+1i*sin(2*pi*f_1*ttt1));
%—————Gaussian Envelope Generation—————

mu=laser_pw_ratio/2.0; %center of gaussian distribution
samp_spacing=1/samp_no_pri;
laser_pw=laser_pw_ratio*pri;

y=zeros(no_of_laser_pulses,samp_no_pri);
T=zeros(no_of_laser_pulses,samp_no_pri);
normalized_end_pri=zeros;
y11=zeros;
y_max=zeros;

for pulse_no=1:no_of_laser_pulses
    normalized_end_pri=1+((samp_no_jitter_pri(pulse_no)-samp_no_pri)/samp_no_pri);
    T(pulse_no,1:samp_no_jitter_pri(pulse_no))=samp_spacing:samp_spacing:normalized_end_pri;
    %samples in PRI(at .1sec)(100ps@ 1:10^9 scale)
    sigma=laser_pw;
    y11 = (1/(sigma*sqrt(2*pi)))*exp(-((T(pulse_no,1:samp_no_jitter_pri(pulse_no))-
mu).^2)/(2*((sigma).^2)));
    y_max=max(y11);
    y(pulse_no,1:samp_no_jitter_pri(pulse_no))=y11/y_max; %normalize
end

gaussian_env_samp_1=zeros(1,samp_no_total);
begin_samp1=zeros(1,no_of_laser_pulses);
end_samp1=zeros(1,no_of_laser_pulses);

for pulse_count1=1:no_of_laser_pulses
    if(pulse_count1==1)
        begin_samp1(pulse_count1)=1;
    else
        begin_samp1(pulse_count1)=end_samp1(pulse_count1-1)+1;
    end
    end_samp1(pulse_count1)=begin_samp1(pulse_count1)+(samp_no_jitter_pri(pulse_count1)-1);

gaussian_env_samp_1(begin_samp1(pulse_count1):end_samp1(pulse_count1))=jitter_amp(pulse_count1)*
y(pulse_count1,1:samp_no_jitter_pri(pulse_count1)); %gaussian_env_samp is the gaussian envelope signal
samples(1-dim array)
end

```



```

gaussian_env_samp=gaussian_env_samp_1;
laser_pulse_out=(gaussian_env_samp.^(.5)).*laser_pulse_out_1d_2; %the laser pulses from the pulsed
laser * Gaussian Envelope
I_in_pulse=laser_pulse_out;

%————— RF signal parameter —————
ant_peak_volt=0.5; % antenna peak voltage
V_lower=-1.0*ant_peak_volt;
V_upper=+1.0*ant_peak_volt;
Vpp=abs(V_upper-V_lower);
V_ant=linspace(V_lower, V_upper, samp_no_total);
time1=samp_time.*linspace(1,samp_no_total,samp_no_total);
V_feedback_pulse_iter=zeros(iteration_no, no_of_laser_pulses);

%————— Ring resonator Parameters —————
a_0=.4;
a_1=.6;
G=4.166;
c=(1-a_0)*(1-a_1); %Multiplying factor
d=(a_0*a_1)*G; %Leakage coefficient

for nnk=1:iteration_no
    nnk %#ok<NOPTS>

%————— Generation different V_ant for each iteration—————
    delta_pi=(nnk-1)*(2*3.141592653/iteration_no) %#ok<NOPTS>
    V_ant1=sin(2*pi*f_0*time1+delta_pi);
    V_ant=ant_peak_volt*V_ant1;%RF voltage – SINE function

%————— Initialization of ant voltage feedback signal calculation—————

    V_feedback_samp=zeros(1,samp_no_total);
    sigma=0.0;
    pulse_count=0.0;
    begin_pulse=0.0;
    end_pulse=0.0;
    dir_transmissivity=zeros(1,samp_no_total);
    dir_I_out=zeros(1,samp_no_total);
    dir_I_out_sq=zeros(1,samp_no_total);
    mag_transmissivity=zeros(1,samp_no_total);
    I_out=zeros(1,samp_no_total);
    sigma_samp_tmp=zeros(1,samp_no_total);
    ring_output_array=zeros(1,samp_no_total);
    photodetector_out=zeros(1,samp_no_total);
    ab=zeros(1,no_of_laser_pulses);
    ae=zeros(1,no_of_laser_pulses);
    ax=zeros(1,no_of_laser_pulses);
    sigma_pulse=zeros(1,no_of_laser_pulses);
    output_envelope_detector=zeros(1,no_of_laser_pulses);
    V_feedback_pulse=zeros(1,no_of_laser_pulses);
    pulse_delay_no=1;
    phase_mod_out=zeros(1,samp_no_total);
    ring_output=zeros(1,samp_no_total);

```

```

%———— Start of Optical Sigma Delta Modulator Loop —————
for ni=1:samp_no_total
    residue1=mod(ni,samp_no_pri);
    if (residue1==1)
        pulse_count=pulse_count+1;
    end
    nk=pulse_count;

    if (pulse_count == 1)
        V_feedback_val=0.0;
        sigma=0.0;
    else
        V_feedback_val=V_feedback_pulse(pulse_count-1);
        sigma=sigma_pulse(pulse_count-1);
    end;

%———— direction_MZI transmissivity calculation —————

    V_ant_val=V_ant(ni);
    V = V_ant_val-V_feedback_val;
    VDC = 0;
    VpiDC = 2;
    phi = (pi*V/Vpi);
    phase = -pi/2;
    theta = (pi*VDC/VpiDC)+phase;
    T1 = (1/2)+(1/2)*cos(phi+theta);%direction transmissivity

%———— direction_MZI output calculation —————

    dir_I_out(ni)=T1*laser_pulse_out(ni); % direction_MZI_output
    dir_I_out_val=dir_I_out(ni);

%———— direction_MZI detector output calculation —————
    dir_I_out_sq(ni) = (abs(dir_I_out_val)^2);% square of direction_MZI detector output

%———— magnitude_MZI transmissivity calculation —————

    phase = pi;
    theta = (pi*VDC/VpiDC)+phase;
    T2 = (1/2)+(1/2)*cos(phi+theta);%magnitude transmissivity

%———— magnitude_MZI output calculation —————

    I_out(ni)=T2*laser_pulse_out(ni); % magnitude_MZI_output
    I_out_val=I_out(ni);

%———— Ring Resonator output calculation —————

    sigma_samp_tmp(ni)=sigma;

    if (sigma==1)

```

```

    phase_mod_out(ni) = (-1)*(I_out_val);%phase modulator output for destructive
interference(sigma=Vpi=1)
else
    phase_mod_out(ni) = (I_out_val);%phase modulator output for constructive interference(sigma=0)
end

if (pulse_count<=pulse_delay_no)
    ring_output(ni) = (I_out_val);%MZI output of pulse#1
else
    ring_output(ni) = c*phase_mod_out(ni) + d*ring_output(ni-(pulse_delay_no*samp_no_pri));
end

ring_output_val= ring_output(ni); % 1-pulse delayed fiber-lattice-accumulator

ring_output_array(ni)=ring_output_val;

%———— photodetector output calculation —————

    photodetector_out(ni) = (abs(ring_output_val)^2);% square of fiber lattice output

%———— direction comparator output calculation —————

residue2=mod(ni,samp_no_pri);
if (residue2==0) % pulse-to-pulse calculation
    begin_pulse=(pulse_count-1)*samp_no_pri+1;
    end_pulse=pulse_count*samp_no_pri;
    ab(pulse_count)=begin_pulse;
    ae(pulse_count)=end_pulse;
    dir_I_out_max=max(dir_I_out_sq(begin_pulse:end_pulse));
    ax(pulse_count)=dir_I_out_max;

    if (dir_I_out_max>dir_comp_th)
        dir_comparator_output = 0.0;%Vpi phase modulator – comparator output–integrate up
    else
        dir_comparator_output = 1.0;%Vpi phase modulator – comparator output–integrate down
    end

    sigma_pulse(pulse_count)=dir_comparator_output;
    sigma_samp(begin_pulse:end_pulse)=sigma_pulse(pulse_count);

%———— output comparator output calculation —————

    photodetector_out_max=max(photodetector_out(begin_pulse:end_pulse));
    output_envelope_detector(pulse_count)=photodetector_out_max;
    output_envelope_detector_samp(begin_pulse:end_pulse)=output_envelope_detector(pulse_count);

    if (photodetector_out_max>mag_comp_th)
        output_comparator_output = ant_peak_volt;%comparator output : V_feedback=1V
    else
        output_comparator_output = -1*ant_peak_volt;%comparator output : V_feedback=-1V
    end
    V_feedback_pulse(pulse_count)=output_comparator_output;

```

```

        V_feedback_samp(begin_pulse:end_pulse)=V_feedback_pulse(pulse_count);
    end

end

%———— End of Optical Sigma Delta Modulator Loop —————

decimation_factor_1=5;
decimation_factor_2=2;
fs=(1/pri)/(decimation_factor_1*decimation_factor_2); %for graph x-axis
filter_order_1=30;
filter_order_2=30;
const11=1.0;

%————— DECIMATE for V_feedback_pulse(modulator output):—
dda1=decimate(V_feedback_pulse,decimation_factor_1,filter_order_1,'fir');
dda2=decimate(dda1,decimation_factor_2,filter_order_2,'fir');
wina1 = blackmanharris(length(dda2));
[decimator_output_mod_output11,wc1]=periodogram(dda2,wina1,'onesided',[],fs);

% —sum of periodogram output for V_feedback_pulse(DECIMATE output) —
decimator_output_modulator_11(nnk,:)=decimator_output_mod_output11;

decimator_output_modulator_sum_11=decimator_output_modulator_sum_11+decimator_output_mod_out
put11;
end

% Normalization of periodogram & plot for V_feedback_pulse—————

decimator_output_modulator_aver_11=decimator_output_modulator_sum_11/iteration_no;
max_mod_out11=max(decimator_output_modulator_aver_11);
decimator_output_modulator_normalize_11=decimator_output_modulator_aver_11/max_mod_out11;

amod11_db=10*log10(decimator_output_modulator_normalize_11);
xaxis=linspace(0,fs/2,length(wc1-1));
xmin=0;
xmax=2.5;
ymin=-90;
ymax=0;
mm1_db = amod11_db
%Remove fo from the spectrum and calculate RMS noise floor
bc1=405; % beginning of deleting point of spectrum
ec1=416;% end of deleting point of spectrum
kr=length(mm1_db);
ar=ec1-bc1+1;
arg1=kr-ar;
bc2=bc1-1;
ec2=ec1+1;
zz5(1:bc2,1)=mm1_db(1:bc2,1);
zz5(bc1:arg1,1)=mm1_db(ec2:kr,1);
nnx=length(zz5);
nf_rms1=-norm(zz5)/sqrt(nnx);
xaxis=linspace(0,fs/2,length(mm1_db-1));

```

```
figure(1001)
plot(xaxis,amod11_db)
grid on;
axis([xmin fs/2 ymin ymax])
xlabel('Frequency(Hz)')
ylabel('Magnitude(dB)')
title(['Normalizd Magnitude Spectrum(Decimate+Period) of Decimator Output for –
OSR=',num2str(oversampling_ratio)])
text(0.03, -75,['NO of pulses:',num2str(no_of_laser_pulses),' PRF=',num2str(prf),'Hz',' SD-
PRI=',num2str(sd_pri),' SD-AMP=',num2str(sd_amp)])
legend('OSR10',2);
text(0.03, -85,['NF=',num2str(nf_rms1)])

save OSR10.mat
```

## LIST OF REFERENCES

- [1] P. M. Aziz, H. V. Sorensen and J. Spiegel, “An overview of sigma delta converters,” *IEEE Signal Processing Magazine*, pp. 61–84, January 1996.
- [2] P. E. Pace, S. A. Bewley and J. P. Powers, “Fiber–lattice accumulator design considerations for optical  $\Sigma\Delta$  analog–digital converters,” *Optical Engineering*, Vol 39, No. 6, pp.1517–1526, June 2000.
- [3] J. M. Butler, “Construction and measurement of an actively mode-locked sigma laser,” M.S. thesis, Naval Postgraduate School, Monterey, California, June 1998.
- [4] J S. A. Bewley, “Fiber lattice accumulator design considerations for optical [sigma delta] digital antennas,” M.S. thesis, Naval Postgraduate School, Monterey, California, December 1998.
- [5] R. Khoini–Poofard and D. A. Johns, “Analysis of sigma delta modulators with zero mean stochastic inputs,” *IEEE Trans. Circuit Syst., II: Analog Digital Signal Process*, 42, pp. 164–175, 1995.
- [6] P. E. Pace, *Advanced Techniques for Digital Receivers*, Artech, Massachusetts, 2000.
- [7] A. F. Atherton, “Integrated optical Fiber Lattice Accumulator,” M.S. thesis, Naval Postgraduate School, Monterey, California, March 1997.
- [8] K. Escobar, “Photonic front–end and comparator processor for a sigma delta modulator,” M.S. thesis, Naval Postgraduate School, Monterey, California, September 2008.
- [9] Byungchae Kim, “Very Compact Ring Resonators with Conventional Waveguides, Total Internal Reflection Mirrors and Etched Beam Splitters,” PhD. dissertation , University of California Santa Barbara, Santa Barbara, California, September 2010.
- [10] Calmar Optcom, “Picosecond Pulsed Fiber Laser Instruction Manual,” 2009.
- [11] Inphi Inc., “4311DZ Mach-Zehnder Driver Data Sheet,” November 2002.
- [12] R. Poore, “Phase Noise and Jitter,” Agilent EEsof EDA, May 2001.
- [13] Maxim Integrated Products, “Clock jitter and phase noise conversion,” Application Note 3359, September 2004.

- [14] Y. W. Tan, H. N. Chang and P. E. Pace, "Effects of amplitude and time jitter on the performance of photonic sigma delta modulators," SPIE Photonics West Conference, San Francisco, January 2011 (To be presented).

## INITIAL DISTRIBUTION LIST

1. Defense Technical Information Center  
Ft. Belvoir, Virginia
2. Dudley Knox Library  
Monterey, California
3. Professor R. Clark Robertson  
Chairman, Department of Electrical & Computer Engineering  
Naval Postgraduate School  
Monterey, California
1. 4. Professor Phillip Pace  
Naval Postgraduate School  
Monterey, California
2. 5. Professor David Jenn  
Naval Postgraduate School  
Monterey, California
6. Mr. James Calusdian  
Naval Postgraduate School  
Monterey, California
7. Professor Tat Soon Yeo  
Director  
Temasek Defence Systems Institute (TDSI)  
National University of Singapore  
Singapore
8. Ms. Tan Lai Poh  
Senior Manager  
Temasek Defence Systems Institute (TDSI)  
National University of Singapore  
Singapore
9. Mr. Tan Yean Wee  
Senior Engineer  
Singapore Technologies Electronic  
Singapore